

VECTOR MESONS IN DENSE MATTER
AND DILEPTON PRODUCTION
IN HEAVY ION COLLISIONS
AT INTERMEDIATE ENERGIES

DISSERTATION

zur Erlangung des Grades eines
Doktors der Naturwissenschaften
der Fakultät für Mathematik und Physik
der Eberhard–Karls–Universität zu Tübingen

vorgelegt von

ELVIRA SANTINI
aus Catania – Italien

2008

Tag der mündlichen Prüfung:

15.02.2008

Dekan:

Prof. Dr. N. Schopohl

1. Berichterstatter:

Prof. Dr. Dr. h.c. mult. A. Fäßler

2. Berichterstatter:

Prof. Dr. C. Fuchs

*Considerate la vostra semenza:
fatti non foste a viver come bruti,
ma per seguir virtute e canoscenza.*

D. ALIGHIERI, *La Divina Commedia*, IF XXVI 118-120

Contents

1	Introduction	1
2	Dileptons and vector mesons: Experimental status	5
2.1	Ultrarelativistic HICs	5
2.2	HICs at intermediate energies	6
2.3	Reactions with elementary projectiles on nuclei	7
3	Elementary sources for dilepton production	9
3.1	Dilepton decay rates of light pseudoscalar mesons	10
3.1.1	Relation between the decays $M \rightarrow M'\gamma^*$ and $M \rightarrow M'\ell^+\ell^-$	10
3.1.2	Decay modes $\pi^0 \rightarrow \gamma e^+e^-$ and $\eta \rightarrow \gamma\ell^+\ell^-$	12
3.2	Decays of the ρ -, ω -, and ϕ -mesons to $\ell^+\ell^-$ pairs	13
3.3	Dilepton decay rates of nucleon resonances	14
3.3.1	The $\gamma^*N \rightarrow R$ helicity amplitudes	14
3.3.2	Extended VMD model	19
4	Vector mesons in the medium	31
4.1	In-medium spectral functions	32
4.2	In-medium self energy: resonant contribution	33
4.2.1	Results	36
4.3	In-medium self energy: non-resonant contributions	39
4.3.1	Results	40
4.4	In-medium resonances: role of self-consistency	44
4.5	Dropping mass scenario	46
5	Dilepton production in HIC	47
5.1	The QMD transport model	47
5.1.1	Basic structure of QMD	48
5.2	Tübingen RQMD	53
5.3	Dileptons within the Tübingen RQMD model	57
5.3.1	Dilepton decays of light mesons	58
5.3.2	Dilepton decays of nucleon resonances	58
5.3.3	Discussion: Nucleon-Nucleon Bremsstrahlung	59
5.3.4	Numerical realization	63

5.3.5	Implementation of the ρ and ω meson in-medium spectral functions	63
5.3.6	Advantages and disadvantages of the present approach	65
5.4	Results	66
6	Summary and Conclusions	79
A	Notation	81
B	The $\gamma^* \rightarrow \ell^+\ell^-$ decay width	85
C	Non-resonant contributions to the forward VN scattering	89
C.1	The Compton-like contribution	89
C.1.1	ω meson	89
C.1.2	ρ meson	92
C.2	The σ -exchange contribution	97
	Bibliography	100
	Zusammenfassung	115
	Acknowledgments	119

Chapter 1

Introduction

In the last two decades substantial experimental and theoretical efforts have been directed to the investigation of the modification of the hadron properties in dense and hot matter. The interest has been triggered by the expectation that a signature of the restoration of the spontaneously broken chiral symmetry at finite density and temperature could be inferred by performing and analyzing appropriate experiments. It is expected that the chiral phase transition would manifest itself in terms of certain changes of the hadron properties. In particular, the relation between medium modification of the hadron masses and chiral symmetry restoration in finite density and high temperature matter has been discussed for a long time. The scalar quark condensate, which due to the spontaneous breaking of the chiral symmetry develops a non-zero value in vacuum, is predicted to decrease with increasing density and temperature [1, 2, 3, 4, 5, 6]. Linking the in-medium modification of the hadron masses directly to the change of the two-quark scalar condensate, one would expect a similar decrease of the hadron masses with increasing density and temperature. The prediction of a dropping of the hadron masses in the nuclear medium driven by the scalar condensate has been formulated in [7] and stimulated the search for signatures of modified hadron properties in different kinds of nuclear reactions. Heavy Ion Collision (HIC) experiments, offering the unique opportunity to investigate the hadron properties at supra-normal densities and high temperature, as well as experiments with elementary projectiles on normal nuclei, due to the expectation that signatures should be already visible at normal matter density, have been involved. Among the hadrons, the attention has particularly focused on the light vector mesons, since their direct decay to a dilepton pair offers the possibility to “detect” the in-medium properties of hadrons using a clean probe. Dileptons, and in general electromagnetic probes, have the advantage that, once produced from the vector meson decay, they leave the reaction zone essentially undistorted by final state interactions and hence carry an undistorted signal of the properties owned by the vector meson in the moment of its decay.

On the other side, the in-medium modification of the spectral properties of the vector mesons has been extensively investigated also in the context of hadronic models [8, 9, 10, 11, 12, 13, 14, 15, 16, 17, 18, 19]. Many-body correlations typically induce a significant reduction of the meson life time and thus its melting in the nuclear environment.

The connection between hadron properties and their in-medium modification on the one hand and the in-medium change of the non-perturbative quark and gluon condensates on the

other hand is not trivial. One approach which aims to establish this connection is the QCD sum rule approach. An early analysis based on QCD sum rules performed by Hatsuda and Lee [20] had supported the conjecture of a dropping of the vector meson masses at finite density made by Brown and Rho [7]. However, the analysis had been performed making the strong assumption that the vector mesons would have zero width in medium. Later it was pointed out [21] that the sum rule approach has only limited predictive power with respect to the specific properties of the hadrons, like their masses or their widths, since it constrains certain integrals over the spectral distribution of the hadron and does not directly constrain the hadron mass and the hadron width separately. Rather, it gives a possible “surface” of allowed values in the mass/width plane. In the case of the ρ meson, for example, a sum rule analysis predicts that in nuclear matter the meson spectral strength is shifted to lower invariant masses. However, it is not possible to deduce only from the sum rule analysis whether the additional strength is due to a dropping of the mass or to a collisional broadening.

The first experimental observations of the modification of the ρ meson spectral properties in hot and dense matter trace back to the nineties, when dilepton spectra in ultrarelativistic heavy ion collisions have been measured by the CERES [22] and HELIOS [23] collaborations at CERN. The dilepton spectra showed a considerable enhancement over the hadronic cocktail in the region below the vector meson peak, which suggested the general moving of spectral strength downward to smaller invariant masses. Whether the presence of spectral strength at lower masses was connected to a dropping of the masses, as predicted in [7, 20], or to a spreading of the spectral function driven by the collisional broadening, as expected from hadronic model calculations [24], could not be clarified by the comparison with the experimental data, mainly due to the low mass resolution of the data in the region of the vector meson peak. Recent higher resolution measurements of dilepton spectra in heavy ion collisions performed by the NA60 collaboration [25] and the CERES collaboration [26] seem to favor an in-medium broadening of the ρ meson over a mass shift.

A second set of heavy ion experiments have been performed at lower laboratory energies (1.0 AGeV) by the DLS collaboration at BEVALAC [27, 28]. Also in this case the low mass region of the dilepton spectra was underestimated by transport calculations, in contrast to similar measurements for the $p+p$ and $p+d$ systems. As opposed to the ultrarelativistic case, the situation did not improve when the in-medium spectral functions or the dropping mass scenario were taken into account [29, 30, 31]. However, in this energy regime which probes the high density/low temperature phase the situation is going to be improved significantly with the already existing and forthcoming measurements of the HADES collaboration at GSI [32, 33].

The aim of this thesis is to perform a systematic study of the in-medium properties of the vector mesons and their influence on dilepton emission in heavy ion collisions at intermediate energies. For this purpose we proceed as follows: first we determine the ρ and ω meson spectral functions in nuclear matter. The self energy that the ρ and ω mesons acquire in nuclear matter due to the excitation of resonance-hole loops is calculated within the extended Vector Meson Dominance (eVMD) model developed in [34]. Possible non-resonant contributions to the vector meson self energies are discussed as well. Then we turn to the analysis of dilepton production in HICs and investigate to which extent different hypotheses

for the in-medium properties of the ρ and ω mesons affect the shape of the dilepton spectra. The production of lepton pairs in intermediate energy heavy ion collisions is described with the Tübingen Relativistic Quantum Molecular Dynamics (RQMD) transport code combined with the eVMD model. In a first step, in-medium modifications of the vector meson properties are introduced either in terms of a dropping mass or in terms of a collisional broadening. Subsequently, the vector meson spectral functions determined within eVMD are included in the calculation of the dilepton spectra. Hence, dilepton production as well as in-medium vector meson properties will be described with the same parameters. The effect the different in-medium scenarios have on the dilepton production rate will be analyzed. Finally, all theoretical calculations are compared with the available HADES data for the C+C reaction at 2 AGeV.

The thesis is organized as follows: in Chapter 2 we briefly summarize the main outcome of different experiments performed in order to study the in-medium modifications of the vector meson properties. Results from heavy ion collision experiments as well as from meson photoproduction and proton induced experiments are reported. This short chapter is rather a prelude aimed to display the status of our present understanding of the problem that is studied in the rest of this work.

In Chapter 3 the main sources of dilepton production in heavy ion collisions at intermediate energies are listed and the theoretical expressions for their dilepton rate are given. In this Chapter, the eVMD model is introduced.

Chapter 4 is devoted to the calculation of the in-medium spectral functions of the ρ and ω mesons within the eVMD model and to the discussion of the effect of possible non-resonant contributions to the vector meson self-energies.

The general features of the Quantum Molecular Dynamics transport model as well as the particular realization of the Tübingen RQMD model are discussed in Chapter 5. The theoretical description of dilepton production within the combined QMD and the eVMD models and the implementation of the in-medium vector meson spectral functions in the dilepton spectra calculations are thereby described. Dilepton spectra are calculated in vacuum and medium using the various in-medium scenarios and compared to the HADES data.

Conclusions and a summary are finally given in Chapter 6.

Chapter 2

Dileptons and vector mesons: Experimental status

2.1 Ultrarelativistic HICs

First dilepton spectra have been measured in the 1990s at CERN SPS by the CERES [22] and HELIOS-3 [23] Collaborations. The CERES Collaboration observed that central nucleus-nucleus (A - A) collisions exhibited a strong enhancement of low mass dilepton production as compared to the proton-nucleus (p - A). Whereas the p - A data could be well reproduced by the so-called hadronic “cocktail” (final state hadron decays with known abundances), the latter strongly underestimated the A - A spectra. A similar enhancement of the low-mass dileptons over the cocktail was also observed by the HELIOS-3 Collaboration.

Since in A - A collisions at SPS energies several hundreds of pions are produced, one possible argument was that the observed increase of dilepton pairs over the cocktail could be attributed to the $\pi^+\pi^- \rightarrow \ell^+\ell^-$ annihilation channel. Therefore, many theoretical groups included this channel in their calculation. Nevertheless it was found that, when using vacuum meson properties, the theoretical results were still in disagreement with the data. All of them underestimated the experimental mass spectra in the mass region 0.3 – 0.6 GeV. It was suggested that vector meson in-medium properties could be responsible for the observed enhancement. For the in-medium vector mesons both the “dropping mass” scenario, conjecturing a direct link between hadron masses and the quark condensate and thus to the restoration of chiral symmetry, and the “melting” scenario, as the effect of a dressing of the mesons induced in medium by many-body correlations, were tested. However, it was found that *both* scenarios, despite the different physics they suggest, could describe the observed phenomena equally well.

A first clarifying answer to this ambiguous situation came in 2006 thanks to the measurement of the dimuon spectrum in In-In collisions at 158 AGeV performed by the NA60 Collaboration [25]. The spectrum, obtained with an unprecedented mass resolution, results to be a mirror of the in-medium ρ meson spectral function under the conditions of ultrarelativistic heavy ion collisions. The NA60 data seem to rule out a naive dropping mass scenario but support the picture of modified vector meson spectral functions as predicted by hadronic many-body theory [35, 36]. At a first glance, the comparison of the NA60 data to thermal

fireball calculations using in-medium electromagnetic rates required a normalization of the integrals of the theoretical spectra to the data in the mass interval $M < 0.9$ GeV [25]. The underlying problem was that in the calculations the absolute yields were overestimated by $\sim 20\%$, although the shape of the predicted in-medium ρ spectral function described the experimental spectra quite well [36]. The discrepancy could be solved by an increase of the transverse fireball expansion which reduces the fireball lifetime and consequently the ρ contribution. Moreover, for a correct determination of the absolute yields, other sources which contribute to the dilepton spectrum besides the ρ meson decays should be taken into account. It results that the addition of QGP emission, correlated charm decays and 4π contributions leads to a satisfactory overall description of the experimental data. The further inclusion of in-medium ω decays improves the agreement between data and theory in the mass region $M = 0.7 - 0.8$ GeV [36].

Recently, the CERES Collaboration has reported on a new measurement of e^+e^- production in central Pb+Au collisions at 158 AGeV performed with the upgraded CERES experiment at CERN-SPS [26]. The new set of data presents an improved mass resolution in the resonance region with respect to the previous set [37]. In comparison to model calculations the data favour models including a substantial in-medium broadening of the ρ meson spectral function over an in-medium dropping vector meson mass.

2.2 HICs at intermediate energies

At lower bombarding energies first dilepton spectra have been measured by the DLS collaboration at BEVELAC [27, 28]. Theoretical calculations based on transport approaches, although able to describe reasonably well the $p+p$ data for 1 – 5 GeV incident energies, strongly underestimated the dilepton yield of the 1 AGeV C+C and Ca+Ca reactions in the invariant mass region $0.15 \leq M_{ee} \leq 0.65$ GeV. As opposed to the case of ultrarelativistic heavy ion collisions, neither the inclusion of in-medium spectral functions for the vector mesons nor the insertion of a dropping of the vector meson mass at finite density according to the Brown-Rho scaling law could solve the discrepancy between the theoretical calculations and the experimental data [29, 30]. This led to the so called DLS puzzle. Other scenarios like an eventual in-medium modification of the η mass have been excluded as a possible resolution of this puzzle. Decoherence effects have been proved to be partially successful in explaining the difference between the DLS data and the theoretical calculations [38]. In lack of a clear theoretical explanation of the DLS data for dilepton production in 1-2 AGeV heavy ion collisions, the high-precision dilepton measurements with the HADES detector at GSI play a crucial role in order to shed light on this puzzling situation.

The dilepton measurements of the DLS Collaboration in C+C and Ca+Ca at 1 AGeV [27] suffered from too low mass resolution in the vicinity of the ω peak in order to make precise statements on the ω in-medium width. However, there is no doubt that the explanation of the DLS data requires a substantial broadening of the ω spectral function. The analysis of [38] showed that the DLS data are compatible with a rather large ω width of $\Gamma_{\omega}^{tot} \sim 150 \div 300$ MeV. The first data from HADES [33] will be analyzed in Chapter 5.

2.3 Reactions with elementary projectiles on nuclei

Complementary to the heavy ion experiments are the γ -nucleus and p -nucleus reactions. Experimental constraints on the in-medium ω and ρ spectral function can presently be derived from the CBELSA/TAPS ($\gamma+A$) experiments [39], the $p+A$ measurements at KEK [40, 41] and the recent $\gamma+A$ measurements from the CLAS Collaboration [42] at JLab.

CBELSA/TAPS investigated in-medium modifications of the ω meson by studying the $\omega \rightarrow \pi^0\gamma$ decay mode via the reaction $\gamma+A \rightarrow \omega+X \rightarrow \pi^0\gamma+X'$. The results obtained for a Nb nucleus have been compared to measurements on a LH₂ target, which were taken as a reference. To partially reduce the number of ω decays occurring outside the target nucleus a kinematic cut on the 3-momentum of the ω meson $|\mathbf{p}_\omega| < 0.5$ GeV has been applied. But still only a fraction of the ω mesons decays inside the medium. The $\pi^0\gamma$ invariant mass for the Nb data present a significant excess on the low-mass side of the ω peak not seen in the LH₂ data. The still present vacuum decays have been eliminated by matching the right hand part of the Nb invariant mass spectrum to the LH₂ data and by subtracting the two spectra from each other. The different assumptions for the subtraction of decays of the ω mesons in vacuum are reflected in the systematic uncertainty. Further details can be found in Ref. [39]. The CBELSA/TAPS collaboration reports an in-medium mass of $M_{\text{medium}} = [722_{-2}^{+2}(\text{stat})_{-5}^{+35}(\text{syst})]$ MeV at an estimated average nuclear density of $0.6\rho_0$, consistent with a scaling of the ω mass by $m = m_0(1 - 0.14\rho/\rho_0)$. The width is found to be $\Gamma = 55$ MeV and is dominated by the experimental resolution [39].

At KEK the E325 collaboration measured the invariant mass spectra of e^+e^- pairs produced in proton-induced nuclear reactions. They investigated possible modification of the spectral shapes of the vector mesons in nuclear matter by studying the direct $\rho, \omega, \phi \rightarrow e^+e^-$ decay modes via the reaction $p+A \rightarrow V+X \rightarrow e^+e^-+X'$ ($V = \rho, \omega, \phi$) using a 12 GeV proton beam on a carbon and a copper target [41]. The invariant mass spectrum was fitted with the combinatorial background and known hadronic sources, $\rho \rightarrow e^+e^-$, $\omega \rightarrow e^+e^-$, $\phi \rightarrow e^+e^-$, $\eta \rightarrow e^+e^-\gamma$ and $\omega \rightarrow e^+e^-\pi^0$, evaluating the combinatorial background with the event-mixing method. A significant excess was found on the low-mass side of the ω peak, whereas the high-mass tail of the ω could be reproduced with the expected shapes. Later, the effect of a possible in-medium modification of the vector meson masses was investigated. We briefly summarize the procedure and refer to [41] for further details. The spectral shapes of the ρ and ω mesons were modified by determining the pole mass with the formula $m_V^*/m_V = 1 - \alpha\rho/\rho_0$ according to the density at the decay point.¹ Fitting again the entire mass region with the same procedure as before, the value $\alpha = 0.092 \pm 0.002$ was extracted.

Finally, the CLAS collaboration at JLab measured the invariant mass spectra of e^+e^- pairs from photoproduction reactions with the purpose to study possible in-medium modification of the vector meson properties from the e^+e^- originating from the $\rho, \omega, \phi \rightarrow e^+e^-$ decays. The reaction studied is $\gamma+A \rightarrow V+X \rightarrow e^+e^-+X'$ ($V = \rho, \omega, \phi$). The measurements have been carried out at photon energies from $E_\gamma = 0.6 - 3.8$ GeV on light (C) and heavier (Fe) targets [42]. The experiment found no signatures for a mass shift but a collisional broadening of the ρ meson. In terms of a $m_\rho^* = m_\rho(1 - \alpha\rho_B/\rho_0)$ scaling law, the extracted value

¹For details on the determination of the decay point we refer to [41].

Experiment	ρ		ω	
	α	Γ [MeV]	α	Γ [MeV]
TAPS			0.14	55
E325	$0.092^{\pm 0.002}$	Γ^{vac}	$0.092^{\pm 0.002}$	Γ^{vac}
CLAS	$0.02^{\pm 0.02}$	$176.4^{\pm 9.5}$ (C), $217.7^{\pm 14.5}$ (Fe)		

Table 2.1: Values for the total vector meson width and for the parameter α entering in the $m_V^* = m_V(1 - \alpha\rho_B/\rho_0)$ scaling law for the vector meson mass extracted by different experiments.

for the parameter α is 0.02 ± 0.02 , i.e. consistent with zero. The values obtained for the ρ meson width are 176.4 ± 9.5 MeV for the carbon and 217.7 ± 14.5 MeV for the iron target.

The outcome of the mentioned experiments is summarized in Table 2.1.

Chapter 3

Elementary sources for dilepton production

At energies of a few AGeV the main sources for dilepton production are the decay of light mesons and the decay of nucleon resonances.

Phenomenological expressions for the dilepton decay rates of different light mesons have been derived in Ref. [43]. There various decay modes of the vector mesons ρ , ω , and $\phi(1020)$ ($= V$), of the pseudoscalar mesons π , η , η' ($= P$), and of the scalar mesons $f_0(980)$ and $a_0(980)$ ($= S$) have been analyzed: direct decays modes $V \rightarrow \ell^+\ell^-$, Dalitz decays of pseudoscalar mesons $P \rightarrow \gamma\ell^+\ell^-$ and scalar mesons $S \rightarrow \gamma\ell^+\ell^-$, Dalitz decays with one meson in the final states $V \rightarrow P\ell^+\ell^-$ and $P \rightarrow V\ell^+\ell^-$ and decays to four-body final states $V \rightarrow PP\ell^+\ell^-$, $P \rightarrow PP\ell^+\ell^-$, and $S \rightarrow PP\ell^+\ell^-$. The analysis showed that in the low mass region of the dilepton spectrum (up to the η meson mass) the two dominant mesonic contributions are the Dalitz decays of the π^0 and η mesons. On the other side, the direct decay of the vector mesons dominates the region around the vector meson peak.

Relativistic phenomenological expressions for the dilepton decay rates of nucleon resonances with arbitrary spin and parity have been derived in Ref. [34]. There the dilepton decay rates of the nucleon resonances with masses below 2 GeV have been estimated using the eVMD model for the transition form factors.

In this Chapter we briefly summarize the results of [43] and [34]. They constitute the basic ground for the investigations and developments presented in the following chapters of this work. Regarding [43], we limit ourselves to report the theoretical expressions for the dilepton rates of the mesonic decay modes which give the dominant contributions. Notice that the $\pi^0 \rightarrow \gamma\ell^+\ell^-$ and $\eta \rightarrow \gamma\ell^+\ell^-$ channels are explicitly included in the applications to dilepton production in HICs performed later on in this work. The direct decay of vector mesons, on the other side, is not explicitly included due to the adoption of a resonance model.¹ Nevertheless, for the sake of completeness, we also report the expressions for the vector meson direct decays.

¹At this stage of our treatment, this statement may sound unclear. It will become clear after the resonance model has been introduced and discussed in Chapter 4.

3.1 Dilepton decay rates of light pseudoscalar mesons

This Section is devoted to the discussion of meson decays $P \rightarrow \gamma \ell^+ \ell^-$ where $P = \pi^0$ and η . The corresponding diagram is shown in Fig. 3.1. These decays are the dominant $e^+ e^-$ modes

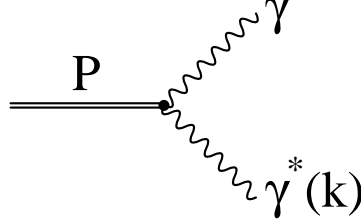


Figure 3.1: Decay of a pseudoscalar meson into a photon and a virtual photon.

for π^0 - and η -mesons and are related to the experimentally measured two photon decays. The uncertainties in the estimates originate only from the poorly known transition form factors in the time-like region. The $\eta\gamma\gamma^*$ transition form factor is in reasonable agreement with the one-pole Vector Meson Dominance (VMD) model predictions [44]. The one-pole VMD approximation for the $P\gamma\gamma^*$ transition form factors is in agreement with the quark counting rules which predict for these form factors a $\sim 1/t$ asymptotics [45]. However, before addressing in particular the $P \rightarrow \gamma \ell^+ \ell^-$ decay, we would like to show in a more extended way the derivation performed in [43] of some useful kinematic relations which simplify the calculations of the decay rates to final states with a dilepton pair. These relations will be often used in the course of this work.

3.1.1 Relation between the decays $M \rightarrow M'\gamma^*$ and $M \rightarrow M'\ell^+\ell^-$

Let us consider decays $M \rightarrow M'\ell^+\ell^-$ where M is a meson, M' is a photon, a meson, or two mesons, and $\ell^+\ell^-$ is an electron-positron or muon-antimuon pair. The results which follow are valid, however, for arbitrary states M' . The decay $M \rightarrow M'\ell^+\ell^-$ proceeds through two steps: $M \rightarrow M'\gamma^*$ and $\gamma^* \rightarrow \ell^+\ell^-$, where γ^* is a virtual photon whose mass M is equal to the invariant mass of the dilepton pair.

The matrix element of the physical process $M \rightarrow M'\gamma$ for a real photon γ has the form

$$\mathcal{M} = \mathcal{M}_\mu \varepsilon_\mu^*(k) \quad (3.1)$$

where $\varepsilon_\mu(k)$ is a photon polarization vector. The matrix element \mathcal{M}_μ is defined also at $k^2 = M^2 \neq 0$ for virtual photons γ^* . As a consequence of the gauge invariance, it is transverse with respect to the photon momentum

$$\mathcal{M}_\mu k_\mu = 0. \quad (3.2)$$

The decay rate $M \rightarrow M'\gamma^*$ can formally be calculated as

$$d\Gamma(M \rightarrow M'\gamma^*) = \frac{1}{2\sqrt{s}} \sum_f \overline{\mathcal{M}_\mu \mathcal{M}_\nu^*} (-g_{\mu\nu}) \frac{(2\pi)^4}{(2\pi)^{3n+3}} d\Phi_{n+1} \quad (3.3)$$

where \sqrt{s} is the mass of the decaying meson and n is the number of particles in the state M' . The phase space in Eq. (3.3) is defined in the usual way

$$d\Phi_k(\sqrt{s}, m_1, \dots, m_k) = \prod_{i=1}^k \frac{d\mathbf{p}_i}{2E_i} \delta^4(P - \sum_{i=1}^k p_i). \quad (3.4)$$

Here, P is the four-momentum of the meson M , $P^2 = s$, and p_i are the momenta of the particles in the final state, including the virtual photon γ^* . In Eq. (3.3), the summation over the final states and averaging over the initial states of the decaying meson is performed. The limit $M^2 \rightarrow 0$ gives the decay rate of the physical process $M \rightarrow M'\gamma$.

The $M \rightarrow M'\ell^+\ell^-$ decay rate is given by

$$d\Gamma(M \rightarrow M'\ell^+\ell^-) = \frac{1}{2\sqrt{s}} \sum_f \overline{\mathcal{M}_\mu \mathcal{M}_\nu^*} j_\mu j_\nu^* \frac{1}{M^4} \frac{(2\pi)^4}{(2\pi)^{3n+6}} d\Phi_{n+2} \quad (3.5)$$

where j_μ is the lepton current. The term $1/M^4$ comes from the photon propagator, and $d\Phi_{n+2}$ is the phase space of n particles in the state M' and of the $\ell^+\ell^-$ pair.

The value $\Gamma(M \rightarrow M'\ell^+\ell^-)$ can be related to the decay rates $\Gamma(M \rightarrow M'\gamma^*)$ and $\Gamma(\gamma^* \rightarrow \ell^+\ell^-)$. The width of the virtual photon can be formally evaluated as the width of an analogous massive vector particle. The direct calculation, performed in detail in Appendix B, gives

$$\boxed{M\Gamma(\gamma^* \rightarrow \ell^+\ell^-) = \frac{\alpha}{3}(M^2 + 2m_\ell^2) \sqrt{1 - \frac{4m_\ell^2}{M^2}}} \quad (3.6)$$

where m_ℓ is the lepton mass and α is the fine-structure constant. The expression for the product of two dilepton currents, summed up over the final states of the $\ell^+\ell^-$ pair, has the form

$$\sum_f j_\mu j_\nu^* = \frac{16\pi\alpha}{3}(M^2 + 2m_\ell^2) \left(-g_{\mu\nu} + \frac{k_\mu k_\nu}{M^2}\right) \quad (3.7)$$

where k is the total momentum of the pair. Factorizing the n -body invariant phase space,²

$$d\Phi_k(\sqrt{s}, m_1, \dots, m_k) = d\Phi_{k-1}(\sqrt{s}, m_1, \dots, m_{k-2}, M) dM^2 \Phi_2(M, m_{k-1}, m_k), \quad (3.9)$$

one obtains from Eqs. (3.3), (3.5), and (3.6) with the help of Eqs. (3.7) and (3.9) the following expression

$$\boxed{d\Gamma(M \rightarrow M'\ell^+\ell^-) = d\Gamma(M \rightarrow M'\gamma^*) M\Gamma(\gamma^* \rightarrow \ell^+\ell^-) \frac{dM^2}{\pi M^4}.} \quad (3.10)$$

²Eq. (3.9) can be proved by inserting the unity decomposition

$$1 = \int d^4q dM^2 \delta(q^2 - M^2) \delta^4(q - p_{k-1} - p_k) \quad (3.8)$$

into Eq. (3.4)

The factor $dM^2/(\pi M^4)$ has the form of a properly normalized Breit-Wigner distribution for a zero-mass resonance.

The two-body phase space in Eq. (3.9) has the form

$$\Phi_2(\sqrt{s}, m_1, m_2) = \frac{\pi p^*(\sqrt{s}, m_1, m_2)}{\sqrt{s}} \quad (3.11)$$

where

$$p^*(\sqrt{s}, m_1, m_2) = \frac{\sqrt{(s - (m_1 + m_2)^2)(s - (m_1 - m_2)^2)}}{2\sqrt{s}} \quad (3.12)$$

is the momentum of the particles 1 and 2 in the c.m. frame.

It is clear from the factorization shown in Eq. (3.10) that in order to derive expressions for the decay rates $M \rightarrow M' \ell^+ \ell^-$ with dileptons in the final state, what one has to determine is the matrix element of the processes $M \rightarrow M' \gamma^*$. Once this matrix element has been calculated, the result for decay rates $M \rightarrow M' \ell^+ \ell^-$ follows automatically. One has just to substitute in Eq. (3.10) the expression for $M\Gamma(\gamma^* \rightarrow \ell^+ \ell^-)$ given by Eq. (3.6). Keeping this in mind, we consider now the processes $\pi^0 \rightarrow \gamma e^+ e^-$ and $\eta \rightarrow \gamma \ell^+ \ell^-$, which give important contributions to the dilepton spectra in HICs.

3.1.2 Decay modes $\pi^0 \rightarrow \gamma e^+ e^-$ and $\eta \rightarrow \gamma \ell^+ \ell^-$

The effective vertex for the $P \rightarrow \gamma\gamma$ decay has the form

$$\delta\mathcal{L}_{P\gamma\gamma} = f_{P\gamma\gamma} \epsilon_{\tau\sigma\mu\nu} \partial_\sigma A_\tau \partial_\nu A_\mu P \quad (3.13)$$

where $P = \pi^0, \eta$ and A_μ is the photon field. The matrix element for the decay $P \rightarrow \gamma\gamma^*$ with a virtual photon γ^* has the form

$$\mathcal{M} = -i f_{P\gamma\gamma} F_{P\gamma\gamma}(M^2) \epsilon_{\tau\sigma\mu\nu} k_\tau \epsilon_\sigma^*(k) k_{1\mu} \epsilon_\nu^*(k_1) \quad (3.14)$$

where k is the virtual photon momentum ($k^2 = M^2$), k_1 is the real photon momentum ($k_1^2 = 0$), and $F_{P\gamma\gamma}(t)$ is the transition form factor $P\gamma\gamma^*$. The comparison of the $P \rightarrow \gamma \ell^+ \ell^-$ decay width with the decay width of a physical process $P \rightarrow \gamma\gamma$ allows to write [44]

$$\boxed{\frac{d\Gamma(P \rightarrow \gamma \ell^+ \ell^-)}{\Gamma(P \rightarrow \gamma\gamma)} = 2 \left(\frac{p^*(\sqrt{s}, 0, M)}{p^*(\sqrt{s}, 0, 0)} \right)^3 |F_{P\gamma\gamma}(M^2)|^2 M\Gamma(\gamma^* \rightarrow \ell^+ \ell^-) \frac{dM^2}{\pi M^4}} \quad (3.15)$$

where $\sqrt{s} = \mu_P$ is the pseudoscalar meson mass.

The form of Eq. (3.15) can be understood with the following considerations:

- the term $M\Gamma(\gamma^* \rightarrow \ell^+ \ell^-) dM^2/(\pi M^4)$ originates from the decomposition (3.10) and its value is given by Eq. (3.6);

- the factor 2 occurs due the identity of photons in the decay $P \rightarrow \gamma\gamma$;
- the product of the cubic term and the absolute square of the form factor gives the ratio between the squares of the matrix element (3.14) at $k^2 = M^2$ and $k^2 = 0$, multiplied by the ratio between the two-particle phase spaces. More precisely one has³

$$\frac{|\mathcal{M}|_{k^2=M^2}^2}{|\mathcal{M}|_{k^2=0}^2} \sim \left(\frac{p^*(\sqrt{s}, 0, M)}{p^*(\sqrt{s}, 0, 0)} \right)^2 |F_{P\gamma\gamma}(M^2)|^2 \quad (3.16)$$

and

$$\frac{\Phi_2(\sqrt{s}, 0, M)}{\Phi_2(\sqrt{s}, 0, 0)} = \frac{p^*(\sqrt{s}, 0, M)}{p^*(\sqrt{s}, 0, 0)}. \quad (3.17)$$

The quark counting rules [45] imply that the form factor $F_{P\gamma\gamma}(t)$ behaves as $\sim 1/t$ at $t \rightarrow \infty$. The experimental data are described reasonably well by the monopole formula

$$F_{P\gamma\gamma}(t) = \frac{\Lambda_P^2}{\Lambda_P^2 - t} \quad (3.18)$$

with $\Lambda_P = 0.75 \pm 0.03$ and 0.77 ± 0.04 , respectively, for the π^0 - and η -mesons [46]. The formula reproduces the asymptotics required by quark counting rules. Such a monopole fit can naturally be interpreted in terms of the vector meson dominance. The values of the Λ_P 's are close to the ρ and ω meson masses.

3.2 Decays of the ρ -, ω -, and ϕ -mesons to $\ell^+\ell^-$ pairs

The diagram for the $V \rightarrow \ell^+\ell^-$ decays with $V = \rho, \omega, \text{ and } \phi$ is shown in Fig. 3.2. In terms

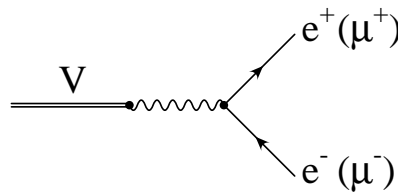


Figure 3.2: Direct decays of vector mesons into electron-positron and muon-antimuon pairs.

of the vector meson fields V_μ the electromagnetic current has the form [47]

$$j_\mu = -e \sum_V \frac{m_V^2}{g_V} V_\mu \quad (3.19)$$

³In Eq. (3.16) we make use of $F_{P\gamma\gamma}(0) = 1$.

where m_V are the vector meson masses and $e = -|e|$ is the electron charge. The $SU(3)$ predictions for the coupling constants, $g_\rho : g_\omega : g_\phi = 1 : 3 : \frac{-3}{\sqrt{2}}$, are in good agreement with the ratios between the values $g_\rho = 5.03$, $g_\omega = 17.1$, and $g_\phi = -12.9$ extracted from the e^+e^- decay widths of the ρ , ω and ϕ mesons with the use of the known expression

$$\Gamma(V \rightarrow \ell^+\ell^-) = \frac{8\pi\alpha^2}{3g_V^2} \left(1 + 2\frac{m_\ell^2}{m_V^2}\right) p^*(m_V, m_\ell, m_\ell), \quad (3.20)$$

with p^* defined in Eq. (3.12).

3.3 Dilepton decay rates of nucleon resonances

This Section is devoted to the description of decays $R \rightarrow N\ell^+\ell^-$ with R being a resonance with arbitrary spin and parity and N a nucleon. The corresponding diagram is shown in Fig. 3.3. We proceed as follows: in Section 3.3.1 the general expression for the $R \rightarrow N\ell^+\ell^-$

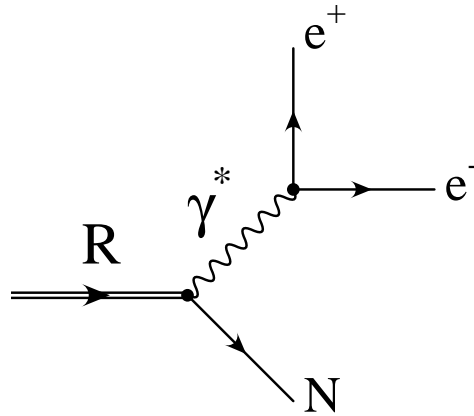


Figure 3.3: Decay of a nucleon resonance to a nucleon and a dilepton pair.

decay width in terms of helicity amplitudes is provided. The helicity amplitudes are then written in terms of three scalar functions called covariant form factors. An explicit expression for the covariant form factors is given in Section 3.3.2 within the vector meson dominance model. After a discussion about the shortcomings of the naive vector meson dominance model the extended vector meson dominance model is introduced. Finally, values for the resonance decay widths determined within the eVMD model are given.

3.3.1 The $\gamma^*N \rightarrow R$ helicity amplitudes

Let us start with the electromagnetic transition current between the nucleon and a nucleon with spin J resonance which has the form

$$J_\mu(p_*, \lambda_*, p, \lambda) = e\bar{u}_{\beta_1 \dots \beta_l}(p_*, \lambda_*) \Gamma_{\beta_1 \dots \beta_l \mu}^{(\pm)} u(p, \lambda) \quad (3.21)$$

where m_* and m are masses, p_* and p are momenta, λ_* and λ are helicities of the resonance and the nucleon, $e = -\sqrt{4\pi\alpha}$ is the electron charge, $\alpha = 1/137$. In the resonance rest frame, $p_* = (m_*, 0, 0, 0)$, $p = (E, 0, 0, -k)$. The spinor $u_{\beta_1 \dots \beta_l}(p_*, \lambda_*)$ is the generalized Rarita-Schwinger spinor that describes fermions with $J = l + \frac{1}{2} \geq \frac{3}{2}$. It is symmetric with respect to the indices $\beta_1 \dots \beta_l$ and traceless. The spinors are normalized by

$$\begin{aligned} \bar{u}(p, \lambda)u(p, \lambda) &= 2m, \\ (-)^l \bar{u}_{\beta_1 \dots \beta_l}(p_*, \lambda_*)u_{\beta_1 \dots \beta_l}(p_*, \lambda_*) &= 2m_*. \end{aligned} \quad (3.22)$$

The matrices $\Gamma_{\beta_1 \dots \beta_l \mu}^{(\pm)}$ stand for the normal- and abnormal parity resonances, $J^P = \frac{1}{2}^-, \frac{3}{2}^+, \frac{5}{2}^-, \dots$ (the upper sign) and $J^P = \frac{1}{2}^+, \frac{3}{2}^-, \frac{5}{2}^+, \dots$ (the lower sign). The $\gamma^*N \rightarrow R$ helicity amplitudes are given by

$$\begin{aligned} \langle J\lambda_* | T | \lambda\lambda_\gamma \rangle &= -J_\mu(p_*, \lambda_*, p, \lambda) \varepsilon_\mu^{(\lambda_\gamma)}(q) = \\ &= -e \bar{u}_{\beta_1 \dots \beta_l}(p_*, \lambda_*) \Gamma_{\beta_1 \dots \beta_l \mu}^{(\pm)} u(p, \lambda) \varepsilon_\mu^{(\lambda_\gamma)}(q). \end{aligned} \quad (3.23)$$

Here $\varepsilon_\mu^{(\lambda_\gamma)}(q)$ are the photon polarization vectors which have the form

$$\begin{aligned} \varepsilon_\mu^{(\pm 1)}(q) &= \frac{1}{\sqrt{2}}(0, \mp 1, -i, 0), \\ \varepsilon_\mu^{(0)}(q) &= \frac{1}{M}(k, 0, 0, \omega), \end{aligned} \quad (3.24)$$

where $q = p_* - p = (\omega, 0, 0, k)$ is the momentum transfer with $q^2 = M^2$. These vectors are transversal, $q_\mu \varepsilon_\mu^{(\lambda)}(q) = 0$, and normalized by

$$\varepsilon_\mu^{(\lambda)}(q)^* \varepsilon_\mu^{(\lambda')}(q) = -\delta_{\lambda\lambda'}. \quad (3.25)$$

The nucleon and photon energies and the photon momentum are

$$E = \frac{m_*^2 + m^2 - M^2}{2m_*}, \quad (3.26)$$

$$\omega = \frac{m_*^2 + M^2 - m^2}{2m_*}, \quad (3.27)$$

$$k = p^*(m_*, m, M), \quad (3.28)$$

with p^* defined in Eq. (3.12). In terms of the helicity amplitudes (3.23) the $R \rightarrow N\gamma^*$ decay width reads:

$$\Gamma(R \rightarrow N\gamma^*) = \frac{k}{8\pi m_*^2} \frac{1}{2J+1} \sum_{\lambda\lambda_\gamma} | \langle \lambda\lambda_\gamma | T | J\lambda_* \rangle |^2. \quad (3.29)$$

There exist six helicity amplitudes, three with positive λ_* 's and three with negative λ_* 's. The P -invariance of the electromagnetic interactions gives a symmetry relation for the amplitudes with opposite signs of the helicities:

$$\langle J - \lambda_* | T | -\lambda - \lambda_\gamma \rangle = \mp \langle J\lambda_* | T | \lambda\lambda_\gamma \rangle. \quad (3.30)$$

Using this property of the helicity amplitudes one obtains the $R \rightarrow N\gamma^*$ decay width in terms of the three helicity amplitudes:

$$\Gamma(R \rightarrow N\gamma^*) = \frac{k}{8\pi m_*^2} \frac{2}{2J+1} \sum_{\lambda_* = -\lambda + \lambda_\gamma > 0} |\langle \lambda \lambda_\gamma | T | J \lambda_* \rangle|^2. \quad (3.31)$$

Once the width $\Gamma(R \rightarrow N\gamma^*)$ is known, the factorization prescription described in Section 3.1.1 can be used to find the dilepton rate

$$d\Gamma(N^* \rightarrow Ne^+e^-) = \Gamma(N^* \rightarrow N\gamma^*) M\Gamma(\gamma^* \rightarrow e^+e^-) \frac{dM^2}{\pi M^4}, \quad (3.32)$$

where $M\Gamma(\gamma^* \rightarrow e^+e^-)$ is the decay width of a virtual photon γ^* into the dilepton pair with invariant mass M , given by Eq. (3.6)

The main notations and kinematic relations have thus been specified. Our main concern is now the determination of the helicity amplitudes $\langle \lambda \lambda_\gamma | T | J \lambda_* \rangle$ of Eq. (3.31). In the expression (3.23) for the helicity amplitudes the unknown quantities are the $\gamma^* N \rightarrow R$ vertices $\Gamma_{\beta_1 \dots \beta_{l\mu}}^{(\pm)}$. To discuss the decomposition of the vertices it is appropriate to separate the case of resonances with spin $J \geq \frac{3}{2}$ from the case of resonances with spin $J = \frac{1}{2}$.

SPIN $J \geq \frac{3}{2}$ RESONANCES. As we have already mentioned, resonances with arbitrary spin have three independent helicity amplitudes in the $\gamma^* N \rightarrow R$ transitions. This means that there are three independent scalar functions to fix the vertices. These functions arise automatically from the decomposition of the $RN\gamma^*$ vertex in terms of covariants. The procedure is analogous to the decomposition of the $pp\gamma^*$ vertex in the electron-proton elastic scattering. As shown in many textbooks (see e.g. [48]), the $pp\gamma^*$ can be expressed in terms of the Dirac and Pauli form factors, $F_1(q^2)$ and $F_2(q^2)$, as schematically shown in Fig. 3.4.

Figure 3.4: Decomposition of the on-shell electromagnetic vertex for a Dirac fermion in terms of the Dirac and Pauli form factors $F_1(q^2)$ and $F_2(q^2)$. If the fermion is a strongly interacting particle such as the proton, the form factors reflect the non-local structure that results from the strong interaction.

In our case, the general $RN\gamma^*$ vertex $\Gamma_{\beta_1 \dots \beta_{l\mu}}^{(\pm)}$ can be decomposed over the Lorentz vectors and the Dirac gamma matrices [49, 50, 51, 34] by writing it first as⁴

$$\Gamma_{\beta_1 \dots \beta_{l\mu}}^{(\pm)} = q_{\beta_1} \dots q_{\beta_{l-1}} \Gamma_{\beta_{l\mu}}^{(\pm)} \quad (3.33)$$

⁴In Eq. (3.33), the symmetrization over the indices β_1, \dots, β_l is assumed.

and then expanding $\Gamma_{\beta\mu}^{(\pm)}$ over a minimal set of covariants. Gauge invariance for on-shell particles requires that

$$q_\mu \Gamma_{\beta\mu}^{(\pm)} = 0 \quad (3.34)$$

which restricts the form of the vertex to a superposition of three covariants [50], i.e.

$$\Gamma_{\beta\mu}^{(\pm)} = \sum_{k=1}^3 \Gamma_{\beta\mu}^{(\pm)k} F_k^{(\pm)}. \quad (3.35)$$

The values $F_k^{(\pm)}$ are scalar functions of q^2 and are called *covariant form factors*. In this representation, the Dirac structure of the transition amplitudes is fully separated off and expressed by the $\Gamma_{\beta\mu}^{(\pm)k}$ matrices. The choice for the covariants $\Gamma_{\beta\mu}^{(\pm)k}$ ($k = 1, 2, 3$) is not unique. The various sets used in the literature [49, 50, 51, 34] can be, however, related to each other with some algebra. We report below the set of gauge invariant covariants used in Ref. [34].

For the normal-parity case, the matrices $\Gamma_{\beta\mu}^{(+)i}$ ($i = 1, 2, 3$) have the form

$$\Gamma_{\beta\mu}^{(+)1} = m_*(q_\beta \gamma_\mu - \not{q} g_{\beta\mu}) \gamma_5, \quad (3.36)$$

$$\Gamma_{\beta\mu}^{(+)2} = (q_\beta P_\mu - q \cdot P g_{\beta\mu}) \gamma_5, \quad (3.37)$$

$$\Gamma_{\beta\mu}^{(+)3} = (q_\beta q_\mu - q^2 g_{\beta\mu}) \gamma_5, \quad (3.38)$$

where γ_μ and γ_5 are defined in Appendix A, $P = \frac{1}{2}(p_* + p)$. For the abnormal-parity case, the matrices $\Gamma_{\beta\mu}^{(-)i}$ ($i = 1, 2, 3$) have been taken as

$$\Gamma_{\beta\mu}^{(-)k} = \Gamma_{\beta\mu}^{(+)k} \gamma_5. \quad (3.39)$$

SPIN $J = \frac{1}{2}$ RESONANCES. The vertex $\Gamma_\mu^{(\pm)}$ ($l = 0$) can also be expanded like in Eq. (3.35). There are two matrices $\Gamma_\mu^{(+)i}$ ($i = 1, 2$) for the normal-parity case $J^P = \frac{1}{2}^-$,

$$\Gamma_\mu^{(+)1} = (q^2 \gamma_\mu - \not{q} q_\mu) \gamma_5, \quad (3.40)$$

$$\Gamma_\mu^{(+)2} = (P \cdot q \gamma_\mu - P_\mu \not{q}) \gamma_5, \quad (3.41)$$

and two matrices for the abnormal-parity case $J^P = \frac{1}{2}^+$,

$$\Gamma_\mu^{(-)k} = \Gamma_\mu^{(+)k} \gamma_5. \quad (3.42)$$

The vertex dimensions are $\Gamma_{\beta_1 \dots \beta_l \mu}^{(\pm)} \sim 1$, $\Gamma_{\beta\mu}^{(\pm)} \sim 1/m_*^{l-1}$, and $F_k^{(\pm)} \sim 1/m_*^{l+1}$.

The helicity amplitudes can be calculated in terms of the covariant form factors $F_k^{(\pm)}$ from

Eq. (3.23). Using the following notations for these amplitudes:⁵

$$\begin{aligned}\mathfrak{F}_{\frac{3}{2}}^{(\pm)} &= \left\langle J\frac{3}{2} \left| T \right| -\frac{1}{2}1 \right\rangle, \\ \mathfrak{F}_{\frac{1}{2}}^{(\pm)} &= \left\langle J\frac{1}{2} \left| T \right| +\frac{1}{2}1 \right\rangle, \\ \frac{M}{m_*} \mathfrak{C}_{\frac{1}{2}}^{(\pm)} &= \left\langle J\frac{1}{2} \left| T \right| -\frac{1}{2}0 \right\rangle,\end{aligned}\tag{3.43}$$

the matrix elements connecting $\mathfrak{F}_{\frac{3}{2}}^{(\pm)}$, $\mathfrak{F}_{\frac{1}{2}}^{(\pm)}$, $\mathfrak{C}_{\frac{1}{2}}^{(\pm)}$ to $F_1^{(\pm)}$, $F_2^{(\pm)}$, $F_3^{(\pm)}$ can be found to be [34, 50]:

SPIN $J \geq \frac{3}{2}$ RESONANCES.

$$\begin{pmatrix} \pm \mathfrak{F}_{\frac{3}{2}}^{(\pm)} \\ -\mathfrak{F}_{\frac{1}{2}}^{(\pm)} \\ \pm \mathfrak{C}_{\frac{1}{2}}^{(\pm)} \end{pmatrix} = \lambda_l^{(\pm)} \frac{2(\pm m)}{3m_{\pm}} \times \begin{pmatrix} \sqrt{\frac{l+2}{2l}} 2m_{\pm} m_* & \sqrt{\frac{l+2}{2l}} m_+ m_- & \sqrt{\frac{l+2}{2l}} 2M^2 \\ \sqrt{\frac{1}{2}} 2(m_{\pm}(\mp m) + M^2) & \sqrt{\frac{1}{2}} m_+ m_- & \sqrt{\frac{1}{2}} 2M^2 \\ 2m_*^2 & 2m_*^2 - \frac{1}{2} \Delta_0^2 & \Delta_0^2 \end{pmatrix} \begin{pmatrix} F_1^{(\pm)} \\ F_2^{(\pm)} \\ F_3^{(\pm)} \end{pmatrix},\tag{3.44}$$

where

$$\begin{aligned}m_{\pm} &= m_* \pm m, \\ \Delta_0^2 &= m_+ m_- + M^2.\end{aligned}$$

The coefficients $\lambda_l^{(\pm)}$ are defined as

$$\lambda_l^{(\pm)} = e \frac{3m_{\pm}}{4(\pm m)} \sqrt{m_{\mp}^2 - M^2} k^{l-1} \sqrt{\frac{2^l (l!)^2 (l+1)}{(2l+1)!}}\tag{3.45}$$

with $J = l + \frac{1}{2}$. Notice that

$$\begin{aligned}\mathfrak{F}_{\frac{3}{2}}^{(-)}(m_*, m) &= -\mathfrak{F}_{\frac{3}{2}}^{(+)}(m_*, -m), \\ \mathfrak{F}_{\frac{1}{2}}^{(-)}(m_*, m) &= +\mathfrak{F}_{\frac{1}{2}}^{(+)}(m_*, -m), \\ \mathfrak{C}_{\frac{1}{2}}^{(-)}(m_*, m) &= -\mathfrak{C}_{\frac{1}{2}}^{(+)}(m_*, -m).\end{aligned}\tag{3.46}$$

⁵These amplitudes describe, respectively, the double-spin-flip, no-spin-flip, and single-spin-flip transitions. For $l = 0$, the amplitude $\mathfrak{F}_{\frac{3}{2}}^{(\pm)}$ should be set equal to zero.

SPIN $J = \frac{1}{2}$ RESONANCES.

$$\begin{pmatrix} \mathfrak{F}_{\frac{1}{2}}^{(\pm)} \\ \pm\sqrt{2}\mathfrak{C}_{\frac{1}{2}}^{(\pm)} \end{pmatrix} = \frac{\lambda_0^{(\pm)}}{m_*} \begin{pmatrix} 2M^2 & m_+m_- \\ -2m_*m_{\mp} & -m_*m_{\pm} \end{pmatrix} \begin{pmatrix} F_1^{(\pm)} \\ F_2^{(\pm)} \end{pmatrix}. \quad (3.47)$$

The coefficients $\lambda_0^{(\pm)}$ are defined by

$$\lambda_0^{(\pm)} = e \frac{m_*}{\sqrt{2}} \sqrt{m_{\pm}^2 - M^2}. \quad (3.48)$$

An explicit expression for the covariant form factors $F_1^{(\pm)}$, $F_2^{(\pm)}$ and $F_3^{(\pm)}$ can be found assuming vector meson dominance.

3.3.2 Extended VMD model

The vector meson dominance model connects the hadronic electromagnetic current with the fields of light vector mesons such as ρ , ω or ϕ , which have the same quantum numbers as the photon, namely spin $J = 1$, parity $P = -1$ and charge conjugation $C = -1$. The connection is obtained by assuming that, to a very good approximation, the hadronic electromagnetic current is a linear combination of the vector meson fields V_μ and has the form [47]

$$J_\mu^{em} = -e \sum_{V=\rho,\omega,\phi} \frac{m_V^2}{g_V} V_\mu. \quad (3.49)$$

Here m_V are the vector meson masses and g_V the corresponding dimensionless coupling constants. As already mentioned in Section 3.2, the $SU(3)$ symmetry predicts for the coupling constants the relation $g_\rho : g_\omega : g_\phi = 1 : 3 : \frac{-3}{\sqrt{2}}$. The magnitude of g_ρ , g_ω and g_ϕ can be determined by measuring the leptonic decays of the vector mesons. The values $g_\rho = 5.03$, $g_\omega = 17.1$, and $g_\phi = -12.9$ extracted from the $V \rightarrow e^+e^-$ decays of the ρ , ω , and ϕ mesons are in good agreement with the $SU(3)$ predictions.

The VMD model has been extensively used to interpret the photo- and electroproduction of hadrons. For example, it describes well the electromagnetic pion form factor:

$$F_\pi(q^2) = \frac{f_{\rho\pi\pi}}{g_\rho} \frac{m_\rho^2}{m_\rho^2 - q^2}, \quad (3.50)$$

with $f_{\rho\pi\pi}$ being the coupling constant of the effective Lagrangian

$$\begin{aligned} \mathcal{L}_{\rho\pi\pi} &= -\frac{1}{2} f_{\rho\pi\pi} \varepsilon_{\alpha\beta\gamma} \rho_\mu^\alpha (\pi^\beta \overleftrightarrow{\partial}_\mu \pi^\gamma) \\ &= -f_{\rho\pi\pi} (\rho_\mu^0 \pi^- i \overleftrightarrow{\partial}_\mu \pi^+ + \rho_\mu^+ \pi^0 i \overleftrightarrow{\partial}_\mu \pi^- + \rho_\mu^- \pi^+ i \overleftrightarrow{\partial}_\mu \pi^0) \end{aligned} \quad (3.51)$$

where $\overleftrightarrow{\partial}_\mu = \overrightarrow{\partial}_\mu - \overleftarrow{\partial}_\mu$. The normalization $F_\pi(0) = 1$ implies

$$f_{\rho\pi\pi}/g_\rho = 1. \quad (3.52)$$

The standard vector meson dominance with the ground-state ρ , ω , and ϕ mesons predicts monopole form factors with $1/q^2$ asymptotics at $q^2 \rightarrow \infty$. Such asymptotics is, according to the quark counting rules [52], valid for the electromagnetic pion form factor.

The description of the resonance decays $\Gamma(R \rightarrow N\gamma^*)$ is usually based on the VMD model. The decays of the N^* resonances proceed through both the ρ and ω mesons. The Δ decays, on the other hand, proceed exclusively through the ρ meson. The approach is schematically depicted in Fig. 3.5. The vector meson couplings with the nucleon resonances $f_{VNR,k}^{(\pm)}$ are

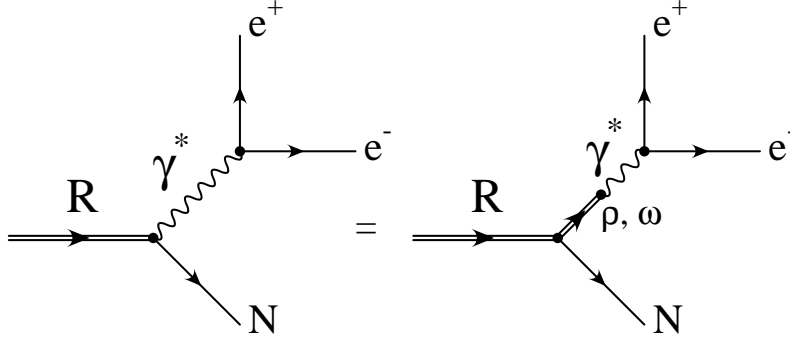


Figure 3.5: Decay of nuclear resonances to dileptons in the VMD model. The $RN\gamma$ transition form factors contain contributions from the ω and ρ mesons.

defined by the T -matrix element of the $VN \rightarrow R$ process

$$\langle J\lambda_* | T | \lambda\lambda_V \rangle = \sum_k f_{VNR,k}^{(\pm)} \bar{u}_{\beta_1 \dots \beta_l}(p_*, \lambda_*) q_{\beta_1} \dots q_{\beta_{l-1}} \Gamma_{\beta_l \mu}^{(\pm)k} u(p, \lambda) \varepsilon_\mu^{(\lambda_V)}(q) \quad (3.53)$$

where the vertices $\Gamma_{\beta_l \mu}^{(\pm)k}$ are the same as for the photon, and $\varepsilon_\mu^{(\lambda_V)}(k)$ is the polarization vector of the vector meson V with momentum q and helicity λ_V .

The combination of Eqs. (3.53) and the VMD current field identity (3.49) allows to calculate the photo- and electroproduction amplitudes

$$\langle J\lambda_* | T | \lambda\lambda_\gamma \rangle = \sum_k \sum_V f_{VNR,k}^{(\pm)} \frac{em_V^2}{g_V} \frac{1}{q^2 - m_V^2} \times \bar{u}_{\beta_1 \dots \beta_l}(p_*, \lambda_*) q_{\beta_1} \dots q_{\beta_{l-1}} \Gamma_{\beta_l \mu}^{(\pm)k} u(p, \lambda) \varepsilon_\mu^{(\lambda_\gamma)}(q). \quad (3.54)$$

The comparison with the expression for the helicity amplitudes (3.23) shows that the covariant form factors have the form

$$F_k^{(\pm)}(M^2) = \sum_V \frac{f_{VNR,k}^{(\pm)}}{g_V} \frac{1}{1 - M^2/m_V^2}. \quad (3.55)$$

The Δ resonance form factors have only contributions from the ρ meson family. If the covariant form factors $F_k^{(\pm)}(M^2)$ are known, the coupling constants $f_{\rho^0 NR,k}^{(\pm)}$ for the Δ resonances can be found from equation

$$f_{\rho^0 N\Delta,k}^{(\pm)} = -\frac{g_\rho}{m_\rho^2} \text{res} \left\{ F_k^{(\pm)}(M^2 = m_\rho^2) \right\}. \quad (3.56)$$

The nucleon resonances N^* receive contributions from the ρ and ω mesons. The couplings with the nucleon resonances are calculated as residues of a superposition for isospin projections $I_3 = +\frac{1}{2}$ and $I_3 = -\frac{1}{2}$:

$$\begin{aligned} f_{\rho^0 NN^*,k}^{(\pm)} &= -\frac{g_\rho}{2m_\rho^2} \text{res} \left\{ F_k^{(\pm)}(M^2 = m_\rho^2)^{I_3=+\frac{1}{2}} - F_k^{(\pm)}(M^2 = m_\rho^2)^{I_3=-\frac{1}{2}} \right\}, \\ f_{\omega NN^*,k}^{(\pm)} &= -\frac{g_\omega}{2m_\omega^2} \text{res} \left\{ F_k^{(\pm)}(M^2 = m_\omega^2)^{I_3=+\frac{1}{2}} + F_k^{(\pm)}(M^2 = m_\omega^2)^{I_3=-\frac{1}{2}} \right\}. \end{aligned} \quad (3.57)$$

The VMD model gives, in principle, an unified description of the radiative and mesonic decays and of the photo- and electroproduction of hadrons. However, two inconsistencies of the standard VMD model have been pointed out [34, 53].

First shortcoming of the standard VMD. We saw that the standard vector meson dominance predicts monopole form factors with $1/q^2$ asymptotics at $q^2 \rightarrow \infty$. The electromagnetic nucleon form factors demonstrate experimentally a dipole behaviour. The quark counting rules for the Sachs form factors predict $G_E(q^2) \sim G_M(q^2) \sim 1/q^4$ at $q^2 \rightarrow \infty$. The VMD model with the ground-state ρ -, ω -, and ϕ -mesons cannot describe the nucleon form factors at low values of q^2 (the isovector charge radius is underestimated) and gives in contrast to the pion incorrect asymptotic behaviour. In order to solve this problem, it was proposed [54, 55, 56, 57] to include in the current (3.49) excited states of the vector mesons ρ' , ρ'' , ... etc. The VMD model extended in this way has been named *extended VMD* (eVMD) model. The eVMD model yields for the nucleon form factors the correct asymptotic behaviour. In addition, the minimal extension of the VMD model improves the description of the $\rho\pi\gamma$ transition form factor that falls off asymptotically as $1/q^4$ [53].

For the $RN\gamma$ transition form factors, in which we are interested, the standard VMD model provides wrong asymptotics too. The quark counting rules predict the following asymptotics for the helicity amplitudes

$$\begin{aligned} \mathfrak{F}_{\frac{3}{2}}^{(\pm)} &= O\left(\frac{1}{(-M^2)^{5/2}}\right), \\ \mathfrak{F}_{\frac{1}{2}}^{(\pm)} &= O\left(\frac{1}{(-M^2)^{3/2}}\right), \\ \mathfrak{C}_{\frac{1}{2}}^{(\pm)} &= O\left(\frac{1}{(-M^2)^{5/2}}\right). \end{aligned} \quad (3.58)$$

Second shortcoming of the standard VMD. The VMD model should give, in principle, an unified description of the radiative $RN\gamma$ and the mesonic RNV decays. However, the standard VMD model underestimates the mesonic branching ratios of various baryon resonances if coupling constants extracted from the radiative branching are used as input. The resonance $N^*(1520)$, for example, is a case for which both, the $N(1520) \rightarrow N\rho$ and $N(1520) \rightarrow N\gamma$ widths are known with a relatively high precision: $B(N(1520) \rightarrow N\rho) = 15 \div 25\%$, $B(N(1520) \rightarrow N\gamma) = 0.46 \div 0.56\%$ ($p\gamma$ mode), $0.30 \div 0.53\%$ ($n\gamma$ mode). The standard VMD model, as it has been used for example in [58], leads to a severe inconsistency: using the coupling constant $f_{N(1520)N\rho} = 7.0$ extracted from the mesonic $N(1520) \rightarrow N\rho$ decay,

R	N_{1440}	N_{1520}	N_{1535}	N_{1650}	N_{1680}	N_{1720}	Δ_{1232}	Δ_{1620}	Δ_{1700}	Δ_{1905}
J^P	$\frac{1}{2}^+$	$\frac{3}{2}^-$	$\frac{1}{2}^-$	$\frac{1}{2}^-$	$\frac{5}{2}^+$	$\frac{3}{2}^+$	$\frac{3}{2}^+$	$\frac{1}{2}^-$	$\frac{3}{2}^-$	$\frac{5}{2}^+$
$f_{RN\rho}$	< 26	7.0	< 2.0	0.9	6.3	7.8	15.3	2.5	5.0	12.2
$f_{RN\rho}^{\gamma}$	1.3	3.8	1.8	< 0.8	3.9	2.2	10.8	0.7	2.7	2.1

Table 3.1: The coupling constants $f_{RN\rho}$ derived from the $R \rightarrow N\rho$ mesonic decays are compared to the coupling constants $f_{RN\rho}^{\gamma}$ fixed from the radiative $R \rightarrow N\gamma$ decays. The numerical values $f_{RN\rho}$ are taken from Ref. [9], with exception of the $\Delta(1232)$ resonance for which the theoretical value from [14] is given and of the $N(1440)$ and $N(1535)$ resonances where the results of the calculations of the authors of Ref. [53] are given. The table is taken from Ref. [53].

the branching ratio for the radiative decay is found to be two to three times larger than the experimental value. Analogous overestimations are observed for almost all other N and Δ resonances for which the experimental $N\rho$ and $N\gamma$ data are available. Table 3.1 summarizes the results.

It is clear that a more accurate description of radiative decays of the baryon resonances requires a model, VMD based, which takes into account the correct asymptotics of the $RN\gamma$ transition form factors and which is able to describe both the $R \rightarrow N\gamma$ radiative decays and the $R \rightarrow N\rho(\omega)$ mesonic decays with the *same* parameters.

In Ref. [34] the eVMD model has been used for the description of the transition form factor of the baryon resonances. As already mentioned, the basic idea of the eVMD model is to include in the current (3.49) excited states of the vector mesons ρ' , ρ'' , ... etc. This results in the addition of new free parameters with respect to the standard VMD model, namely the couplings of the ρ' , ρ'' , ..., to the resonances ($f_{\rho'NR,k}^{(\pm)}$, $f_{\rho''NR,k}^{(\pm)}$, ...) and to the photon ($g_{\rho'}$, $g_{\rho''}$, ...). However, the constraints (3.58) can be used to reduce the number of free parameters of the model. Thus, the eVMD model provides the correct asymptotics of the $RN\gamma$ transition form factors *ab initio*. Moreover, the model provides an unified description of photo- and electroproduction data and the vector meson decays of the baryon resonances.

We report below the main steps that lead to the expression of the covariant form factors $F_1^{(\pm)}$, $F_2^{(\pm)}$ and $F_3^{(\pm)}$ in terms of the free parameters of the eVMD model. For this purpose, we separate the case of resonances with spin $J \geq \frac{3}{2}$ from the case of resonances with spin $J = \frac{1}{2}$.

SPIN $J \geq \frac{3}{2}$ RESONANCES. Taking into account that $\lambda_l^{(\pm)} = O((-M^2)^{l-1/2})$ at $M^2 \rightarrow -\infty$, one

gets the asymptotics of the covariant form factors $F_k^{(\pm)}(M^2)$ at $M^2 \rightarrow -\infty$:

$$\begin{aligned} F_1^{(\pm)}(M^2) &= O\left(\frac{1}{(-M^2)^{l+2}}\right), \\ F_2^{(\pm)}(M^2) &= O\left(\frac{1}{(-M^2)^{l+3}}\right), \\ F_3^{(\pm)}(M^2) &= O\left(\frac{1}{(-M^2)^{l+3}}\right). \end{aligned} \quad (3.59)$$

These constraints can be resolved with a minimal set of parameters to give

$$\boxed{\begin{aligned} F_1^{(\pm)}(M^2) &= \frac{C_{10}^{(\pm)} + C_{11}^{(\pm)} M^2}{\prod_{i=1}^{l+3} (1 - M^2/m_i^2)}, \\ F_2^{(\pm)}(M^2) &= \frac{C_{20}^{(\pm)}}{\prod_{i=1}^{l+3} (1 - M^2/m_i^2)}, \\ F_3^{(\pm)}(M^2) &= \frac{C_{30}^{(\pm)}}{\prod_{i=1}^{l+3} (1 - M^2/m_i^2)}. \end{aligned}} \quad (3.60)$$

Here, $C_{kj}^{(\pm)}$ are free parameters of the extended VMD model, $l+3$ is the total number of the vector mesons. For each form factor, the quark counting rules reduce the number of free parameters from $l+3$ to 2 for $k=1$ and to 1 for $k=2,3$. The knowledge of the four parameters $C_{10}^{(\pm)}$, $C_{11}^{(\pm)}$, $C_{20}^{(\pm)}$, and $C_{30}^{(\pm)}$ is therefore sufficient to fix $F_k^{(\pm)}(M^2)$. In the zero-width limit, the multiplicative representation (3.60) is completely equivalent to an additive representation of Eq. (3.55), according to the known theorems of complex analysis of rational functions.

SPIN $J = \frac{1}{2}$ RESONANCES. For the two helicity amplitudes $\mathfrak{F}_{\frac{1}{2}}^{(\pm)}$ and $\mathfrak{C}_{\frac{1}{2}}^{(\pm)}$, the constraints to the asymptotics are given by Eqs. (3.58). Taking into account that $\lambda_0^{(\pm)} = O((-M^2)^{1/2})$ at $M^2 \rightarrow -\infty$, one gets

$$F_{1,2}^{(\pm)}(M^2) = O\left(\frac{1}{(-M^2)^3}\right). \quad (3.61)$$

The general representation for the covariant form factors in the spin- $\frac{1}{2}$ case has the form

$$\boxed{F_k^{(\pm)}(M^2) = \frac{C_{k0}^{(\pm)}}{\prod_{i=1}^3 (1 - M^2/m_i^2)}}. \quad (3.62)$$

The parameters $C_{kj}^{(\pm)}$ of the extended VMD model, entering Eqs. (3.60) and (3.62), have been determined in [34] from the fit to the photo- and electroproduction data [59, 60, 61, 62, 63] and the vector meson decay amplitudes of the nucleon resonances [59, 64, 65, 66, 67]. The number of the vector mesons required for each isotopic channel to ensure the correct asymptotic behavior depends on the total spin of the nucleon resonance. For spin- J resonances, one needs $l+3$ excited vector mesons with the same quantum numbers. The

nucleon resonances considered in [34] have spins J from $\frac{1}{2}$ to $\frac{7}{2}$. It means that at most 6 excited vector mesons for each isotopic channel are needed. The following masses have been used: 0.769, 1.250, 1.450, 1.720, 2.150, 2.350 (in GeV). The numbers appearing on the 1 and 3 - 5 positions are masses of the physical ρ mesons according to the PDG [59]. For discussions on the possible existence of vector mesons with masses around 1.250 GeV see [43] and [34]. The last mass was set equal to 2.350 GeV for an estimate. In principle the inclusion of the heavy vector mesons can also be considered as a phenomenological approach to obtain a physically correct asymptotic behaviour of the form factors. However, the results on the dilepton emission do anyhow not depend strongly on the exact numerical values of the masses of the excited vector mesons, since the dilepton energy spectrum extends only slightly above 1 GeV for the nucleon resonances with masses of about 2 GeV. The authors assumed further a degeneracy between the ρ and ω families. The strange ϕ mesons are decoupled in the eVMD model from the nucleons due to the OZI⁶ rule.

For the nucleon resonance decays into the vector mesons, the authors used the data from PDG [59]. When these data are not available, the Manley and Saleski results (MS) of the multichannel πN partial wave analysis [64] were used. In other cases, they used the quark model predictions by Koniuk (K) [66] with 50% errors and $0.05 \text{ MeV}^{1/2}$ errors if the values are close to zero. In a few cases, the results of the multichannel πN partial-wave analysis of Longacre and Dolbeau (LD) [65] with 50% errors and quark model predictions of Capstick and Roberts (CR) [67] were used, when other results did not agree with the most recent PDG constraints to the total vector meson decay widths. The PDG and MS data were included to the χ^2 with greater weights. In [34] details on the fitting procedure are given separately for each one of the 25 resonances considered. We restrict ourselves to list the sources used to fix the couplings of the resonances which enter in the calculations that will be presented in Chapter 4 and Chapter 5 of this work. For a more complete description of the fitting procedure as well for the discussion on the relative sign of the photo- and electroproduction amplitudes and amplitudes for the nucleon resonance decays into the vector mesons we address the reader to Ref. [34].

$N(1535)\frac{1}{2}^-$: The experimental values for $A_{1/2}$ are from Ref. [68]. The $N\rho$ mode $s_{1/2}$ is taken from PDG. The $N\rho$ mode $d_{3/2}$ is taken from MS. The ω meson mode $d_{3/2}$ is set equal to zero.

$N(1650)\frac{1}{2}^-$: The $N\rho$ mode $s_{1/2}$ is taken from PDG. The mode $d_{3/2}$ is taken from PDG. The $N\omega$ modes are from K.

$N(1520)\frac{3}{2}^-$: The experimental values for $A_{1/2}$ and $A_{3/2}$ are from Ref.[68]. The modes $d_{1/2}$ and $d_{3/2}$ are taken from K. The mode $s_{3/2}$ is taken from PDG.

$N(1440)\frac{1}{2}^+$: The experimental values for $A_{1/2}$ are from Ref.[68]. The mode $p_{1/2}$ is taken from PDG. The value of the mode $p_{3/2}$ is taken from K.

$N(1720)\frac{3}{2}^+$: The $N\rho$ mode $p_{1/2}$ from MS and the mode $p_{3/2}$ from LD seems to be overestimated in view of the PDG value $\sqrt{\Gamma_{N\rho}^{tot}} = 11 \pm 2 \text{ MeV}^{1/2}$ for the total $N\rho$ width. The modes $p_{1/2}$, $p_{3/2}$ and $f_{3/2}$ are taken from K. The $N\omega$ modes from K are included to the fit.

⁶The Okubo-Zweig-Iizuka (OZI) rule states that processes with disconnected quark lines in the initial or final state are suppressed.

$N(1680)_{\frac{5}{2}}^{+}$: The experimental values for $A_{1/2}$ and $A_{3/2}$ are from Ref. [68]. The $N\rho$ mode $f_{1/2}$ is from K. The modes $f_{3/2}$ and $p_{3/2}$ are from PDG. The $N\omega$ modes are from K.

$\Delta(1620)_{\frac{1}{2}}^{-}$: PDG values are used.

$\Delta(1700)_{\frac{3}{2}}^{-}$: K values are used for the modes $d_{1/2}$ and $d_{3/2}$. The PDG absolute value is used for the $s_{3/2}$ mode.

$\Delta(1232)_{\frac{3}{2}}^{+}$: The data in the space-like region on the magnetic transition form factor are from Refs. [61, 60, 62]. Into the fit the experimental results of Refs. [69, 70, 71, 63, 72, 73] for the ratio G_C/G_M and of Refs. [63, 72, 70, 73] for the ratio G_E/G_M are included. The amplitudes $A_{3/2}$ and $A_{1/2}$ at $M = 0$ are given by PDG.

$\Delta(1905)_{\frac{5}{2}}^{+}$: CR values are used for the f -modes and PDG for the $p_{3/2}$ -mode.

$\Delta(1950)_{\frac{7}{2}}^{+}$: PDG gives an upper limit of $6 \text{ MeV}^{1/2}$ for the total $N\rho$ width. MS and K results are above this limit, therefore the estimates of CR have been used.

In Table 3.2 we show the parameters $C_{kj}^{(\pm)}$ of the extended VMD model for the above listed nucleon resonances. The eVMD model results for the vector meson decay amplitudes of the nucleon resonances are listed in Tables 3.3 and 3.4. Finally, the dilepton widths of the nucleon resonances are shown in Table 3.5.

Resonance	J^P	C_{10}	C_{11}	C_{20}	C_{30}
$N^*(1535)$	$\frac{1}{2}^-$	0.979		0.006	
		1.787		-0.062	
$N^*(1650)$	$\frac{1}{2}^-$	0.232		-0.186	
		-0.394		0.157	
$N^*(1520)$	$\frac{3}{2}^-$	2.186	-1.236	-1.976	-0.159
		-0.220	1.899	-0.316	-0.249
$N^*(1440)$	$\frac{1}{2}^+$	0.863		1.023	
		0.084		-0.699	
$N^*(1720)$	$\frac{3}{2}^+$	0.000	0.608	0.187	-5.312
		0.051	-0.304	0.194	1.630
$N^*(1680)$	$\frac{5}{2}^+$	2.487	-0.700	-2.116	-0.797
		-0.793	4.929	0.735	-6.297
$\Delta(1620)$	$\frac{1}{2}^-$	-0.155		-0.081	
$\Delta(1700)$	$\frac{3}{2}^-$	-0.630	-0.298	1.080	-0.473
$\Delta(1232)$	$\frac{3}{2}^+$	1.768	0.025	-1.096	-0.926
$\Delta(1905)$	$\frac{5}{2}^+$	-0.209	0.090	0.157	-1.145
$\Delta(1950)$	$\frac{7}{2}^+$	0.867	-1.250	-0.138	1.619

Table 3.2: Residues $C_{jk}^{(\pm)}$ of the extended VMD model, entering Eqs. (3.60) and (3.62), in units $\text{GeV}^{-(l+1)}$ where $l = J - \frac{1}{2}$. The N^* residues are shown in two rows for the proton and neutron resonances, respectively.

Resonance	Ref.	$N\rho$	$N\rho$	$N\rho$	$\sqrt{\Gamma_{N\rho}^{tot}}$	$N\omega$	$N\omega$	$N\omega$	$\sqrt{\Gamma_{N\omega}^{tot}}$
		$s_{1/2}$	$d_{3/2}$			$s_{1/2}$	$d_{3/2}$		
$N^*(1535)\frac{1}{2}^-$	VMD	-2.13	-0.25		2.15	1.43	0.05		1.43
	MS	-1.7 ± 0.5	-1.3 ± 0.6		2.2 ± 0.6				
	PDG	-2.0 ± 0.9			< 2.7				
$N^*(1650)\frac{1}{2}^-$	VMD	-1.45	1.04		1.78	-0.97	-0.02		0.97
	MS	0.0 ± 1.6	2.2 ± 0.9		2.2 ± 0.9				
	PDG	$\pm 1.6\pm 1.2$	3.4 ± 1.0		3.6 ± 0.9				
		$d_{1/2}$	$d_{3/2}$	$s_{3/2}$		$d_{1/2}$	$d_{3/2}$	$s_{3/2}$	
$N^*(1520)\frac{3}{2}^-$	VMD	-0.37	-0.17	-5.14	5.16	-0.02	0.03	0.28	0.29
	MS	0	0	-5.1 ± 0.6	5.1 ± 0.6				
	PDG			-4.9 ± 0.6	4.9 ± 0.6				
		$p_{1/2}$	$p_{3/2}$			$p_{1/2}$	$p_{3/2}$		
$N^*(1440)\frac{1}{2}^+$	VMD	-0.29	0.61		0.67	0.00	0.00		0.00
	PDG	$\pm 3.7\pm 2.2$			< 6				
		$p_{1/2}$	$p_{3/2}$	$f_{3/2}$		$p_{1/2}$	$p_{3/2}$	$f_{3/2}$	
$N^*(1720)\frac{3}{2}^+$	VMD	11.03	-2.56	1.02	11.37	5.29	-2.09	0.14	5.69
	MS	18 ± 5	0	0	18 ± 5				
	PDG				11 ± 2				
		$f_{1/2}$	$f_{3/2}$	$p_{3/2}$		$f_{1/2}$	$f_{3/2}$	$p_{3/2}$	
$N^*(1680)\frac{5}{2}^+$	VMD	-1.35	-1.23	-2.62	3.20	0.09	0.40	0.58	0.71
	MS	0	-1.7 ± 0.6	-2.8 ± 0.7	3.3 ± 0.7				
	PDG		-2.0 ± 0.6	-2.8 ± 1.4	3.4 ± 1.1				

Table 3.3: Predictions of the extended VMD model for the partial widths of the N^* resonance decays into the ρ and ω meson channels, inclusive of the sign of the amplitudes. The data quoted by PDG [59] and the results of the multichannel πN partial-wave analysis MS [64] are given for comparison. The widths are in MeV.

Resonance	Ref.	$N\rho$	$N\rho$	$N\rho$	$\sqrt{\Gamma_{N\rho}^{tot}}$
		$s_{1/2}$	$d_{3/2}$		
$\Delta(1620)_{\frac{1}{2}}^{-}$	VMD	4.05	-0.02		4.05
	MS	6.2 ± 0.9	-2.4 ± 0.2		6.6 ± 0.8
	PDG	4.2 ± 1.4	-2.2 ± 1.5		4.9 ± 1.5
		$d_{1/2}$	$d_{3/2}$	$s_{3/2}$	
$\Delta(1700)_{\frac{3}{2}}^{-}$	VMD	-1.66	0.66	6.67	6.91
	MS	0	0	6.8 ± 2.3	6.8 ± 2.3
	PDG			$\pm 6.7\pm 2.4$	11 ± 3
		$f_{1/2}$	$f_{3/2}$	$p_{3/2}$	
$\Delta(1905)_{\frac{5}{2}}^{+}$	VMD	-1.40	-0.46	17.46	17.53
	MS	0	0	16.8 ± 1.3	16.8 ± 1.3
	PDG			20 ± 6	> 17
		$f_{1/2}$	$f_{3/2}$	$h_{3/2}$	
$\Delta(1950)_{\frac{7}{2}}^{+}$	VMD	1.28	-2.38	0.28	2.72
	MS	0	11.4 ± 0.5	0	11.4 ± 0.5
	PDG				< 6

Table 3.4: The ρ meson modes of the Δ resonances. The notations are the same as in Table 3.3.

Resonance	$\Gamma_{e^+e^-}$ [keV]	$\Gamma_{\mu^+\mu^-}$ [keV]
$N^*(1535)_{\frac{1}{2}}^-$	2.01	1.87
	5.30	4.85
$N^*(1650)_{\frac{1}{2}}^-$	3.23	0.79
	2.00	0.31
$N^*(1520)_{\frac{3}{2}}^-$	6.02	0.73
	4.42	0.41
$N^*(1440)_{\frac{1}{2}}^+$	1.40	0.22
	0.56	0.05
$N^*(1720)_{\frac{3}{2}}^+$	7.93	7.77
	3.14	2.77
$N^*(1680)_{\frac{5}{2}}^+$	2.58	0.43
	1.47	1.13
$\Delta(1620)_{\frac{1}{2}}^-$	1.33	0.88
$\Delta(1700)_{\frac{3}{2}}^-$	6.10	1.65
$\Delta(1232)_{\frac{3}{2}}^+$	5.02	0.04
$\Delta(1905)_{\frac{5}{2}}^+$	10.51	10.36
$\Delta(1950)_{\frac{7}{2}}^+$	3.18	0.81

Table 3.5: The decay widths of the nucleon resonances into the e^+e^- and $\mu^+\mu^-$ pairs. The first line of the N^* resonances with $I = 1/2$ refers to the proton, the second one to the neutron resonances.

Chapter 4

Vector mesons in the medium

The in-medium properties of hadrons are generally expressed in terms of the self energy Σ . The self energy determines the spectral function of the quasi-particle in the medium. As long as the self energy shows only a moderate energy dependence, the real part of Σ can be interpreted in terms of a mass shift while the imaginary part generates the in-medium width. To leading order in density the self energy is determined by the forward scattering length of the hadron with the surrounding particles. Since the ρ -nucleon and ω -nucleon scattering lengths are unknown from the experimental side, these quantities have to be determined theoretically.

This Chapter is devoted to the description of the properties that the ρ and ω mesons acquire when they are embedded in the nuclear medium. After introducing some basic concepts in Section 4.1, we apply in Section 4.2 the Nucleon Resonance Dominance (NRD) model to calculate the forward scattering of vector mesons on nucleons and then determine the in-medium spectral functions of the ρ and ω mesons. The nucleon resonance dominance model is not a field theory in the strict sense where corresponding Feynman diagrams are evaluated, but an effective model which has, however, some similarity to a field theory based on Feynman diagrams with the intermediate resonances in the s -channel of vector meson and nucleon scattering (see Fig. 4.1). The model assumes that vector meson production runs over the excitation of nucleon resonances. Such an approach was applied in many previous investigations of vector mesons properties in the nuclear medium [74, 75, 76, 18, 17]. The present approach differs with respect to previous investigations by the fact that in the NRD+eVMD model the corresponding couplings of resonances to nucleon and vector meson are of relativistic form and kinematically complete. The inclusion of possible non-resonant contributions to the forward vector meson-nucleon scattering and the influence of in-medium resonances on the vector meson self energies are discussed in Section 4.3 and Section 4.4 respectively. Finally, in Section 4.5 we briefly report the main features of the analysis that led to the conjecture of the “dropping mass” in-medium scenario for the vector mesons.

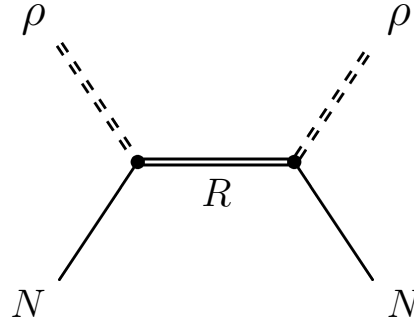


Figure 4.1: Resonance contribution to the ρN scattering amplitude.

4.1 In-medium spectral functions

The spectral function of a particle is defined as the imaginary part of the propagator. In vacuum the spectral functions of the ρ and ω mesons depend only on their invariant mass and the spectral distribution of the longitudinal and transversal modes are the same. In nuclear matter, instead, the acquired self energy depends separately on both the energy p^0 and the three-momentum \mathbf{p} of the vector meson $V = \rho, \omega$. Moreover, the transverse and longitudinal propagation modes receive different in-medium modifications. This results in a different spectral distribution of the longitudinal and transversal modes or, in other words, in a transversal and longitudinal spectral function:

$$A_V^{T/L}(p^0, \mathbf{p}) = -\frac{1}{\pi} \frac{\text{Im} \Sigma_V^{\text{tot}(T/L)}(p^0, \mathbf{p})}{(p^2 - m_V^2 + \text{Re} \Sigma_V^{\text{tot}(T/L)}(p^0, \mathbf{p}))^2 + \text{Im} \Sigma_V^{\text{tot}(T/L)}(p^0, \mathbf{p})^2}. \quad (4.1)$$

Here m_V is the pole mass of the vector meson. $\Sigma^{\text{tot}(T/L)}$ is the transverse or longitudinal part of the total self energy of the vector meson which can be decomposed into a vacuum self energy $\Sigma_V^{(0)}$ and an in-medium part $\Sigma^{T/L}(p^0, \mathbf{p})$:

$$\Sigma_V^{\text{tot}(T/L)}(p^0, \mathbf{p}) = \Sigma_V^{(0)}(p^2) + \Sigma_V^{T/L}(p^0, \mathbf{p}). \quad (4.2)$$

The vacuum self energy $\Sigma_V^{(0)}$ is determined by the corresponding vacuum width

$$\Im \Sigma_V^{(0)} = -m_V \Gamma_V^{\text{tot}}(M), \quad \Re \Sigma_V^{(0)} = 0. \quad (4.3)$$

Here $\Gamma_\rho^{\text{tot}}(M)$ and $\Gamma_\omega^{\text{tot}}(M)$ are essentially given by the dominating decay widths of the ρ meson into two pions and of the ω meson into three pions respectively.

The two pion decay width of the ρ meson is parameterized as

$$\Gamma_\rho^{\text{tot}}(M) = \Gamma_\rho^{\text{tot}}(m_\rho) \frac{m_\rho}{M} \left(\frac{k_\pi(M, m_\pi, m_\pi)}{k_\pi(m_\rho, m_\pi, m_\pi)} \right)^3 \Theta(M^2 - 4m_\pi^2) \quad (4.4)$$

where¹ $k_\pi(M, m_\pi, m_\pi) = p^*(M, m_\pi, m_\pi)$ is the momentum of the pions in the rest frame of the decaying ρ having mass M ; m_ρ is the physical ρ mass and $\Gamma_\rho^{\text{tot}}(m_\rho) = 150$ MeV the on-shell

¹ p^* has been defined in Section 3.1.1, Eq. (3.12).

decay width. Eq. (4.4) can be understood as follows: the energy dependence of the width around threshold is determined by the orbital angular momentum l of the $\pi\pi$ system in the $\rho \rightarrow \pi\pi$ decay as

$$\Gamma_{\rho}^{\text{tot}}(M) \sim \left(k_{\pi}(M, m_{\pi}, m_{\pi}) \right)^{2l+1}, \quad (4.5)$$

where one power of k_{π} is due to the two-body phase space and the remaining powers originate from the square of the matrix element of the process. Since the $\rho \rightarrow \pi\pi$ decay proceeds as a p -wave², one has $\Gamma_{\rho}^{\text{tot}} \sim k_{\pi}^3$. Despite its simplicity, Eq. (4.4) contains precisely the energy dependence of the imaginary part of the ρ meson vacuum self energy that comes out of a one loop calculation.

The three pion decay width of the ω meson can be calculated according to the two-step process $\omega \rightarrow \rho\pi \rightarrow 3\pi$ as proposed by Gell-Mann, Sharp, and Wagner [77]. The corresponding result can be parametrized in the simple form

$$\Gamma_{\omega}^{\text{tot}}(M) = \Gamma_{\omega}^{\text{tot}}(m_{\omega}) \frac{m_{\omega}}{M} \left(\frac{M^2 - 9m_{\pi}^2}{m_{\omega}^2 - 9m_{\pi}^2} \right)^3 \Theta(M^2 - 9m_{\pi}^2) \quad (4.6)$$

with m_{ω} the physical ω mass and $\Gamma_{\omega}^{\text{tot}}(m_{\omega}) = 8.4$ MeV the on-shell decay width.

In the following we will determine the in-medium part of the self energy Σ_V .

4.2 In-medium self energy: resonant contribution

To lowest order in the nuclear density ρ_B the self energy Σ_V of a vector meson V in isotopically symmetric nuclear medium is determined by the invariant VN forward scattering amplitude A_{VN}

$$\Sigma_V(p^0, \mathbf{p}, \rho_B) = - \int_F A_{VN}(p, p_N) 2 \cdot 2 \frac{d^3 \mathbf{p}_N}{2E_N (2\pi)^3}. \quad (4.7)$$

Here $p = (p^0, \mathbf{p})$ and $p_N = (E_N, \mathbf{p})$ are the 4-momenta of the vector meson V and the nucleon, where V refers either to a ρ^0 or a ω meson. Due to isosymmetry of the medium the self energy Σ_V for ρ^{\pm} mesons is the same as for ρ^0 meson. The forward scattering amplitude A_{VN} is the same for proton ($N = p$) and neutron ($N = n$) scattering. The integral in (4.7) runs over the nucleon momenta within the Fermi volume, denoted here by F . By performing the integration in the rest frame of nuclear matter F is simply the Fermi sphere with Fermi momentum p_F determined by nuclear matter density ρ_B

$$\rho_B = \frac{2}{3\pi^2} p_F^3. \quad (4.8)$$

The amplitude A_{VN} is expressed as the sum over resonances of amplitudes for resonant scattering of Breit-Wigner form

$$A_{VN} = - \sum_R \frac{(2J_R + 1) 8\pi s}{2 \cdot 3} \frac{\Gamma_{R \rightarrow NV}(s, p^2)}{k (s - M_R^2 + i\sqrt{s}\Gamma_R^{\text{tot}}(s))}. \quad (4.9)$$

²We remind that the pion is a pseudoscalar particle, $J_{\pi} = 0$, and the ρ meson is a vector particle, $J_{\rho} = 1$. Therefore in the $\rho \rightarrow \pi\pi$ decay angular momentum conservation imposes the $\pi\pi$ system to be in a state with relative orbital angular momentum $l = 1$.

In (4.9) $s = (p_N + p)^2 = \mu^2$ is the running mass squared of the baryon resonance, J_R its spin, M_R its pole mass and k is the c.m. momentum in the VN scattering. The width $\Gamma_{R \rightarrow NV}(s, p^2)$ refers to the decay of the baryon resonance to a nucleon and a vector meson with fixed mass squared $p^2 = M^2$. The width $\Gamma_R^{\text{tot}}(\mu)$ is given by ³

$$\Gamma_R^{\text{tot}}(\mu) = \Gamma_{R \rightarrow N\pi}(\mu) + \Gamma_{R \rightarrow N\rho}(\mu) + \Gamma_{R \rightarrow N\omega}(\mu) + \delta\Gamma_R \quad (4.11)$$

and refers to the decays of the resonance R not modified by the medium, in particular, with the vacuum spectral functions for the decay products.

This represents the lowest order approximation in the calculation of the medium contribution Σ_V to the total self energy $\Sigma_V^{\text{tot}} = \Sigma_V + \Sigma_V^{(0)}$ of the vector meson V . In the next order the medium modification of the resonance spectral function including the modification of the resonance width due to the modifications of the products of the resonance decay should be taken into account. This leads to a self-consistency problem.

Let us now discuss each term of the *r.h.s.* of Eq. (4.11) separately:

- $\Gamma_{R \rightarrow N\pi}(\mu)$ is the energy dependent $N\pi$ partial decay width scaled according to the $N\pi$ phase space and the Blatt-Weisskopf suppression factor:

$$\Gamma_{R \rightarrow N\pi}(\mu) = \Gamma_{R \rightarrow N\pi}(M_R) \frac{M_R^2}{\mu^2} \left(\frac{q}{q_r} \right)^{(2l_\pi+1)} \left(\frac{\delta^2 + q_r^2}{\delta^2 + q^2} \right)^{(l_\pi+1)} \Theta(\mu - (m_N + m_\pi)) \quad (4.12)$$

where $q = q(\mu, m_N, m_\pi)$ and $q_r = q(M_R, m_N, m_\pi)$ are the pion (or nucleon) three-momenta in the rest-frame of the resonance with mass μ and M_R respectively and l_π is relative orbital angular momentum of the $N\pi$ system. The parameter δ in the cutoff function has a value $\delta = 0.3$ GeV for the $\Delta(1232)$ resonance and $\delta^2 = (M_R - m_N - m_\pi)^2 + \frac{\Gamma_R^{\text{tot}}(M_R)^2}{4}$ for the higher baryon resonances.

- $\Gamma_{R \rightarrow N\rho}(\mu)$ is the energy dependent $N\rho$ partial decay width given by

$$\Gamma_{R \rightarrow N\rho}(\mu) = \int_{4m_\pi^2}^{(\mu-m_N)^2} dM^2 \Gamma_{R \rightarrow N\rho}(\mu, M) A_\rho(M) \quad (4.13)$$

where $\Gamma_{R \rightarrow N\rho}(\mu, M)$ stands for the width of a resonance with mass μ decaying into a nucleon and a ρ meson with fixed mass M and

$$\mathcal{A}_\rho(M) = \frac{1}{\pi} \frac{m_\rho \Gamma_\rho^{\text{tot}}(M)}{(M^2 - m_\rho^2)^2 + (m_\rho \Gamma_\rho^{\text{tot}}(M))^2} \quad (4.14)$$

is the vacuum spectral function of the ρ meson. The integration over A_ρ is motivated by the fact that the ρ meson, being an unstable particle, does not exist as asymptotic state. The physical situation one has to evaluate is rather the one showed in Fig. 4.2.

³In the case of the $N^*(1535)$ resonance the $N\eta$ decay channel contributes to $\sim 45\%$ of the total width and Eq.(4.11) reads :

$$\Gamma_R^{\text{tot}}(\mu) = \Gamma_{R \rightarrow N\pi}(\mu) + \Gamma_{R \rightarrow N\eta}(\mu) + \Gamma_{R \rightarrow N\rho}(\mu) + \Gamma_{R \rightarrow N\omega}(\mu) + \delta\Gamma_R . \quad (4.10)$$

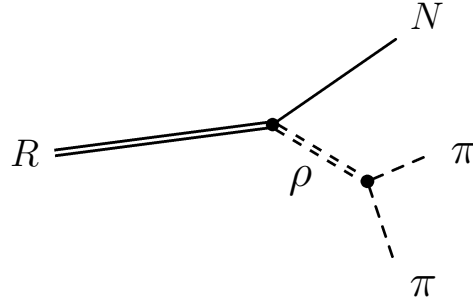


Figure 4.2: Decay of a resonance into a nucleon and two pions via an intermediate ρ meson.

- $\Gamma_{R \rightarrow N\omega}(\mu)$ is the energy dependent $N\omega$ partial decay width. A $\Delta \rightarrow N\omega$ decay would violate isospin conservation. Therefore one has $\Gamma_{R \rightarrow N\omega}(\mu) = 0$ for all resonances of the Δ family. For resonances $R = N^*$ one has:

$$\Gamma_{R \rightarrow N\omega}(\mu) = \int_{9m_\pi^2}^{(\mu - m_N)^2} dM^2 \Gamma_{R \rightarrow N\omega}(\mu, M) \mathcal{A}_\omega(M) \quad (4.15)$$

where $\Gamma_{R \rightarrow N\omega}(\mu, M)$ stands for the width of a resonance with mass μ decaying into a nucleon and a ω meson with fixed mass M and

$$\mathcal{A}_\omega(M) = \frac{1}{\pi} \frac{m_\omega \Gamma_\omega^{\text{tot}}(M)}{(M^2 - m_\omega^2)^2 + (m_\omega \Gamma_\omega^{\text{tot}}(M))^2} \quad (4.16)$$

is the vacuum spectral function of the ω meson.

- Finally, $\delta\Gamma_R = \Gamma_R^{\text{tot}}(M_R) - \Gamma_{R \rightarrow N\pi}(M_R) - \Gamma_{R \rightarrow N\rho}(M_R) - \Gamma_{R \rightarrow N\omega}(M_R)$ ensures the normalization of the total width at the resonance pole mass. The introduction of this term is due to the fact that in some cases the sum of the channels considered does not exhaust the total width.

At this point it is clear that the width $\Gamma_{R \rightarrow NV}(s, p^2)$ appearing in Eq. (4.9), (4.13)⁴, (4.15) is the key quantity which has to be determined in order to have access to the vector meson spectral functions in nuclear matter. As already shown in Chapter 3, the width $\Gamma_{R \rightarrow NV}(s, p^2)$ can be expressed in terms of the helicity amplitudes $A_{\frac{3}{2}}, A_{\frac{1}{2}}, S_{\frac{1}{2}}$ of the $R \rightarrow NV$ decay

$$\Gamma_{R \rightarrow NV}(s, p^2) = \frac{k}{8\pi s} \frac{2(A_{\frac{3}{2}}^2 + A_{\frac{1}{2}}^2 + S_{\frac{1}{2}}^2)}{(2J_R + 1)}. \quad (4.17)$$

These amplitudes have been parameterized within the relativistic approach developed in Ref. [34] and presented in Chapter 3.

The transverse and longitudinal self energies Σ_V^T and Σ_V^L can be then obtained by the following substitutions in (4.17)

$$\frac{2}{3}(A_{\frac{3}{2}}^2 + A_{\frac{1}{2}}^2 + S_{\frac{1}{2}}^2) \rightarrow (A_{\frac{3}{2}}^2 + A_{\frac{1}{2}}^2) \frac{1 + \cos^2 \theta}{2} + 2S_{\frac{1}{2}}^2 \frac{\sin^2 \theta}{2}, \quad (4.18)$$

$$\frac{2}{3}(A_{\frac{3}{2}}^2 + A_{\frac{1}{2}}^2 + S_{\frac{1}{2}}^2) \rightarrow 2S_{\frac{1}{2}}^2 \cos^2 \theta + (A_{\frac{3}{2}}^2 + A_{\frac{1}{2}}^2) \sin^2 \theta, \quad (4.19)$$

⁴Isospin symmetry implies $\Gamma_{\Delta^* \rightarrow N\rho} = \frac{3}{2}\Gamma_{\Delta^* \rightarrow N\rho^0}$ and $\Gamma_{N^* \rightarrow N\rho} = 3\Gamma_{N^* \rightarrow N\rho^0}$.

N^*	J^P	L_{212J}	Δ	J^P	L_{212J}
$N^*(1535)$	$\frac{1}{2}^-$	S_{11}	$\Delta(1620)$	$\frac{1}{2}^-$	S_{31}
$N^*(1650)$	$\frac{1}{2}^-$	S_{11}	$\Delta(1700)$	$\frac{3}{2}^-$	D_{33}
$N^*(1520)$	$\frac{3}{2}^-$	D_{13}	$\Delta(1232)$	$\frac{3}{2}^+$	P_{33}
$N^*(1440)$	$\frac{1}{2}^+$	P_{11}	$\Delta(1905)$	$\frac{5}{2}^+$	F_{35}
$N^*(1720)$	$\frac{3}{2}^+$	P_{13}	$\Delta(1950)$	$\frac{7}{2}^+$	F_{37}
$N^*(1680)$	$\frac{5}{2}^+$	F_{15}			

Table 4.1: List of the resonances included in the calculation of the helicity amplitudes entering into Eq. (4.17).

where θ is the polar angle of vector meson momentum in the c.m. system. The polarization averaged self energy Σ_V reads then

$$\Sigma_V = \frac{2\Sigma_V^T + \Sigma_V^L}{3}. \quad (4.20)$$

The resonances included in the calculation of the width $\Gamma_{R \rightarrow NV}(s, p^2)$ are listed in Table 4.1. The same relativistic approach and the same set of nucleon resonances used for this calculation has been successfully applied to dilepton and vector meson production in pp collisions [53, 78, 79].

4.2.1 Results

In the following we discuss first the results of the non self-consistent approach. Analogous lowest order calculations have been performed e.g. in Ref. [11].

ρ -meson spectral function

Fig. 4.3 shows the ρ spectral function in nuclear matter at nuclear saturation density $\rho_0 = 0.16 \text{ fm}^{-3}$. Longitudinal (\mathcal{A}^L) and transverse (\mathcal{A}^T) spectral functions are found to be rather similar. This means that unpolarized spectral functions can be used in the calculations of dilepton spectra.

We observe a slight upwards mass shift of the ρ and a substantial broadening. At low momenta the spectral functions show a clear two peak structure which vanishes with increasing vector meson momentum. The results shown in Fig. 4.3 are in qualitative and quantitative agreement with previous calculations based on the resonance model assumption [18]. Although the various approaches are based on different ways to describe the corresponding transition form factors, eVMD in the present case, and parameters are partially fixed in a different way, this fact demonstrates the stability of the essential features predicted by these types of models.

The emerging two-peak structure can be understood as follows: value and sign of the self energy $\Re\Sigma_V$ depend on the pole positions of the particular resonances. If the vector meson mass is small, the invariant mass of vector meson plus nucleon is below the pole

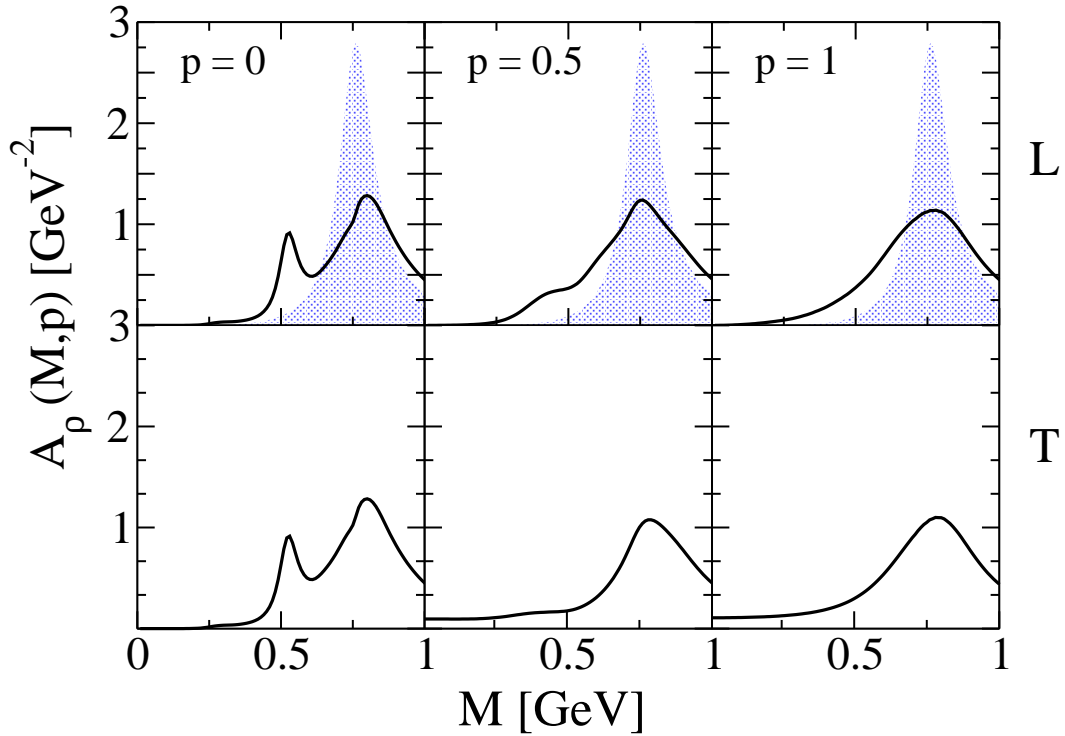


Figure 4.3: Longitudinal (L) and transverse (T) ρ spectral functions in nuclear matter at saturation density for various momenta p (in GeV). The shaded area shows the vacuum spectral function.

masses of the relevant nucleon resonances. Therefore the real part of the vector meson self energy is negative. This is a typical example for level repulsion (vector meson plus nucleon and nucleon resonance). Consequently, the factor $(m^2 - m_V^2 - \Re\Sigma_V)^2$ in the denominator of the vector meson spectral function, Eq. (4.1), is small or even equal to zero. Thus the first peak in the spectral function emerges at a vector meson mass around 0.5 GeV. The major contribution which generates the first peak comes from the $N^*(1520)$ which is in agreement with the findings reported in Ref. [18]. If the vector meson mass squared lies in the vicinity of its vacuum value m_V^2 , the invariant mass of vector meson plus nucleon lies above the pole masses of the relevant nucleon resonances and the real part of the vector meson self energy is positive. Therefore we obtain the second peak in the spectral function at a vector meson mass slightly above m_V . At high vector meson momenta the invariant mass of vector meson plus nucleon is always above the pole masses of the relevant nucleon resonances. As a result the spectral function has only one single peak slightly above m_V .

The dependence of the ρ meson spectral function on the nuclear density is shown in Fig. 4.4. The figure displays the unpolarized spectral function of a ρ meson at rest in the frame of the surrounding medium at ρ_0 and at $2\rho_0$ nuclear density. With increasing density we observe a further shift of strength away from the original pole mass, i.e. the first branch in the spectral distribution is slightly enhanced and even shifted to lower masses, while the second peak is slightly shifted upwards and additionally broadened.

In this context it should be noted that the resonance model predictions stand in contrast to the coupled channel calculations of Ref. [11] which predict no significant medium depen-

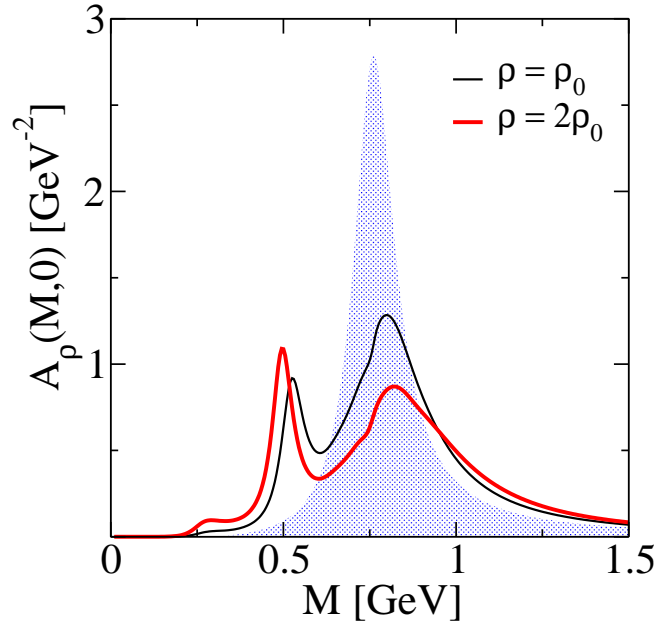


Figure 4.4: Unpolarized ρ meson spectral function at rest in nuclear matter at saturation density and twice saturation density. The shaded area displays the vacuum spectral function.

dence of the ρ , neither concerning a mass shift nor a broadening. The reason for the much less pronounced shift to lower masses resulting from the approach of [11] lies mainly in the much weaker coupling to the $N^*(1520)$ found in [11]. For this resonance the value of $\Gamma_{N\rho} \sim 2$ MeV [11] has to be compared to $\Gamma_{N\rho} \sim 25$ MeV from [34, 18]. The latter value is, however, in agreement with PDG [80] and the Manley/Saleski analysis [64].

ω -meson spectral function

For the ω we observe a behaviour which is qualitatively similar to that of the ρ -meson. Fig. 4.5 shows the ω spectral function in nuclear matter at nuclear saturation density. Longitudinal (\mathcal{A}^L) and transverse (\mathcal{A}^T) spectral functions are again found to be rather similar. In both cases the ω pole mass is slightly shifted upwards and the ω is substantially broadened around its quasi-particle pole. At ρ_0 we obtain an in-medium ω width of 300 MeV.⁵

As in the case of the ρ , the coupling to low lying resonances leads to the appearance of a first peak in the spectral function which lies around $0.5 \div 0.55$ GeV. With increasing momentum this peak is washed out and disappears finally.

The first branch in the spectral distribution is mainly generated by the $N^*(1535)$ resonance. As discussed in detail in Refs. [34, 78], in the NRD+eVMD model a strong $N^*(1535)N\omega$ coupling is implied by the available electro- and photoproduction data. However, the $N\omega$ decay of this resonance has not been measured directly, and therefore input from quark model predictions had to be used to fix the entire set of eVMD model parameters. Nevertheless, within such a procedure a strong $N^*(1535)N\omega$ coupling seems practically unavoidable. In $pp \rightarrow pp\omega$ production the large $N^*(1535)N\omega$ decay mode leads to substantial contributions

⁵The width has been evaluated as $-\Im\Sigma_{\omega}^{\text{tot}}(m_{\omega}, \mathbf{p} = 0)/m_{\omega}$.

in a kinematical regime where the ω is far off-shell, i.e. at small invariant masses. This is reflected in an enhancement in the cross section around threshold [78]. Existing data [81, 82, 83] do, however, not rule out such a behaviour. A closer inspection of the experimentally observed background contributions may provide important information concerning this question.

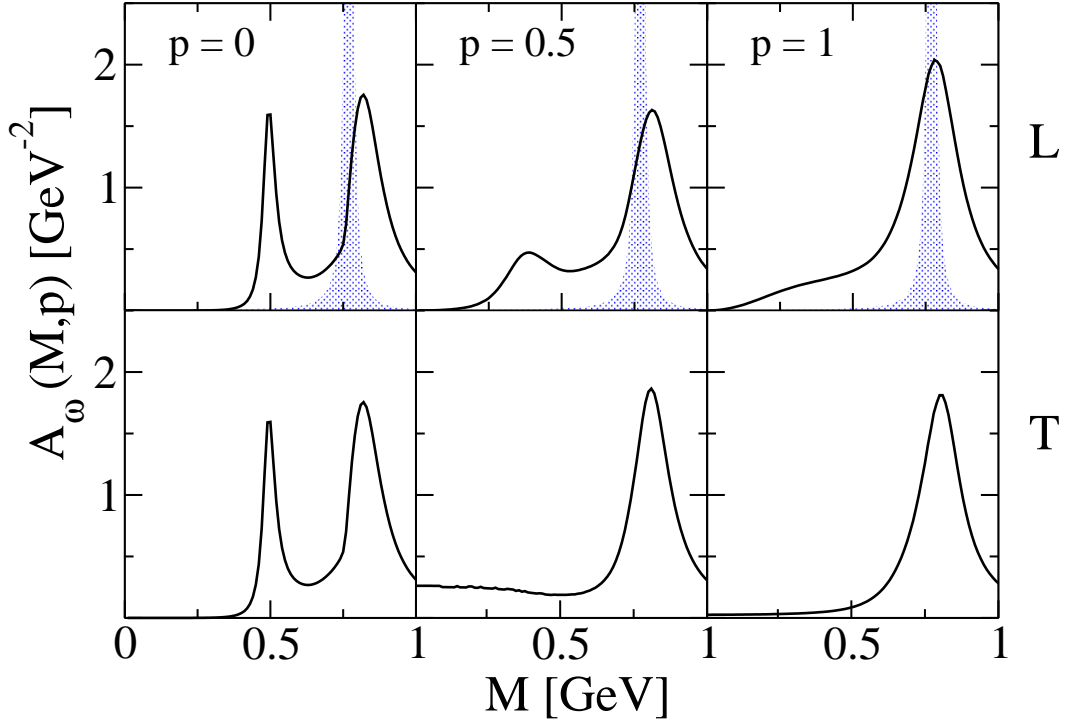


Figure 4.5: Longitudinal (L) and transverse (T) ω spectral functions in nuclear matter at saturation density for various momenta p (in GeV). The shaded area shows the vacuum spectral function.

The nuclear matter density dependence of the ω meson spectral function is shown in Fig. 4.6. The figure shows the unpolarized spectral function at rest at ρ_0 and $2\rho_0$ nuclear density. As in the case of the ρ meson we observe a shift of the second peak which belongs to the original ω pole towards higher masses with increasing density while the first peak is shifted to lower masses.

4.3 In-medium self energy: non-resonant contributions

Up to now we have not discussed possible non-resonant contributions to the forward vector meson-nucleon scattering. The reason is twofold: first of all, we cannot fix the non-resonant amplitudes with the same accuracy as the resonant ones. Secondly, if we fix them with the available accuracy, we would find that non-resonant amplitudes approximately cancel each other in the sum. For example, in the case of the ρ meson there exist the Compton scattering amplitude, which gives a positive contribution to the real part of the ρ meson self energy, and the amplitude due to σ meson exchange, which gives a negative contribution to it (the latter is of the same origin as the attractive part of NN interaction). The unknown $\rho\rho\sigma$ coupling

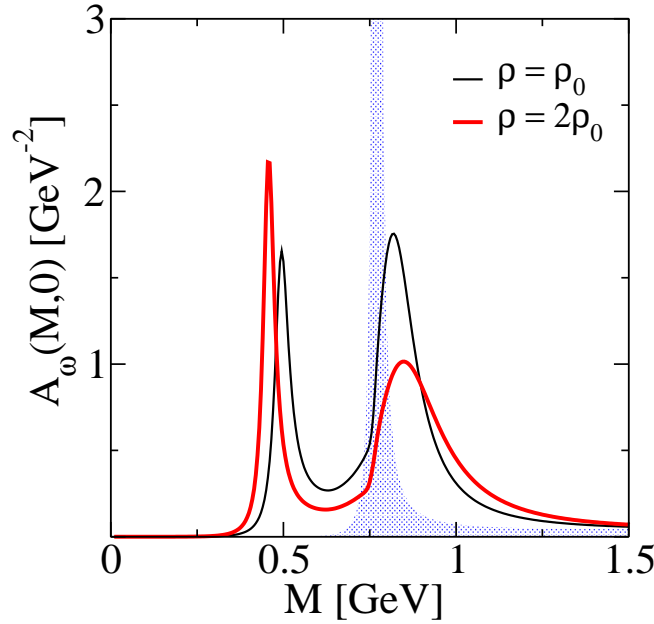


Figure 4.6: Unpolarized ω meson spectral function at rest in nuclear matter at saturation density and twice saturation density. The shaded area displays the vacuum spectral function.

constant can be extracted from the width of the $\rho^0 \rightarrow \pi^+\pi^-\pi^+\pi^-$ decay if one assumes that this decay goes over an intermediate $\rho^0\sigma$ state.

Details on the calculation of the two contributions from Compton scattering (Σ^{Compt}) and σ -exchange ($\Sigma^{\sigma\text{-exch}}$) are given in Appendix C.1. For the estimate shown in Fig. 4.7 the corresponding $NN\rho$ tensor coupling and $NN\sigma$ coupling strength were taken from the Bonn one-boson-exchange model [84] for nucleon-nucleon scattering ($g_{NN\rho} = 19.8$, $g_{NN\sigma} = 10$). The error band for $\Sigma^{\sigma\text{-exch}}$ is due to the relatively large uncertainty in the four- π decay of the ρ meson

$$BR(\rho^0 \rightarrow \pi^+\pi^-\pi^+\pi^-) = (1.8 \pm 0.9) \times 10^{-5}.$$

However, from Fig. 4.7 one sees that the two contributions from Compton scattering (Σ^{Compt}) and σ -exchange ($\Sigma^{\sigma\text{-exch}}$) are of different sign and comparable magnitude. For the mean values of the branching ratio $BR(\rho^0 \rightarrow \pi^+\pi^-\pi^+\pi^-)$ they almost cancel out completely and changes of the ρ meson spectral function are insignificant.

To account for non-resonant contributions to the ω spectral function within the present scheme we assume an $\omega\omega\sigma$ coupling three times larger than that for $\rho\rho\sigma$ which is motivated by the comparison with the two pion coupling. The $NN\omega$ vector coupling ($g_{NN\omega} = 15.9$) is again taken from the Bonn potential [84].

4.3.1 Results

ρ meson spectral function

The influence of the non-resonant contributions on the ρ meson spectral function is displayed in Fig. 4.8 and Fig. 4.9. Fig. 4.8 shows the longitudinal and transverse ρ spectral function

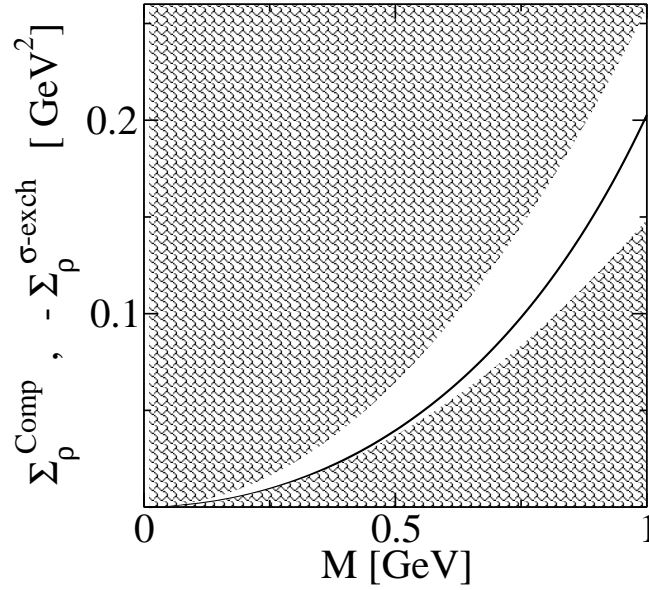


Figure 4.7: Non-resonant contributions to ρ meson self energy from Compton scattering amplitude (solid line) and from the amplitude due to exchange by σ meson (unshaded region). The region corresponds to the error in the branching ratio $Br(\rho^0 \rightarrow \pi^+\pi^-\pi^+\pi^-) = (1.8 \pm 0.9) \times 10^{-5}$.

in nuclear matter at nuclear saturation density, while Fig. 4.9 shows the unpolarized spectral function of a ρ meson at rest in nuclear matter at saturation density and twice saturation density. The spectral distributions obtained from calculations which take into account the non-resonant contributions to the forward vector meson-nucleon scattering are compared to the corresponding ones, presented in Section 4.2, obtained from calculations which take only resonant contributions into account. As can be seen, the addition of non-resonant contributions does not appreciably modify the ρ meson spectral function.

ω -meson spectral function

In the case of the ω the influence of non-resonant contributions is found to be more pronounced than in the case of the ρ , as shown in Fig. 4.10 and Fig. 4.11. The non-resonant contributions tend to increase the repulsive mass shift of the ω pole and they strongly suppress the first peak in the spectral function. However, the qualitative features of the spectral distributions are not changed.

Comparing with other works, it should be mentioned that in the pure resonance model approach of Ref. [74] no such additional peak has been observed. The ω meson spectral functions obtained within the coupled-channel approach of Ref. [11] and within the coupled-channel K -matrix of Ref. [19] have qualitative similarity with those from the present approach.

All approaches come practically to the same conclusions: an upward mass shift, a broadening of the ω and the appearance of an additional branch in the ω spectral function.

This branch appears at the same position and is in both cases generated by the $N^*(1535)$. However, in all approaches the ω survives as a quasi-particle, at least at moderate densities

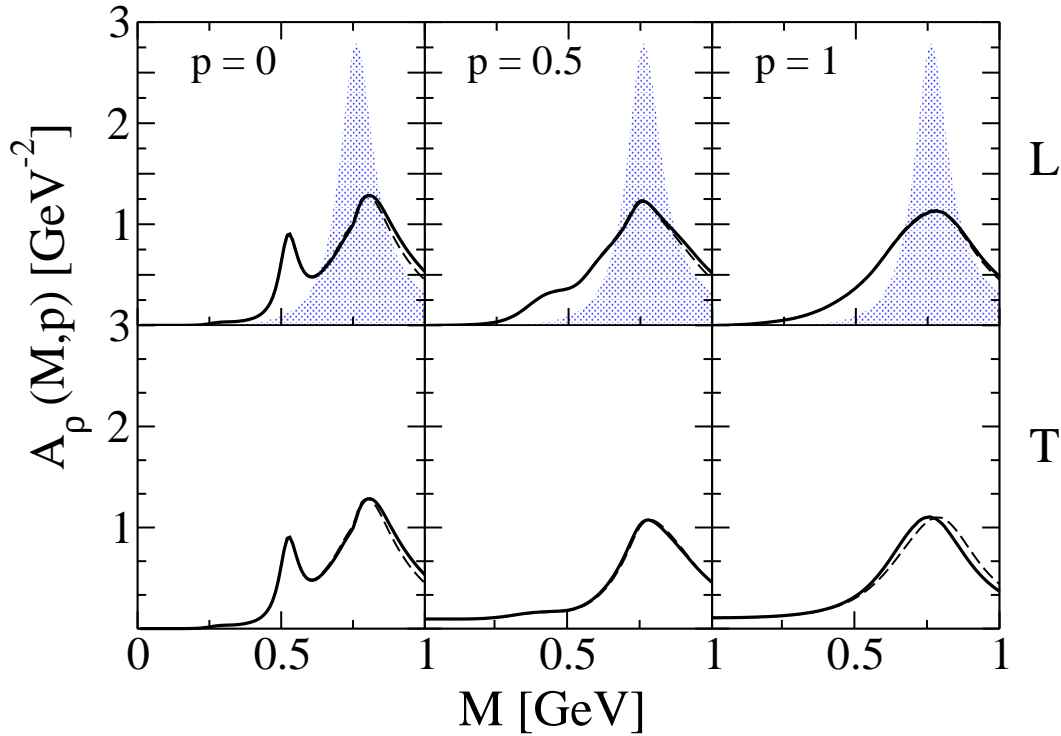


Figure 4.8: Longitudinal (L) and transverse (T) ρ spectral functions in nuclear matter at saturation density for various momenta p (in GeV). Dashed lines stand for the resonance approximation, solid lines represent calculations where non-resonant contributions have been included as well. The shaded area shows the vacuum spectral function.

up to ρ_0 , i.e. there the spectral function is still dominated by the main branch corresponding to the original ω pole. The predictions for the density dependence of the spectral function are similar on a qualitative level, i.e. when going from one to two times nuclear density the suppression of the branch corresponding to the ω pole is of similar size.

However, on a quantitative level the models come to different conclusions. While the broadening of the ω is similar in Refs. [11] and [19] the mass shift is much larger in Ref. [11] ($\Delta m_\omega \sim 46$ MeV at ρ_0) than in Ref. [19] ($\Delta m_\omega \sim 10$ MeV at ρ_0). In the present case the in-medium modifications of the ω meson are even more pronounced compared to [11, 19], i.e. the broadening and the upwards mass shift are larger ($\Delta m_\omega \sim 75$ MeV at ρ_0).

A comparison to predictions from QCD sum rules [85, 86] turns out to be difficult since the ω properties depend strongly on higher order condensates. Sum rules leave space for upward and downward mass shifts and the parameters related to the higher order terms in the operator product expansion have finally to be fixed from experiments [86]. Moreover, in these approaches it is assumed that the ω maintains its quasi-particle properties. However, due to the distinct two-peak structure of the present spectral distributions it is not possible to assign a common mass shift to an ω quasi-particle pole.

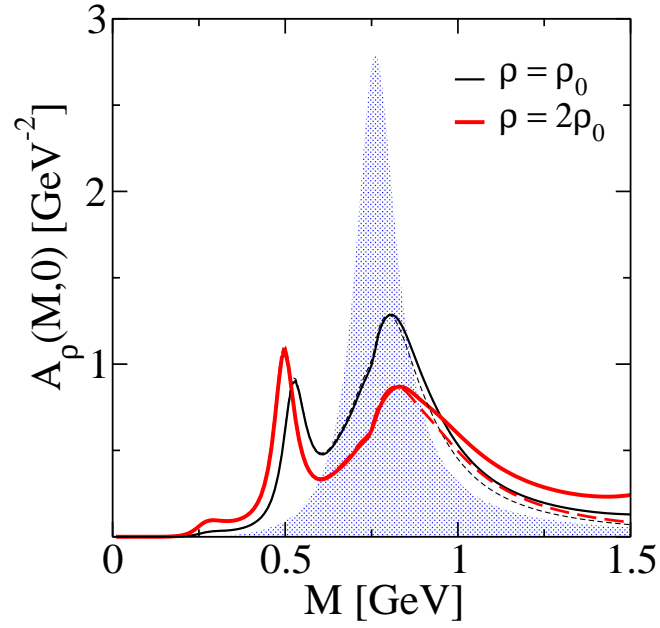


Figure 4.9: Unpolarized ρ meson spectral function at rest in nuclear matter at saturation density and twice saturation density. Dashed lines stand for the resonance approximation, solid lines represent calculations where non-resonant contributions have been included as well. The shaded area displays the vacuum spectral function.

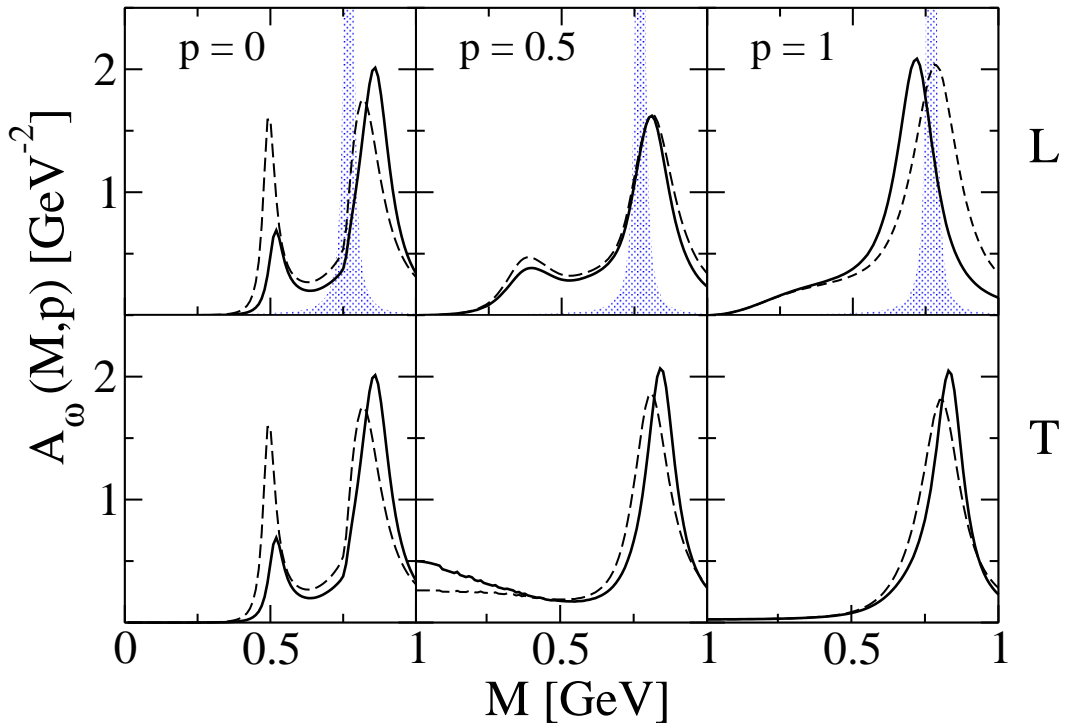


Figure 4.10: Longitudinal (L) and transverse (T) ω spectral functions in nuclear matter at saturation density for various momenta p (in GeV). Dashed lines stand for the resonance approximation, solid lines represent calculations where non-resonant contributions have been included as well. The shaded area shows the vacuum spectral function.

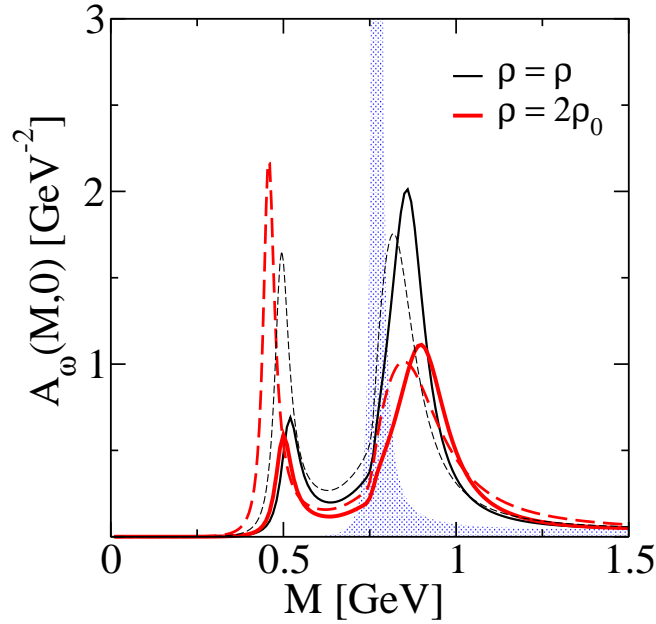


Figure 4.11: Unpolarized ω meson spectral function at rest in nuclear matter at saturation density and twice saturation density. Dashed lines stand for the resonance approximation, solid lines represent calculations where non-resonant contributions have been included as well. The shaded area displays the vacuum spectral function.

4.4 In-medium resonances: role of self-consistency

As the next step, we took into account the changes induced by the in-medium vector mesons on the total width of the nucleon resonances. This leads to a self-consistent determination of the self energies of the vector mesons in nuclear matter.

The first iteration corresponds to the determination of the self energies of the ρ and ω mesons from Eqs. (4.2-4.9) considering vacuum spectral functions for the decay products of each nucleon resonance in Eq. (4.9). Thus, one assumes that the decay of each resonance is not modified by the medium. In fact, the results shown in the previous sections correspond to this first iteration, if considered in the context of a self-consistent calculation.

In the second iteration, one determines the total width of the nucleon resonances from Eq. (4.11) inserting this time the in-medium spectral functions of the vector mesons obtained from the first iteration and calculates again the self energies of the vector mesons with the use of Eqs. (4.2-4.9). Thus, one includes the modification of the resonance width due to the modifications of the resonance decay products.

The procedure is repeated until convergence. We found that the convergence is obtained already after the third iteration.

As a side result of our self-consistent calculation, we find that the widths of the nucleon resonances are enhanced in medium due to the fact that the vector meson spectral functions show a significant spectral strength at small invariant masses. A similar outcome emerged from the analysis performed in Ref. [9].

The resulting unpolarized vector meson spectral functions are shown in Fig. 4.12 and Fig. 4.13 for the ρ and ω meson respectively. They refer to saturation density. We observe

that the self-consistent calculation leads predominantly to a reduction of the lower mass peak. This result is in qualitative agreement with the findings of Ref. [18], where the role of a self-consistent iteration scheme on the ρ meson spectral function has been investigated.

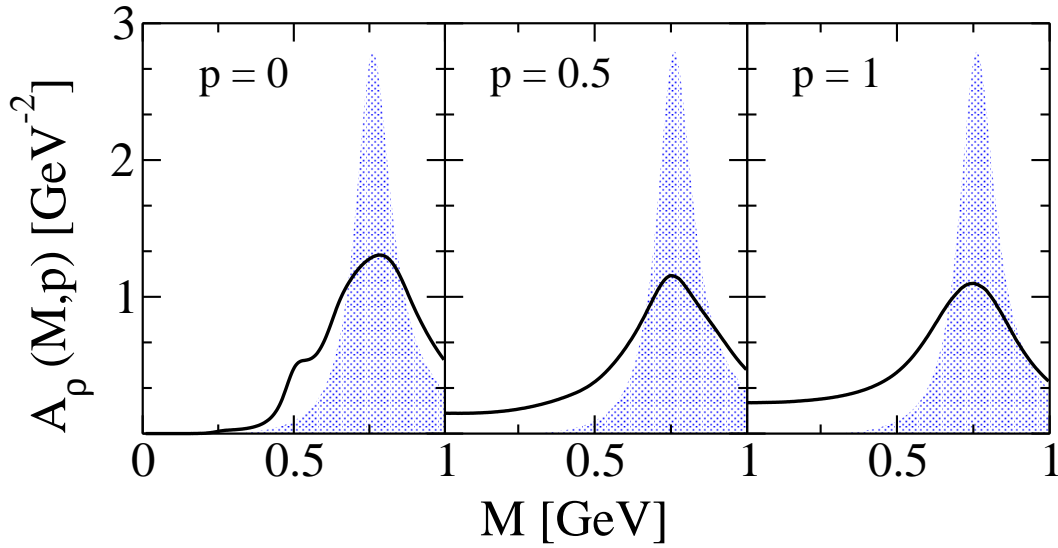


Figure 4.12: Unpolarized spectral functions of the ρ meson in nuclear matter at saturation density for various momenta p (in GeV). Modification of the resonance width due to the modification of the spectral properties of the vector mesons are taken into account and a self-consistent calculation is performed. The shaded area shows the vacuum spectral function.

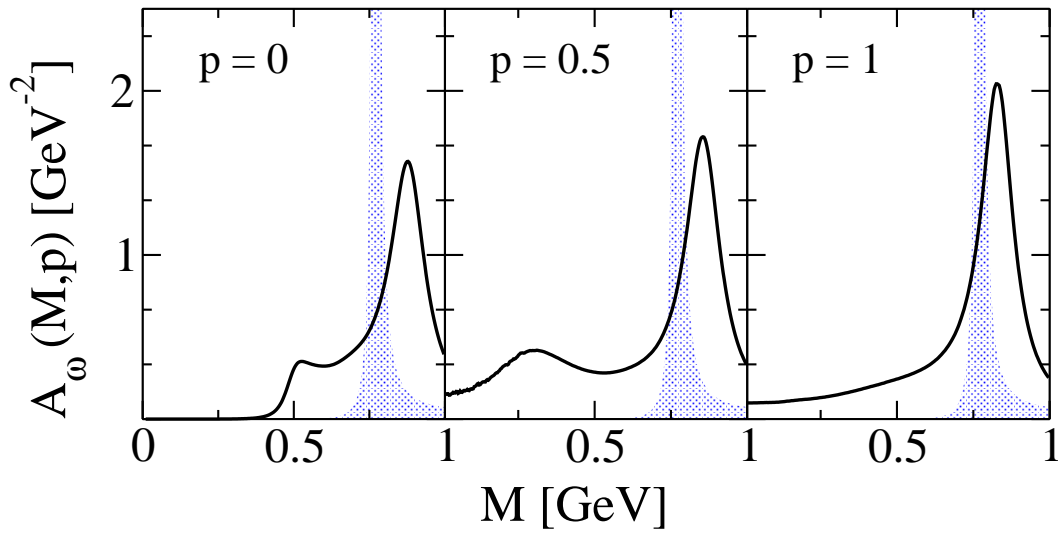


Figure 4.13: Unpolarized spectral functions of the ω meson in nuclear matter at saturation density for various momenta p (in GeV). The broadening of the nucleon resonance widths induced by the in-medium spectral properties of the vector mesons is taken into account and a self-consistent calculation is performed. The shaded area shows the vacuum spectral function.

4.5 Dropping mass scenario

As already anticipated in the introduction, the search for signatures of a dropping meson mass was mainly triggered by the theoretical works of Brown and Rho [7] and of Hatsuda and Lee [20] published at the beginning of the '90s. The mean field based analysis of effective Lagrangians performed by Brown and Rho suggested that the meson masses decrease with the density according to a scaling law that was named, after the authors, ‘‘Brown-Rho scaling’’ and reads

$$\Phi(\rho) \equiv \frac{f_\pi^*}{f_\pi} = \frac{m_N^*}{m_N} = \frac{m_\rho^*}{m_\rho} = \frac{m_\omega^*}{m_\omega}. \quad (4.21)$$

Here f_π is the pion decay constant, m_N the nucleon mass, m_ρ and m_ω the ρ and ω meson masses respectively; f_π^* , m_N^* , m_ρ^* , m_ω^* denote the correspondent density dependent quantities. Since one has $m_N^*/m_N \approx 0.8$ at $\rho = \rho_0$, Eq. (4.21) implies that the vector meson masses should decrease to 80% of their vacuum value already at saturation density.

This scaling law found support in the QCD sum rule calculations performed by Hatsuda and Lee [20], who extracted the medium dependence of the non-strange vector meson masses as

$$\frac{m_{\rho,\omega}^*}{m_{\rho,\omega}} = 1 - (0.18 \pm 0.06) \frac{\rho}{\rho_0}. \quad (4.22)$$

However, in deriving Eq. (4.22) the resonance part of the in-medium spectral density was parametrized, in analogy to the vacuum case, by a delta function (narrow width approximation)

$$\rho_V(q_0) \sim \delta(q_0^2 - m_V^{*2}) + \text{continuum}, \quad (4.23)$$

which means that Eq. (4.22) was obtained and *is valid* in the limit of narrow meson width.

This issue was later investigated by Leupold *et al.* [21] who replaced the delta function parametrization by a schematic Breit-Wigner spectral function. This analysis pointed out that QCD sum rules do not give any stringent prediction for a dropping of vector masses when taking into account a possible broadening of the meson widths. A significant broadening of the strength distributions is, however, expected by hadronic model calculations and, at least for the ρ meson, experimentally confirmed by the measurements of the NA60 collaboration [25]. We recall that the same measurement seems to rule out a simple dropping mass scenario for the ρ meson.

Chapter 5

Dilepton production in HIC

5.1 The QMD transport model

The Quantum Molecular Dynamics (QMD) model is a microscopic dynamical n -body approach to heavy ion reactions which simulates the whole time evolution of the nucleus-nucleus collision on an event by event basis. The ability of QMD to simulate individual collision events significantly facilitates the contact with actual collision experiments and has been a main reason for extensive usage of this approach for confronting theory with experiment.

Many versions of the QMD approach have been developed, most of them being rooted in the code originally developed by Aichelin and coworkers [87]. Extensions to relativistic kinematics have been made, most notably Relativistic Quantum Molecular Dynamics (RQMD) [88, 89] and further extensions towards ultrarelativistic collisions, named UrQMD [90, 91], have been widely applied to relativistic nuclear collisions and have had considerable success in reproducing many aspects of the data.

For our investigation of dilepton production in heavy ion collisions at intermediate energies we employ a particular realization of the QMD model currently used in Tübingen: the Tübingen Relativistic Quantum Molecular Dynamics (Tübingen RQMD). The Tübingen RQMD transport code [92] applied for the present investigations is based on relativistic kinematics but not formulated covariantly. Thus, despite the analogy in the name, it differs from the RQMD model originally developed by Sorge et al. [88].¹ Besides the code used

¹The Relativistic Quantum Molecular Dynamics (RQMD), as originally developed by Sorge et al. [88], represents a fully covariant description of a classical N -particle system based on Dirac's Constrained Hamilton Dynamics [93]. The N -body Hamiltonian is thereby expressed by $2N - 1$ constraints ϕ_i ,

$$H = \sum_{i=1}^{2N-1} \lambda_i \phi_i , \quad (5.1)$$

where the first N constraints are given by the mass-shell conditions and the remaining $N - 1$ constraints serve to fix the world lines of the particles, i.e. to ensure world line invariance and causality. A final time constraint which does not enter the Hamiltonian fixes an overall evolution time of the system.

The complete set of $2N - 1$ constraints generates the equations of motions for canonically conjugate coordinates and momenta,

$$dq_i^\mu / d\tau = \{H, q_i^\mu\} \quad , \quad dp_i^\mu / d\tau = \{H, p_i^\mu\} \quad , \quad (5.2)$$

here, a fully covariant RQMD code has been developed by the Tübingen group in the early 1990s [89] and has even been extended to the application of relativistic scalar-vector mean field dynamics [94] going thereby beyond the the original RQMD approach of Ref. [88]. However, the application at low relativistic energies (SIS) revealed insignificant differences between the two approaches, QMD with relativistic kinematics and full RQMD, what concerns physical observables, in the latter case, however, by the price of extensive numerical effort. Therefore the present as well as most previous investigations on particle production are based on the standard QMD (relativistic kinematics) approach. The only mesons included dynamically are the pions, but heavier mesons (K , η , ρ , ω , ...) are treated perturbatively. The model is particular suited for studies of subthreshold meson production at SIS energies. It has been extensively applied to kaon production at subthreshold energies [95, 96] and has also been used for dilepton production [38]. For the latter application, the Tübingen model has been extended to include all nuclear resonances with masses below 2 GeV, in total 11 N^* and 10 Δ resonances [38].

We present below some basic aspects of the QMD model. For a more detailed description we refer to Ref. [87]. The particular realization of the Tübingen RQMD model used for the description of dilepton production in heavy ion collisions will be discussed later.

5.1.1 Basic structure of QMD

In the following the QMD approach is sketched in its original non-relativistic formulation.

In QMD each nucleon is represented by a coherent state of the form

$$\psi_i(\mathbf{x}, \mathbf{r}_i, \mathbf{p}_i, t) = \left(\frac{2}{\pi L} \right)^{3/4} e^{-\frac{(\mathbf{x}-\mathbf{r}_i(t))^2}{L}} e^{i\mathbf{p}_i(t) \cdot \mathbf{x}} \quad (5.3)$$

characterized by the 6 time dependent parameters $\mathbf{r}_i(t)$, $\mathbf{p}_i(t)$. The width L is related to the extension of the wave packet in the phase space and is kept constant in the calculations ($L = 4.33 \text{ fm}^2$).² The nuclear wave function is assumed to be the direct product on n coherent states (5.3)

$$\Psi = \prod_i \psi_i(\mathbf{x}, \mathbf{r}_i, \mathbf{p}_i, t) . \quad (5.4)$$

Thus the standard QMD neglects antisymmetrization. The computational time scales like $(A_P + A_T)^4$, being A_T and A_P the number of nucleons of the target and projectile nucleus respectively, if a Slater determinant is used, while in QMD it scales like $(A_P + A_T)^2$. First successful attempts to simulate heavy ion reactions with antisymmetrized states have been performed within the Fermionic Molecular Dynamics (FMD) [97, 98, 99, 100, 101] and the

where $\{\cdot, \cdot\}$ denotes the Poisson bracket. To compute the evolution of the system, i.e. integrating the set of above equations of motion (5.2), one must determine the unknown Lagrange multipliers $\lambda_i(\tau)$. While Hamilton Constrained Dynamics provides the most exact solution toward the relativistic N -body problem, the numerical effort is prohibitively large since the computational time scales with N^3 .

²The width of a coherent state $L = L(t)$ increases as function of time if propagated with the free Schrödinger equation. In the QMD approach the width is kept constant, i.e. no spreading of the wave function is allowed. This is motivated by the observation that otherwise the nucleus as a whole would spread in coordinate space as a function of time.

Antisymmetrized Molecular Dynamics (AMD) [102, 103, 104] approaches. In both realizations the system is represented by a Slater determinant and the equations of motion are derived from the time-dependent variational principle. The FMD approach, though originally launched for applications in nuclear collision dynamics, has become one of the most promising quantum many-body approaches for nuclear structure studies. It permits the use of realistic nuclear forces and tames the repulsive hard core by use of the unitary correlation operator method [105, 106]. AMD differs from FMD mainly in that stochastic terms have been added to the equation of motion so that many configurations can appear through the reaction dynamics. The introduction of two-nucleon collisions is similar to QMD.

³ AMD has been successfully applied to fragmentation reactions, such as central collisions in the energy region of several tens of MeV/nucleon for light and heavy systems [107, 108]. While these treatments are much better grounded in basic theory, they are relatively complicated to apply and, as a result, their applications have been considerably more limited relative to the range of observables calculated with the Boltzmann and QMD approaches. Moreover, these refinements, though conceptually important, are less urgent in the context of high energy collisions where these quantum effects are less apparent.

The initial values of the parameters are chosen in QMD in such a way that the ensemble of $A_T + A_P$ nucleons gives a proper density distribution as well as a proper momentum distribution of the target and projectile nuclei.

The Wigner transform of the coherent states (5.3) are Gaussians in momentum and coordinate space. The Wigner distribution function f_i of the nucleon i reads:

$$f_i(\mathbf{x}, \mathbf{p}, t) = \frac{1}{(2\pi)^3} \int e^{-i\mathbf{p}\cdot\mathbf{x}_{12}} \psi_i(\mathbf{x} + \mathbf{x}_{12}/2, t) \psi_i^*(\mathbf{x} - \mathbf{x}_{12}/2, t) d^3x_{12} \quad (5.5)$$

$$= \frac{1}{\pi^3} e^{-(\mathbf{x}-\mathbf{r}_i(t))^2 \frac{2}{L}} e^{-(\mathbf{p}-\mathbf{p}_i(t))^2 \frac{L}{2}}. \quad (5.6)$$

The n -body Wigner distribution $f^{(N)}$ is the direct product of the Wigner distributions of the n coherent states. Therefore the single particle density in coordinate space

$$\rho(\mathbf{x}, t) = \sum_{i=1}^N \delta(\mathbf{x} - \mathbf{x}_i) \int f^{(N)}(\mathbf{x}_1, \dots, \mathbf{x}_N, \mathbf{p}_1, \dots, \mathbf{p}_N, t) d^3p_1 \dots d^3p_N d^3x_1 \dots d^3x_N \quad (5.7)$$

results ($N = A_P + A_T$)

$$\rho(\mathbf{x}, t) = \sum_{i=1}^{A_P+A_T} |\Psi_i(\mathbf{r}, t)|^2 = \sum_{i=1}^{A_P+A_T} \left(\frac{2}{\pi L} \right)^{3/2} e^{-\frac{(\mathbf{x}-\mathbf{r}_i(t))^2}{L/2}}. \quad (5.8)$$

The equations of motion of the many-body system are calculated by means of a variational principle. For the coherent states (5.3) and a Hamiltonian of the form $H = \sum_i T_i +$

³A technical difference originates due to the antisymmetrization. The antisymmetrization implies that the wave packet centroids cannot be interpreted as the positions and momenta of nucleons. Rather, the physical coordinates are introduced as nonlinear functions of the centroids [103] and the two-nucleon collisions are performed by using these physical coordinates. There then appear Pauli-forbidden phase-space regions coordinates into which the physical coordinates will never enter, for any values of the centroid variables. These regions are regarded as Pauli-blocked and not allowed as final state of a collision. Another difference from QMD is the fact that the physical momentum in AMD is the momentum centroid of a Gaussian phase space distribution, while the momentum variable in QMD usually represents the definite momentum of a nucleon.

$\frac{1}{2} \sum_{ij} V_{ij}$, where T_i is the kinetic energy and V_{ij} the mutual interaction between two nucleons, the variation yields [87, 90, 109]:

$$\dot{\mathbf{r}}_i = \frac{\mathbf{p}_i}{m} + \nabla_{\mathbf{p}_i} \sum_j \langle V_{ij} \rangle = \nabla_{\mathbf{p}_i} \langle H \rangle \quad (5.9)$$

$$\dot{\mathbf{p}}_i = -\nabla_{\mathbf{r}_i} \sum_{j \neq i} \langle V_{ij} \rangle = -\nabla_{\mathbf{r}_i} \langle H \rangle \quad (5.10)$$

with $\langle V_{ij} \rangle = \int d^3x_i d^3x_j \Psi_i^* \Psi_j^* V(x_i, x_j) \Psi_i \Psi_j$. These are the time evolution equations which are solved numerically. Thus the variational principle yields the same time evolution of the parameters \mathbf{r}_i , \mathbf{p}_i as one would obtain by moving the centroids of the wave function (5.3) according to the classical Hamilton equations:

$$\dot{\mathbf{p}}_i = -\frac{\partial \langle H \rangle}{\partial \mathbf{r}_i} \quad \text{and} \quad \dot{\mathbf{r}}_i = \frac{\partial \langle H \rangle}{\partial \mathbf{p}_i}. \quad (5.11)$$

The expectation value of the QMD Hamiltonian

$$\langle H \rangle = \sum_i \frac{p_i^2}{2m_i} + \sum_i \sum_{j>i} \int f_i(\mathbf{x}_i, \mathbf{p}_i, t) V^{ij} f_j(\mathbf{x}_j, \mathbf{p}_j, t) d^3x_i d^3x_j d^3p_i d^3p_j \quad (5.12)$$

is obtained by the convolution of the distribution functions f_i and f_j with the mutual interaction V^{ij} between the nucleons i and j . The potential V^{ij} contains a contact Skyrme-type interaction supplemented by a phenomenological momentum dependence V_{ij}^{Sk} , a finite range Yukawa-type potential V_{ij}^{Yuk} and an effective Coulomb interaction V_{ij}^{Coul}

$$V^{ij} = V_{\text{Skyrme}}^{ij} + V_{\text{Yuk}}^{ij} + V_{\text{Coul}}^{ij}. \quad (5.13)$$

The Yukawa potential

$$V_{\text{Yuk}}^{ij} = t_5 \frac{\exp\{-|\mathbf{x}_i - \mathbf{x}_j|/\mu\}}{|\mathbf{x}_i - \mathbf{x}_j|/\mu} \quad (5.14)$$

mainly serves to improve the surface properties and the stability of the initialized nuclei when used in heavy ion collisions. The Coulomb interaction between the nucleons is taken into account through the effective potential:

$$V_{\text{Coul}}^{ij} = \frac{Z_{\text{eff}}^2 e^2}{|\mathbf{x}_i - \mathbf{x}_j|}. \quad (5.15)$$

where the effective charge $Z_{\text{eff}} = (Z_T + Z_P)/(A_P + A_T)$ is attributed to all nucleons.

The Skyrme-type potential, written in the form of two-particle interactions, reads:

$$V_{\text{Skyrme}}^{ij} = t_1 \delta(\mathbf{x}_i - \mathbf{x}_j) + t_\gamma \delta(\mathbf{x}_i - \mathbf{x}_j) (\rho_{\text{int}}^{ij})^{\gamma-1}(\mathbf{x}_i) + t_3 \ln^2(1 + t_4 (\mathbf{p}_i - \mathbf{p}_j)^2) \delta(\mathbf{x}_i - \mathbf{x}_j). \quad (5.16)$$

Let us clarify the form of expression (5.16). For simplicity we neglect the momentum dependent part of the interaction and discuss only the static part. Let us start with the local Skyrme-type interaction

$$V_{\text{Skyrme}}(\mathbf{x}_1, \mathbf{x}_2, \mathbf{x}_3) = t_1 \delta(\mathbf{x}_1 - \mathbf{x}_2) + t_2 \delta(\mathbf{x}_1 - \mathbf{x}_2) \delta(\mathbf{x}_1 - \mathbf{x}_3). \quad (5.17)$$

The folding over the Wigner distributions f_i and f_j yields the expectation value:

$$\langle V^{ij(2)} \rangle = \int f_i(\mathbf{x}_i, \mathbf{p}_i, t) f_j(\mathbf{x}_j, \mathbf{p}_j, t) V^{(2)}(\mathbf{x}_i, \mathbf{x}_j) d^3x_i d^3x_j d^3p_i d^3p_j \quad (5.18)$$

$$\langle V^{ijk(3)} \rangle = \int f_i(\mathbf{x}_i, \mathbf{p}_i, t) f_j(\mathbf{x}_j, \mathbf{p}_j, t) f_k(\mathbf{x}_k, \mathbf{p}_k, t) V^{(3)}(\mathbf{x}_i, \mathbf{x}_j, \mathbf{x}_k) d^3x_i d^3x_j d^3x_k d^3p_i d^3p_j d^3p_k \quad (5.19)$$

where $V^{(2)}$ and $V^{(3)}$ are the two- and three-body parts of the interaction defined in Eq. (5.17). Performing the integration one sees that the two-body potential for the particle i , $U^{i(2)} = \sum_{j; j \neq i} \langle V^{ij(2)} \rangle$, can be written as

$$U^{i(2)} = t_1 \rho_{\text{int}}^i(\mathbf{r}_i) \quad (5.20)$$

where the interaction density $\rho_{\text{int}}^i(\mathbf{r}_i)$ is

$$\rho_{\text{int}}^i(\mathbf{r}_i) = \frac{1}{(\pi L)^{3/2}} \sum_{j \neq i} e^{-(\mathbf{r}_i - \mathbf{r}_j)^2/L}. \quad (5.21)$$

As we have seen, the interaction density arises due to the folding of the two Gaussian wave packets with fixed width in coordinate space. This density has the same form as the single particle density (5.8), but omits the nucleon at the location j and has twice the width of the single particle density. The three-body potential for the particle i , $U^{i(3)} = \sum_{j,k; j \neq i, k \neq i} \langle V^{ijk(3)} \rangle$, can be approximated as a function of $\rho_{\text{int}}^i(\mathbf{r}_i)$ [87]:

$$U^{i(3)} \approx t_2 \left(\frac{2}{\pi L} \right)^3 3^{-\frac{3}{2}} \sum_{j,k; j \neq i, k \neq i} e^{-\frac{(\mathbf{r}_i - \mathbf{r}_j)^2 + (\mathbf{r}_i - \mathbf{r}_k)^2}{L}} \propto t_2 [\rho_{\text{int}}^i(\mathbf{r}_i)]^2. \quad (5.22)$$

The quadratic density dependence of the three particle term (5.22) may be generalized to arbitrary exponents for the density:

$$U^{i(3)} \propto t_2 [\rho_{\text{int}}^i(\mathbf{r}_i)]^2 \rightarrow t_\gamma [\rho_{\text{int}}^i(\mathbf{r}_i)]^\gamma. \quad (5.23)$$

This is important for the investigation of the influence which different compressibilities, i.e. different equations of state, have on observables. Then, however, the interpretation of $U^{i(3)}$ as three-body interaction is no longer valid.

In nuclear matter, where the density is constant, one convolutes the potentials with the distribution functions assuming an infinite homogeneous distribution. Thus the interaction density (5.21) as used e.g. in (5.20) and (5.22) can be replaced by the position independent nuclear matter density. In nuclear matter the potential has therefore the form:

$$U = \alpha \cdot \left(\frac{\rho}{\rho_0} \right) + \beta \cdot \left(\frac{\rho}{\rho_0} \right)^\gamma + \delta \cdot \ln^2 \left(\varepsilon \cdot (\Delta \vec{p})^2 + 1 \right) \cdot \left(\frac{\rho}{\rho_0} \right). \quad (5.24)$$

The parameters μ and t_5 of the Yukawa interaction have been adjusted in order to give the best preservation of the nuclear surface, obtaining $\mu = 1.5$ fm and $t_5 = -6.66$ MeV [87]. The parameters $\alpha, \beta, \gamma, \delta, \varepsilon$ in Eq. (5.24) are determined in order to reproduce simultaneously

κ (MeV)	α (MeV)	β (MeV)	γ	δ (MeV)	ε (GeV^{-2})	EOS
200	-390	320	1.14	1.57	500	soft
380	-130	59	2.09	1.57	500	hard

Table 5.1: Parameter sets for the potential used in the QMD model.

the correct momentum dependence of the nucleon-nucleus optical potential [110, 111] as well as the saturation density ($\rho_0 = 0.16 \text{ fm}^{-3}$) and the binding energy ($E_B = -16 \text{ MeV}$) for a given incompressibility κ . Two different equations of state are commonly used: a hard equation of state with a compressibility of $\kappa = 380 \text{ MeV}$ and a soft equation of state with a compressibility of $\kappa = 200 \text{ MeV}$ [112, 113]. The standard values of the parameters $\alpha, \beta, \gamma, \delta, \varepsilon$ used in the QMD model can be found in Ref. [87, 109]. For completeness, we list them in Table (5.1).

Stochastic collisions of particles are included by standard Monte Carlo procedures. The collision probabilities are determined by a geometrical minimal distance criterium, in analogy to the cascade models: two particles collide if their minimum distance d , i.e. the minimum relative distance of the centroids of the Gaussians during their motion, in their c.m. frame fulfills the requirement:

$$d \leq d_0 = \sqrt{\frac{\sigma_{\text{tot}}}{\pi}}, \quad \sigma_{\text{tot}} = \sigma(\sqrt{s}, \text{collision type}). \quad (5.25)$$

where the cross section is assumed to be the free cross section of the regarded collision type ($N - N, N - \Delta, \dots$). For each collision the phase space densities in the final states are checked in order to assure that the final distribution in phase space is in agreement with the Pauli principle ($f \leq 1$). The phase space density f'_i at the final states $1'$ and $2'$ is measured and interpreted as a blocking probability. Thus, the collision is only allowed with a probability of $(1 - f'_1)(1 - f'_2)$. If the collision is not allowed the particles remain at their original momenta.

The main steps to perform the simulation of a single event with QMD can be summarized as follows:

Initialization: Projectile and target nuclei are initialized according to an initial Wigner distribution function $f(\mathbf{r}, \mathbf{p}, t = 0)$. This distribution is constrained by the requirements to reproduce the ground state properties of the two nuclei, essentially radii and binding energies.

Propagation: For each time step the particles (nucleons and eventually produced baryon resonances and mesons) are propagated according to the equation of motions (5.11) with a given Hamiltonian $\langle H \rangle$.

Collisions: Within the considered time step, two particles close in coordinate space such that condition (5.25) is fulfilled can potentially perform a collision. For each potential collision one checks whether its final state is Pauli-blocked. If this is the case, the momenta of collision partners are kept unchanged – i.e. the collision does not occur

–, otherwise the momenta are changed according to the angular distribution of this particular channel.

5.2 Tübingen RQMD

In order to study dilepton production in heavy ion collisions, the Tübingen RQMD transport code [92] has been extended and all nucleon resonances with mass below 2 GeV have been included [38]. These are altogether 11 N^* and 10 Δ resonances. The corresponding masses and decay widths are listed in Tables 5.2 and 5.3.

The various resonance states can be populated either in baryon-baryon collisions, or in pion absorption processes, or in the decay of a higher order resonance. In the Tübingen RQMD model the following inelastic channels can lead to the excitation of a resonance in a baryon-baryon collision: $NN \rightarrow N\Delta_{1232}$, $NN \rightarrow NN^*$, $NN \rightarrow N\Delta^*$, $NN \rightarrow \Delta_{1232}\Delta_{1232}$, $NN \rightarrow \Delta_{1232}N^*$, $NN \rightarrow \Delta_{1232}\Delta^*$ and $NR \rightarrow NR'$. Here the Δ_{1232} is explicitly listed, whereas higher excitations of the Δ resonance have been denoted as Δ^* . R and R' denote two generic resonances. In addition, all possible elastic baryon-baryon collisions are taken into account in RQMD. Elastic scattering is considered on the same footing for all the particles involved. Matrix elements for elastic reactions are assumed to be the same for nucleons and nucleon resonances. Thus elastic NR and RR cross sections are determined from the elastic pp or np cross sections, depending on the total charge. Regarding the inelastic cross-sections, the production cross sections for the $\Delta(1232)$ and the $N^*(1440)$ resonances in the $NN \rightarrow N\Delta_{1232}$, $NN \rightarrow NN^*(1440)$ and $NN \rightarrow \Delta_{1232}\Delta_{1232}$ reactions are taken from [114]. These cross sections were determined within the framework of a one-boson-exchange model. For the higher lying resonances the parametrizations for the production cross-section are taken from Refs. [90, 115]. In [90], an effective parametrization based on simple phase space considerations has been employed and free parameters have been tuned to experimental measurements. Thus, inelastic collisions are considered according to the expression [90]:

$$\sigma_{1,2 \rightarrow 3,4} \sim \frac{\langle p_f \rangle}{p_i s} |\mathcal{M}|^2 \quad (5.26)$$

where p_i and $\langle p_f \rangle$ are the momenta of the incoming and outgoing particles in the center of mass frame. In the case that the outgoing particles are stable particles with a well-defined mass $\langle p_f \rangle$ has the standard expression:

$$\langle p_f \rangle = p_f = p^*(\sqrt{s}, m_3, m_4) \quad (5.27)$$

with p^* defined in Eq. (3.12). In the case that one of the final particle is a resonance, i.e. an unstable particle, the phase space is averaged over the corresponding spectral function

$$\langle p_f \rangle = \int p^*(\sqrt{s}, m_N, \mu) dW_R(\mu) \quad (5.28)$$

where $dW_R(\mu)$ is the resonance Breit-Wigner distribution. In the general case that both final states in Eq. (5.26) are resonances, p_f is averaged over both resonances

$$\langle p_f \rangle = \int p^*(\sqrt{s}, \mu, \mu') dW_R(\mu) dW_{R'}(\mu') . \quad (5.29)$$

Res.	Mass [MeV]	Γ_{tot} [MeV]	$N\omega$		$N\rho$		$N\pi$	$N\pi\pi$	$\Delta_{1232\pi}$	$N_{1440\pi}$	$N\eta$
N_{1440}	1440	200	$< 10^{-4}$	(-)	0.45	(-)	140	10	50	-	-
N_{1520}	1520	125	0.08	(-)	26.63	(-)	75	18.75	31.25	-	-
N_{1535}	1535	150	2.05	(-)	4.62	(-)	82.5	7.5	-	7.5	52.5
N_{1650}	1650	150	0.94	(-)	3.17	(-)	97.5	7.5	15	7.5	7.5
N_{1675}	1675	140	0.003	(-)	3.50	(-)	63	77	-	-	-
N_{1680}	1680	120	0.50	(-)	10.24	(24)	78	18	-	-	-
N_{1700}	1700	100	-	(-)	-	(5)	10	45	35	-	5
N_{1710}	1710	110	-	(-)	-	(5.5)	16.5	22	22	11	22
N_{1720}	1720	184 (150)	32.4	(-)	129.3	(37.5)	22.5	67.5	15	-	-
N_{1900}	1870	500	-	(275)	-	(25)	175	-	25	-	-
N_{1990}	1990	550	-	(-)	-	(82.5)	27.5	137.5	165	82.5	-

Table 5.2: List of N^* resonances which are included in the QMD transport model. The table shows the resonance masses and the total and partial widths of the included decay channels in MeV. The values of $\Gamma_{N\omega}$ and $\Gamma_{N\rho}$ are given at the resonance pole masses. The values in brackets as well as the other decay channels are taken from [90] and used for the reaction dynamics.

Res.	Mass [MeV]	Γ_{tot} [MeV]	N_{ρ}	N_{π}	$\Delta_{1232\pi}$	$N_{1440\pi}$
Δ_{1232}	1232	115	~ 0 ^a (–)	115	–	–
Δ_{1600}	1700	200	– (–)	30	110	60
Δ_{1620}	1675	180	16.4 (–)	45	108	27
Δ_{1700}	1750	300	47.7 (30)	60	165	45
Δ_{1900}	1850	240	– (36)	72	72	60
Δ_{1905}	1880	363 (280)	307.3 (168)	56	28	28
Δ_{1910}	1900	250	– (100)	87.5	37.5	25
Δ_{1920}	1920	150	– (45)	22.5	45	37.5
Δ_{1930}	1930	250	– (62.5)	50	62.5	75
Δ_{1950}	1950	250	– (37.5)	112.5	50	50

Table 5.3: List of Δ resonances which are included in the QMD transport model. The table shows the resonance masses and the total and partial widths of the included decay channels in MeV. The values of $\Gamma_{N\rho}$ are given at the resonance pole masses. The values in brackets as well as the other decay channels are taken from [90] and used for the reaction dynamics.

^aAt the resonance pole $\Gamma_{N\rho}$ is practically zero for the Δ_{1232} due to vanishing phase space. However, the ρ meson coupling constants of this resonance, in particular the magnetic one, are large [34] and thus the Δ_{1232} has non-vanishing off-shell contributions.

The integrations are performed over kinematically defined limits. \mathcal{M} in Eq. (5.26) is the matrix element of the cross section and the proportionality sign accounts for possible overall (iso-)spin coefficients. For most of the cases we use expressions for the matrix elements from Ref. [90]. However, when parameterizations of the matrix elements are given in Ref. [115], we make use of these expressions.

The cross-section for the reactions $NR \rightarrow NR'$ is determined from the known channels $NN \rightarrow NR$ and $NN \rightarrow NR'$ by

$$\sigma_{NR \rightarrow NR'} = I \frac{0.5(|\mathcal{M}_{NN \rightarrow NR}|^2 + |\mathcal{M}_{NN \rightarrow NR'}|^2)2(2J_{R'} + 1)}{16\pi p_i s} \langle p_f \rangle. \quad (5.30)$$

In Eq. (5.30) I is an isospin coefficient, depending on the resonance type, and $J_{R'}$ denotes the spin of R' .

For all resonances we use mass-dependent widths in expressions (5.28)-(5.30), namely

$$\Gamma(\mu) = \Gamma_R \left(\frac{p}{p_r} \right)^3 \left(\frac{p_r^2 + \delta^2}{p^2 + \delta^2} \right)^2. \quad (5.31)$$

In (5.31) p and p_r are the c.m. momenta of the pion in the resonance rest frame evaluated at the resonance running and pole mass, respectively. $\delta = 0.3$ is chosen for the Δ_{1232} and $\delta = \sqrt{(m_R - m_N - m_\pi)^2 + \Gamma^2/4}$ for all other resonances.

Backward reactions, e.g. $NR \rightarrow NN$, are treated by detailed balance

$$\sigma_{3,4 \rightarrow 1,2} \sim \frac{|p_{1,2}|^2}{|p_{3,4}|^2} \sigma_{1,2 \rightarrow 3,4} \quad (5.32)$$

where the proportionality sign is due to overall (iso-)spin factors.

The resonances as well as the pions originating from their decay are dynamically treated, i.e. in a non-perturbative way.

Pion-baryon collisions are treated as two-stage processes, i.e. first the pion is absorbed by a nucleon or a baryon resonance forming a new resonance state with subsequent decay. The pion absorption by nucleons is treated in the standard way [90, 92, 115] and the pion absorption by resonances is proportional to the partial decay width of the reverse process [115]

$$\sigma_{\pi R \rightarrow R'} = \frac{2J_{R'} + 1}{(2S_a + 1)(2S_b + 1)} \frac{4\pi}{p_i^2} \frac{s(\Gamma_{R' \rightarrow R\pi})^2}{(s - m_{R'}^2)^2 + s\Gamma_{R'}^2}. \quad (5.33)$$

The decay of baryon resonances is treated as proposed in [116, 117, 118, 119], i.e. the resonance life time is given by the spectral function

$$\tau_R(\mu) = 4\pi\mu \frac{dW_R(\mu)}{d\mu^2}. \quad (5.34)$$

Here we use constant widths when considering resonance decays. The decay channels which are taken into account are listed in Tables 5.2 and 5.3 together with their corresponding branching ratios. For the mass system under consideration pion multiplicities are reasonably well reproduced by the present description. E.g. inclusive π^+ cross sections in C+C reactions

measured by the KaoS collaboration [120] can be reproduced by the present description within error bars.

As mentioned, nucleons, pions and baryon resonances with masses below 2 GeV are the dynamical hadronic degrees of freedom included in RQMD. In addition to them, the Tübingen RQMD model includes the Λ and Σ baryons as well as the K^+ , η , ρ , ω and ϕ mesons treating them perturbatively, as generally done for subthreshold particles.⁴ To treat a particle perturbatively means to neglect the feedback of this particle on the overall reaction dynamics. In this method, the dynamical degrees of freedom are not affected by the production of one of these mesons. The method allows to artificially enhance the corresponding production cross sections in the simulation in order to collect the necessary statistics. The production of the particle occurs every time energy conservation allows it and the produced particle is assigned a “probability to exist”, i.e. of having been indeed produced, determined by the ratio of its production cross section to the total two-body scattering cross section. For details regarding the treatment of the strange particles in RQMD we refer the reader to Ref. [96].

Concerning the η , the fit of [121] is in good agreement with the exclusive $pp \rightarrow pp\eta$ production data from COSY [122] around threshold. Thus in this case the cross section from [121] is used and the production through the decay of nucleon resonances is neglected. As a consistency check, the η yield obtained by the two production mechanisms $NN \rightarrow NN\eta$ and $NN \rightarrow RN \rightarrow NN\eta$ has been compared and it was found that both lead to almost identical η yields in heavy ion reactions [38]. To avoid double counting only one of the channels should be included. In line with experimental data [123] for the η an iso-spin factor of

$$\sigma(pn \rightarrow pn\eta) = 6.5\sigma(pp \rightarrow pp\eta) \quad (5.35)$$

is assumed. The η absorption runs over the dominating channel $\eta + N \rightarrow N^*(1535)$. The corresponding η production cross sections in C+C collisions are consistent with the experimental results of Ref. [124].

5.3 Dileptons within the Tübingen RQMD model

In the energy range of a few AGeV one can identify three main classes of processes that lead to dilepton emission: decays of light unflavoured mesons, decays of N^* and Δ resonances and nucleon-nucleon bremsstrahlung. Dilepton production through the bremsstrahlung mechanism has in detail been studied by the Gießen group in [125]. For the energy range of interest in this work bremsstrahlung contributes in a significant way to the dilepton spectrum only at small invariant masses. By far the dominant contributions result from diagrams which involve the excitation of an intermediate Δ resonance. Within the present framework the inclusion of such contributions would, however, lead to a double counting and therefore we omitted up to now [53, 38, 126] and also omit in this work explicit bremsstrahlung contributions.

However, it has been pointed out [127] that in a recent calculation performed by the Rossendorf group [128] the contribution of the pn bremsstrahlung was found to be up to a

⁴If the threshold for hadron production in elementary NN reactions exceeds the heavy ion laboratory energy one speaks about subthreshold production.

factor four larger than in Ref. [125] and of comparable size as the corresponding contribution running via intermediate Δ resonances. The issue is at present a topic of debate.

We describe below the realization within the RQMD model of dilepton emission originated by decays of light unflavoured mesons and decays of nucleon resonances. The controversy about the nucleon-nucleon bremsstrahlung contribution is more extensively discussed in Section 5.3.3.

5.3.1 Dilepton decays of light mesons

At incident energies of few AGeV the cross sections for meson $\mathcal{M} = \eta, \eta', \rho, \omega, \phi$ production are small and these mesons do not play an important role in the dynamics of heavy ion collisions. Their production can thus be treated perturbatively. The decay of a meson to a dilepton pair takes place through the emission of a virtual photon. The differential branching ratios for the decay of a meson to a final state Xe^+e^- can be written as

$$dB(\mu, M)^{\mathcal{M}, \pi \rightarrow e^+ e^- X} = \frac{d\Gamma(\mu, M)^{\mathcal{M}, \pi \rightarrow e^+ e^- X}}{\Gamma_{\text{tot}}^{\mathcal{M}, \pi}(\mu)}, \quad (5.36)$$

with μ the meson mass and M the dilepton mass. As already mentioned in Chapter 3, three types of such decays have been considered: direct decays $\mathcal{M} \rightarrow e^+e^-$, Dalitz decays $\mathcal{M} \rightarrow \gamma e^+e^-$, $\mathcal{M} \rightarrow \pi(\eta)e^+e^-$ and four-body decays $\mathcal{M} \rightarrow \pi\pi e^+e^-$. The comprehensive study on the decay of light mesons to a dilepton pair performed in [43] showed that, assuming a nucleon resonance dominance model for the production of ρ and ω mesons, the remaining decay channels that are most important quantitatively for heavy ion collisions at 1 and 2 AGeV are $\pi^0 \rightarrow \gamma e^+e^-$ and $\eta \rightarrow \gamma e^+e^-$. The $\pi^0 \rightarrow \gamma e^+e^-$ and $\eta \rightarrow \gamma e^+e^-$ decay rates are given by expression (3.15) of Section 3.1.2. For the η we include η absorption from the dominating channel $\eta + N \rightarrow N^*(1535)$ explicitly. Since chiral perturbation theory predicts practically no modification of the in-medium η mass [129], we do not include a possible η mass shift.

5.3.2 Dilepton decays of nucleon resonances

In terms of the branching ratios for the Dalitz decays of the baryon resonances, the cross section for e^+e^- production from the initial state X' together with the final state NX can be written as

$$\frac{d\sigma(s, M)^{X' \rightarrow NX e^+ e^-}}{dM^2} = \sum_R \int_{(m_N + M)^2}^{(\sqrt{s} - m_X)^2} d\mu^2 \frac{d\sigma(s, \mu)^{X' \rightarrow RX}}{d\mu^2} \sum_V \frac{dB(\mu, M)^{R \rightarrow VN \rightarrow Ne^+ e^-}}{dM^2}. \quad (5.37)$$

Here, μ is the running mass of the baryon resonance R with the cross section $d\sigma(s, \mu)^{X' \rightarrow XR}$ and $dB(\mu, M, \rho_B)^{R \rightarrow VN \rightarrow Ne^+ e^-}$ is the differential branching ratio for the Dalitz decay $R \rightarrow Ne^+e^-$ through the vector meson V

$$\frac{dB(\mu, M)^{R \rightarrow VN \rightarrow Ne^+ e^-}}{dM^2} = \frac{d\Gamma(\mu, M)^{R \rightarrow VN \rightarrow Ne^+ e^-} / dM^2}{\Gamma_{\text{tot}}^R(\mu)}, \quad (5.38)$$

with the Dalitz decay width $d\Gamma(\mu, M)^{R \rightarrow VN \rightarrow Ne^+e^-} / dM^2$ of the resonance given by (3.32) and the total width $\Gamma_{\text{tot}}^R(\mu)$ of the resonance given by (4.11). Thus Eq. (5.37) describes baryon induced and pion induced dilepton production, i.e. the initial state can be given by two baryons $X' = NN, NR, R'R$ or it runs through pion absorption $X' = \pi N$. In the resonance model both processes are treated on the same footing by the decay of intermediate resonances.

For the description of the dilepton production through baryon resonances we consider the same set of resonances which has successfully been applied to the description of dilepton and vector meson production in pp collisions [53, 78, 79]. It includes only the well established (4*) resonances listed by the PDG [80] and is smaller than the complete set of resonances included in the RQMD model.

5.3.3 Discussion: Nucleon-Nucleon Bremsstrahlung

Dilepton production in elementary nucleon-nucleon reactions has been studied within microscopic models by various authors [125, 128, 130]. In the evaluation of the $NN \rightarrow NNe^+e^-$ cross section two major channels have been taken into account:

- pure nucleonic bremsstrahlung, i.e. diagrams with intermediate nucleons. For the following let us distinguish the isospin dependences in

$$pp \rightarrow ppe^+e^- \quad (5.39)$$

$$np \rightarrow npe^+e^- \quad (5.40)$$

- diagrams with intermediate Δ resonances

$$NN \rightarrow N\Delta \rightarrow NNe^+e^- . \quad (5.41)$$

Among the authors of Refs. [125, 130] there exists an agreement that the Δ channel (5.41) is the dominant one. For pp collisions it turned out to be almost one order of magnitude larger than the channel (5.39) and for np collisions about a factor 3 larger than the channel (5.40). The results of [125] show clearly that at the three beam energies considered in [125], 1.04 GeV, 2.09 GeV and 4.88 GeV, in all cases the dominant contribution arises from the intermediate state consisting of the Δ isobar resonance. In fact, the total yields are almost equal to the contribution of the Δ amplitude alone [125].

The contribution of the nucleonic bremsstrahlung to the low mass dilepton spectra is *relatively* small and can therefore be safely neglected in transport calculations (see below).

A contradictory behavior was found in [128]. There the channel (5.40) was found to be of comparable size as the corresponding contribution from intermediate Δ 's. This finding stands in particular in contradiction to the work of Shyam and Mosel [125]. This is quite puzzling since [128] uses exactly the same meson-nucleon vertices (including the same energy dependence) as [125] to evaluate the corresponding diagrams. Also the photon-nucleon vertices are the same. It is therefore unclear, how a four times larger cross section for the channel (5.40) can be obtained. This discrepancy is currently under discussion.

Realization in transport calculations. The diagram with intermediate Δ states can be factorized into the reaction $NN \rightarrow N\Delta$ with subsequent Δ Dalitz decay $\Delta \rightarrow Ne^+e^-$. Such processes are standardly included in transport calculations. To add the corresponding contribution (5.41) is therefore double counting.

The pure nucleonic bremsstrahlung can be added without explicitly⁵ running into the double counting problem. However, taking the cross sections from [125], it is significantly smaller than the Δ Dalitz and can therefore be neglected, as done e.g. by the Tübingen RQMD group.

Other transport groups [30, 58] included the pn bremsstrahlung in the soft photon approximation. In such an approximation very similar cross sections to the ones calculated in [125, 130] are obtained (see [127]). The pp bremsstrahlung has been discarded by them on the basis of its smallness in comparison to the Δ Dalitz decay contribution.

In this respect, a remark can be made based on results previously published by the different groups. In Ref. [38] dilepton production in pp and pd reactions in the energy range $T = 1 \div 5$ GeV has been analyzed. There no explicit nucleonic bremsstrahlung contribution has been taken into account. The corresponding spectra are reported in Figs. 5.1 and 5.2. At low energies, $T = 1.04$ and $T = 1.27$ GeV, the theoretical $pd \rightarrow e^+e^-X$ cross sections significantly underestimate the experimental data. Such a strong underestimation does not emerge for the $pp \rightarrow e^+e^-X$ cross sections, nor it does at higher energies, at which anyhow the η contribution becomes dominant at low invariant masses. The discrepancy between theoretical calculations and experimental spectra observed in the pd spectra leaves therefore room for the conjecture that a channel, which has the property of being significant in pn collisions and negligible in pp collisions, is not accounted for in the theoretical calculations. Being the large pn bremsstrahlung of [128] a possible candidate for such a channel, we conclude that the results of [38] are not openly incompatible with the hypothesis of [128].

A similar enhancement of the pd data over the model results in the mass region of the η decay was found in the analysis performed by the UrQMD group [30]. Note that in [30] explicit pn bremsstrahlung was included in the soft-photon approximation.⁶ The authors concluded that pn bremsstrahlung is relatively unimportant.

On the other side, the same reactions have been analyzed in Ref. [58]. The authors took explicitly into account pn bremsstrahlung using the soft photon approximation [131] and discarded pp bremsstrahlung. They found that the DLS data for *both* the pp and pd reactions were reasonably well described within their approach [58]. It is hard to think that a similar agreement could be reached under the assumption that the pn bremsstrahlung contribution would be enhanced by a factor four, as expected from the cross sections given in Ref. [128].

⁵There are still cases in which the simple addition of the nucleonic bremsstrahlung at the level of the cross sections would be incorrect. In models fixing the resonance Dalitz decays by fitting available experimental data exclusively within a resonance model, like e.g. the eVMD model, a proper treatment would require the coherent addition of the pure nucleonic contribution to the resonant one and a refitting of the couplings.

⁶To extrapolate to the case of hard and massive virtual photons, a phase space correction was applied by multiplying the cross section with the ratio of the phase space integrals with/without virtual photon. Further details can be found in Ref. [30].

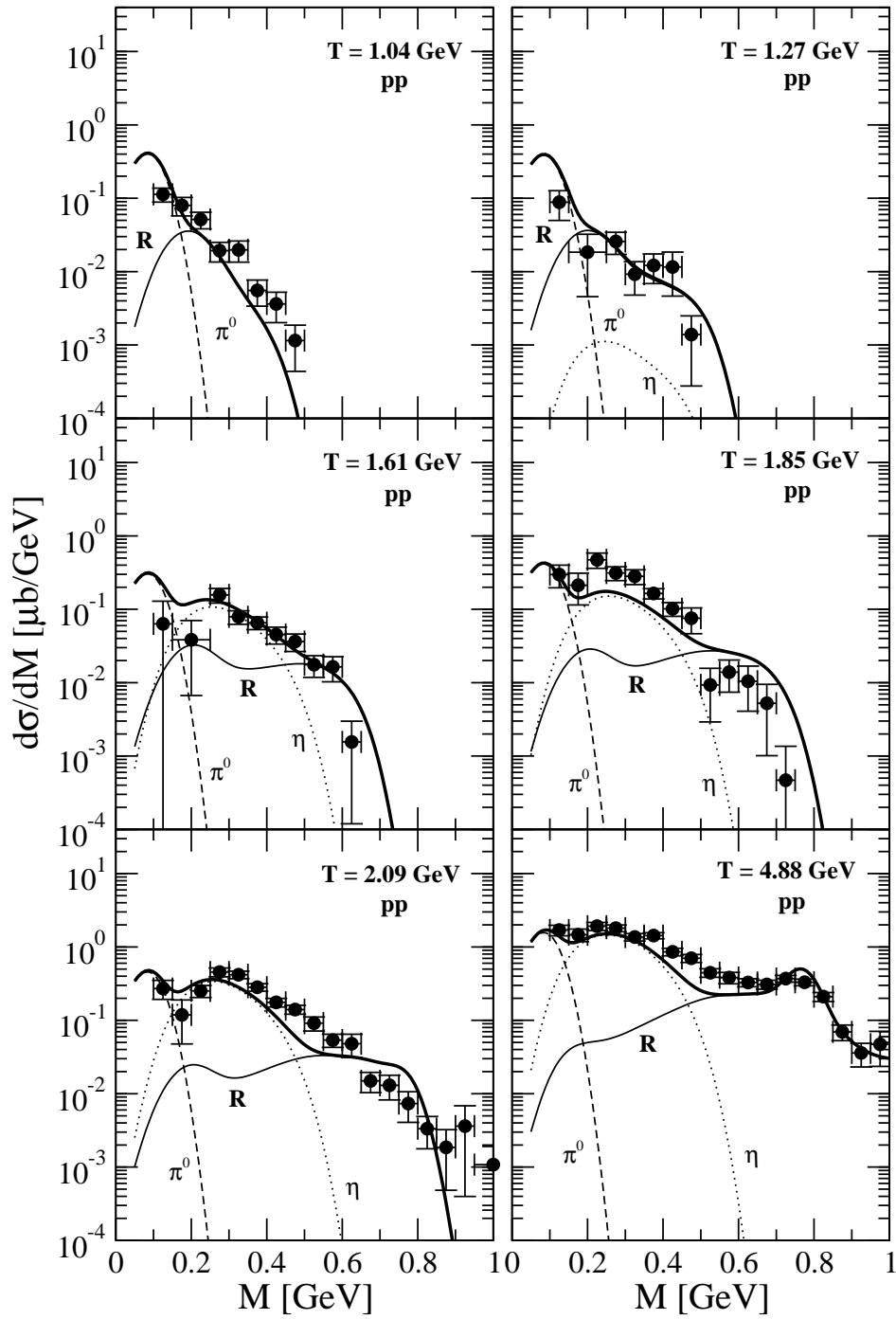


Figure 5.1: The differential $pp \rightarrow e^+e^-X$ cross sections at various proton kinetic energies are compared to the DLS data [28]. (Figure taken from [38]).

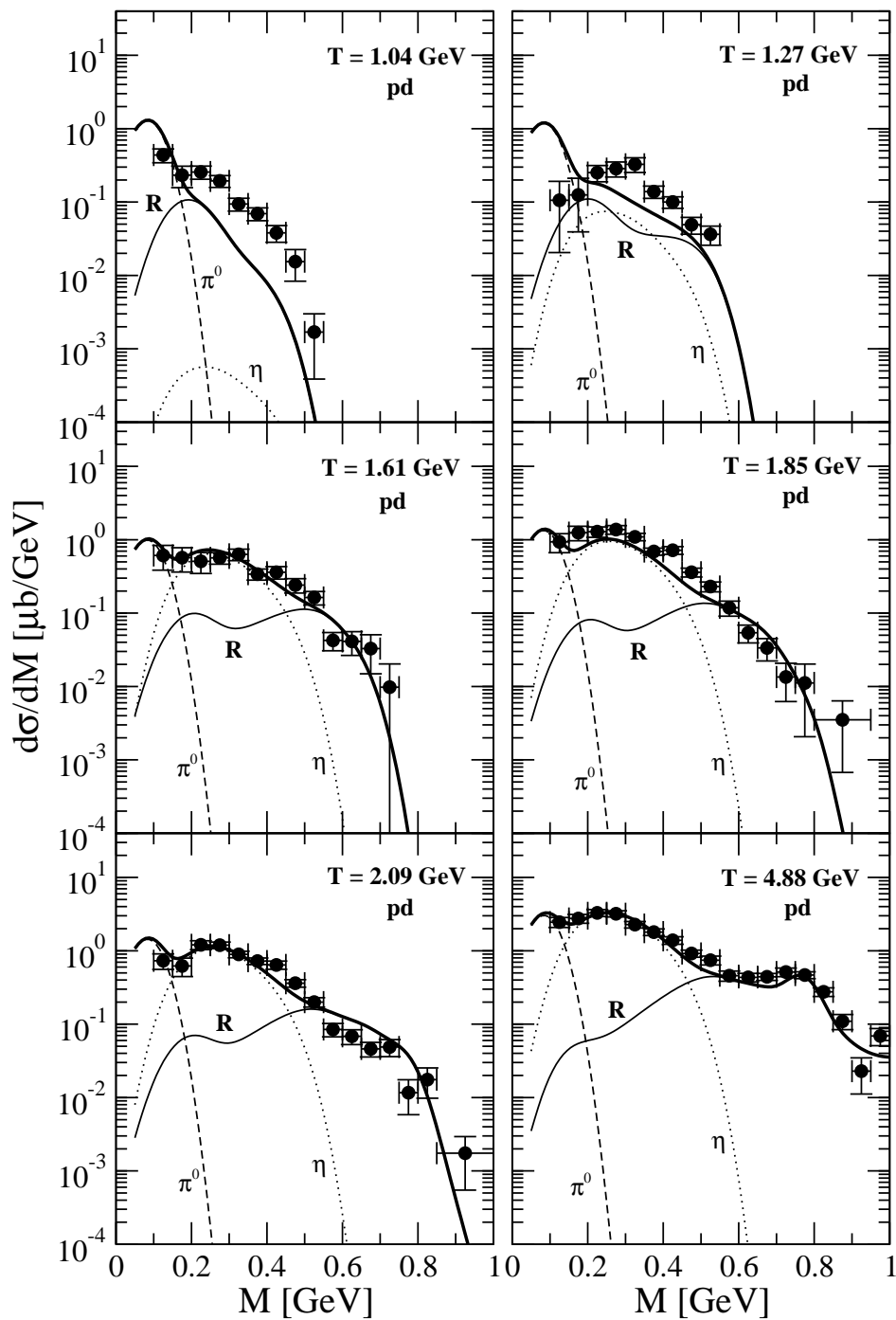


Figure 5.2: The differential $pd \rightarrow e^+e^-X$ cross sections at various proton kinetic energies are compared to the DLS data [28]. (Figure taken from [38]).

5.3.4 Numerical realization

In this Section we give technical details concerning the way the contribution of nucleon resonances to the dilepton yield is operatively extracted.

As already mentioned in Section 5.2, the various nucleon resonances are produced and propagated in the RQMD transport code. In the course of their propagation, resonances can scatter elastically and inelastically. The included scattering channels have been already listed in Section 5.2. At the beginning of each time step dt baryon-baryon collisions are performed. The process can lead to the production of new resonances or to the absorption of resonances previously present. Resonance decays are eventually performed at the end of the time step. The probability for a resonance to decay is estimated as

$$\mathcal{P}_{\text{dec}} = 1 - e^{-\frac{dt}{\gamma_R \tau_R}}, \quad (5.42)$$

where γ_R represents a Lorentz factor and τ_R is the resonance life time (5.34). Knowing the decay probability, whether a resonance decays or not is then decided by application of standard Monte Carlo techniques. Those resonances *which decay* are stored. In particular, the resonance running mass, the components of its 3-momentum and the local baryon density at the decay point are stored. For these resonances the dilepton branching is calculated from (5.38).

Thus, dilepton production is determined in terms of dilepton rates. Advantages and disadvantages of this approach will be discussed in Section 5.3.6, as some of the arguments will be better understood after the implementation of the ρ and ω meson in-medium spectral functions has been described.

5.3.5 Implementation of the ρ and ω meson in-medium spectral functions

In Section 3.3.1 we saw that, due to the P-invariance of the electromagnetic interaction, the resonances with arbitrary spin have only three independent helicity amplitudes in the $\gamma^*N \rightarrow R$ transitions. Therefore there are three independent scalar functions to fix the vertices. We showed that the three scalar functions arising from the decomposition of the $\gamma^*N \rightarrow R$ vertex over the Lorentz vectors and the Dirac matrices are functions of the mass squared M^2 of the virtual photon and are called covariant form factors. In the eVMD model each of these covariant form factors is expressed as a linear superposition of the contributions from the intermediate vector mesons of the ρ and ω family:

$$F_k^{(\pm)}(M^2) = \sum_i \mathcal{M}_{ki}^{(\pm)} \quad (5.43)$$

where $k = 1, 2, 3$ stands for each of the form factors, (\pm) denotes states of normal and abnormal parity respectively and the sum is over the intermediate mesons. The amplitude

$$\mathcal{M}_{k,i}^{(\pm)} = h_{ki}^{(\pm)} \frac{m_i^2}{m_i^2 - im_i \Gamma_i - M^2} \quad (5.44)$$

represents the contribution of the i^{th} vector meson to the form factor of type k . The residues $h_{ki}^{(\pm)}$ contain the parameters of the model.

In this representation, the insertion of the in-medium properties of the ω and ρ vector mesons is straightforward. In the medium, the transition amplitudes $\mathcal{M}_{k,i}^{(\pm)}$ ($i = \rho, \omega, \dots$) are directly modified by the vector meson self energies and read

$$\mathcal{M}_{k,i=V}^{(\pm)} = h_{kV}^{(\pm)} \frac{m_V^2 + \text{Re}\Sigma_V^{\text{tot}}}{m_V^2 + \text{Re}\Sigma_V^{\text{tot}} + i\text{Im}\Sigma_V^{\text{tot}} - M^2}. \quad (5.45)$$

We include the self energy contributions for the ground state ρ and ω mesons in the transition. For the excited states ρ', ρ'', \dots the self energies are unknown and thus we keep for these states their vacuum properties.

As in Ref. [38, 126] we also consider scenarios where the in-medium properties of the vector mesons are based on different model assumptions, namely a simple Brown-Rho or Hatsuda-Lee scaling of the vector meson masses [7, 20] and a collisional broadening of the vector meson widths. In the latter case the self energies are given by

$$\begin{aligned} \text{Im}\Sigma_V^{\text{tot}} &= -m_V \left(\Gamma_V^{(0)}(M) + \Gamma_V^{\text{coll}}(\rho, M) \right) \\ \text{Re}\Sigma_V^{\text{tot}} &= 0. \end{aligned} \quad (5.46)$$

In Eqs. (5.46) the energy dependence due to the two-, respectively three-pion decay of the vector meson is kept in the vacuum contribution to the total width, while the collisional broadening due to the interaction with the surrounding nucleons is absorbed into a density and energy dependent part. The issue of the energy dependence of the collisional width will be discussed in detail in Section 5.4. The Brown-Rho scaling is introduced through the replacement $m_V \rightarrow m_V^* = m_V(1 - \alpha \frac{\rho_B}{\rho_0})$, as done e.g. in [132]. In particular, in this case one has

$$\text{Re}\Sigma_V^{\text{tot}} = \left(m_V - \alpha \frac{\rho_B}{\rho_0} \right)^2 - m_V^2. \quad (5.47)$$

As usual, the mass shift entering into the real part can be adjusted by the parameter α . Like in the case of full spectral functions the self energy components enter into the amplitudes (5.45). In this context it is important to note that the modification of the amplitudes (5.45) leads to a *coherent* summation of the ρ and ω in-medium contribution to the transition form factors (5.43).

Doing so, this approach goes beyond the standard – even off-shell – transport approach where spectral properties are treated at the level of cross sections [29, 133, 134]. The latter always leads to an incoherent summation of the contributions from different hadrons.

The self energy appearing in Eq. (5.45) is a function $\Sigma_V^{\text{tot}}(M, |\mathbf{p}|, \rho_B)$ of the vector meson running mass, of the modulus of its 3-momentum in the nuclear matter rest frame and of the local density of the surrounding matter. In the rest frame L^* of a resonance R with mass μ , decaying into a nucleon and a vector meson of mass M , the modulus $|\mathbf{p}^*|$ of the momentum of the meson is fixed by energy conservation. If \mathbf{p}_R is the momentum of the resonance R in

the c.m. frame L of the colliding nuclei and $\mathbf{v}_R = \mathbf{p}_R / \sqrt{\mathbf{p}_R^2 + \mu^2}$ is its velocity, the vector meson momentum in L is given by the Lorentz transformation

$$|\mathbf{p}|^2 = (\gamma_R |\mathbf{v}_R| E^* + \gamma_R p_L^*)^2 + p_T^{*2} \quad (5.48)$$

where

$$p_L^* = |\mathbf{p}^*| \cos \theta \quad (5.49)$$

$$p_T^* = |\mathbf{p}^*| \sin \theta \quad (5.50)$$

with θ being the polar angle of the meson in L^* if one chooses the z -axis of this frame pointing in the direction of \mathbf{v}_R . Since $|\mathbf{p}^*|$ is fixed, in terms of the L frame variables one has $\Sigma_V^{\text{tot}} = \Sigma_V^{\text{tot}}(M, \cos \theta, \rho_B)$ and the decay amplitude averaged over the angles is:

$$\Gamma(R \rightarrow N\gamma^*)(\mu, M, \rho_B) = \int_{-1}^{+1} \frac{d \cos(\theta)}{2} \Gamma(R \rightarrow N\gamma^*)(\mu, M, \cos \theta, \rho_B). \quad (5.51)$$

Eq. (5.51) is implementable in the framework of QMD. For each resonance, QMD provides the values of the 3-momentum components (necessary to perform the Lorentz boost), of the mass (distributed over a Breit-Wigner) and of the local density of the surrounding matter at the point of the decay.

As discussed in Ref. [18], the excitation of particle-hole pairs in the meson spectral function generates resonance-nucleon scattering terms in the resonance self energy and thus the in-medium broadening of the resonance. We have seen that nucleon resonances are dynamically treated in the RQMD model and resonance-nucleon scattering is explicitly performed. Thus, the in-medium broadening of nucleon resonances is taken into account in the transport approach *dynamically*.⁷ No in-medium spectral functions of the vector mesons are therefore included in the total width $\Gamma_{\text{tot}}^R(\mu)$ appearing in the denominator of (5.38).

An observable tightly connected to a correct treatment of the resonance dynamics in HIC transport calculations is provided by the pion multiplicity. As previously mentioned, inclusive π^+ cross sections in C+C reactions measured by the KaoS Collaboration [120] can be reproduced by the present description within error bars. This gives, at least on a global level, manifest credit to our treatment.

5.3.6 Advantages and disadvantages of the present approach

Some of the advantages of our approach have been explicitly discussed. Others could be deduced from the content which has been exposed. However, for a better overview we summarize them here in a compact list:

⁷In simpler terms the argument can be qualitatively expressed as follows: the broadening of a nucleon resonance corresponds to a smaller value of its life time. In medium, the occurrence of absorption processes shortens the mean life time of a resonance: whereas in vacuum its disappearance is exclusively due to its decay, in medium the resonance can disappear also due to absorption. An absorbed resonance is removed and replaced by a new particle. The resonance will not appear among the stored resonances which decay, therefore it will not contribute to the dilepton branching.

- ⁸Dilepton rates are calculated in the framework of a microscopic hadronic model: the eVMD model. We have therefore direct access to the expressions of the *amplitudes* determining the contribution of the intermediate vector meson to the transition form factors. In-medium properties can thus be included at the level of these amplitudes (see (5.45)). It follows that we are able to resolve the *coherent* summation of the ρ and ω meson in-medium contributions. Note that the coherent summation involves the account for interference terms between the two vector mesons. These interference terms, naturally present in a proper quantum mechanical treatment, are absent in approaches operating at the level of cross sections.
- The vector mesons play in the eVMD model the role of intermediate virtual particles in the RNe^+e^- vertices. They are therefore fully treated as virtual particles.
- The approach represents a *unified* description of dilepton and vector meson production as well as their in-medium modifications. The same model parameters govern all these interconnected processes.

A drawback of our approach is that the dynamical propagation of the vector mesons is neglected. In particular, in-medium properties are determined by the local density at the decay point of the nucleon resonance, whereas in a dynamical treatment a vector meson would propagate within a system in evolution. Thus the various interactions determining its in-medium properties would occur at a density typical of the position reached by the vector meson in the evolving system. Eventually, some vector mesons could escape the fireball and decay in vacuum. Unfortunately, the formidable task of including consistently full off-shell particles characterized by their (in-medium) spectral function in a dynamical approach has not been done yet. Note that, analogously, no explicit dynamical propagation of the vector mesons is present in the fireball models successfully applied at SPS energies for the study of vector meson in-medium properties (see e.g. [14, 24, 36]). In those models, in-medium effects enter in the expression for the dilepton rates too.

5.4 Results

In this Section we provide theoretical calculations of the dilepton emission in heavy ion collisions at intermediate energy. In particular, we address the reaction C+C at 2 AGeV for which experimental data have been already published by the HADES collaboration. The main purpose is to compare calculations that include in-medium effects in a more traditional way, i.e. via Brown-Rho scaling of the vector masses and empirical collisional broadening of the decay width, with results which are obtained using ρ and ω mesons described by the in-medium spectral functions presented in Chapter 4 of this work. Particular emphasis is also put on remaining – and rarely discussed – model uncertainties which are inherent in a transport theoretical treatment.

⁸Discussed in Section 5.3.5

In the transport calculation the reaction has been treated as minimal bias collisions with respective maximal impact parameter $b_{max} = 6.0$ fm. For the nuclear mean field a soft momentum dependent Skyrme force ($K=200$ MeV) is used [87] which provides also a good description of the subthreshold K^+ production in the considered energy range [95]. In order to compare to the HADES data, dilepton events originated from the different considered sources have been generated in the phase space. After smearing over the experimental momentum resolution, the acceptance filter function provided by the HADES collaboration has been applied. Events with opening angle $\theta_{e^+e^-} \leq 9^\circ$ have been rejected, according to the treatment of the experimental data. The spectrum is then normalized to the corresponding π^0 multiplicity.

Vacuum

We start by addressing the results obtained without any additional medium effects concerning the dilepton production. In Fig. 5.3 the dilepton spectrum obtained within the vacuum formulation of the NRD+eVMD model is compared to the HADES data [33]. The experimental data are slightly underestimated in the mass region $m_\pi \leq M \leq 0.4$ GeV and overestimated in the region of the vector meson peak. Indeed, already the comparison with DLS data had shown that the eVMD model in its pure vacuum formulation fails in describing dilepton production in heavy ion collisions [38]. However, the vacuum calculation is a good reference point to isolate, where possible, those sources which dominantly contribute to the spectrum in a certain invariant mass region. Once the dominant sources have been identified, it is interesting to look separately at their modifications due to in-medium-effects. For this purpose we also show separately in Fig. 5.3 the contributions to the spectrum of the decays of the pseudoscalar η and π^0 mesons and all the N^* as well as the Δ resonances. In addition, the $\Delta(1232) \rightarrow Ne^+e^-$ decay channel is explicitly shown. In what follows, we will investigate the modification of the Dalitz decays of the baryon resonances $R \rightarrow Ne^+e^-$ when in-medium properties of the ρ and ω mesons are taken into account. Since we introduce no in-medium modifications of the $\pi^0 \rightarrow \gamma e^+e^-$ and $\eta^0 \rightarrow \gamma e^+e^-$ channels, the contribution to the dilepton spectrum due to the π^0 and η Dalitz decay will remain unchanged in the course of our analysis.

Collisional broadening

Let us now turn to the introduction of in-medium effects according to the standard treatments and address first to Fig. 5.4 where the HADES data are compared to calculations where the possible broadening of the vector meson spectral function in medium is effectively taken into account through the introduction of a collisional width Γ_V^{coll} . We present calculations where a linear parametrization of the type $\Gamma_V^{tot}(\rho) = \Gamma_V^{vac} + \rho/\rho_0 \Gamma_V^{coll}(\rho_0)$ has been used to estimate the vector meson in-medium width $\Gamma_V^{tot}(\rho)$. Fig. 5.4(a) refers to the assumption $\Gamma_\rho^{tot}(\rho_0) = 200$ MeV and $\Gamma_\omega^{tot}(\rho_0) = 60$ MeV, which reflects the estimates of the CLAS and TAPS experiments for the collisional broadening of ρ and ω meson respectively. Fig. 5.4(b) refers to the assumption $\Gamma_\rho^{tot}(\rho_0) = 250$ MeV, $\Gamma_\omega^{tot}(\rho_0) = 125$ MeV, which reflects the estimates emerged from the analysis performed in [38]. We observe a suppression of the peak

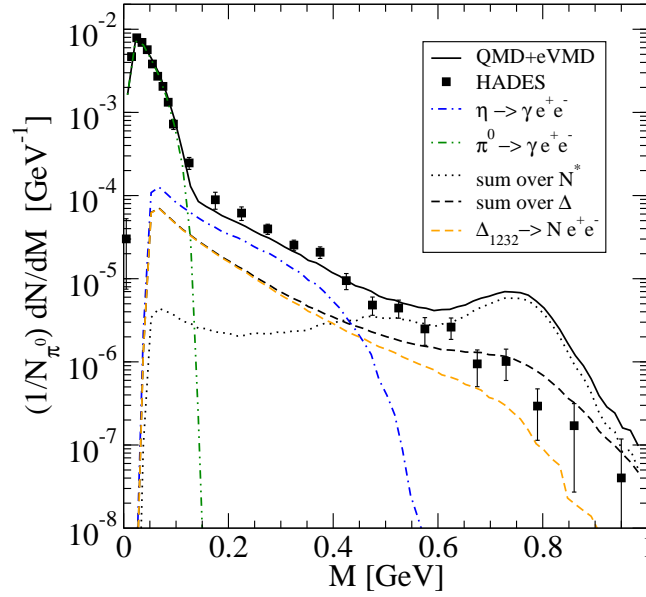


Figure 5.3: The dilepton spectrum in C+C reaction at 2.0 AGeV as predicted by the vacuum NRD+eVMD model is compared to the HADES data [33]. The contribution of the different types of sources taken into account in the calculation is explicitly shown.

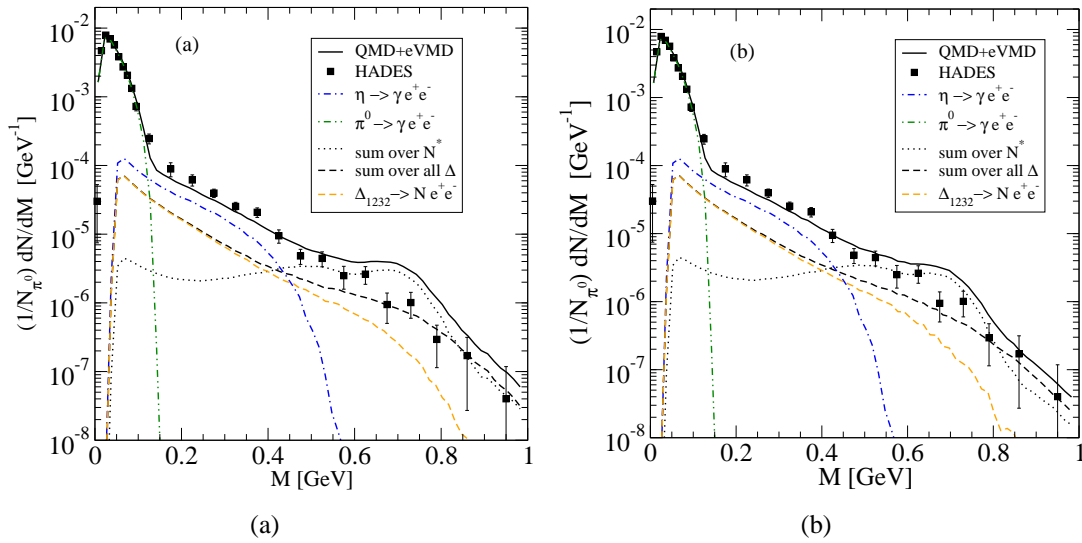


Figure 5.4: Dilepton spectrum in C+C collisions at 2.0 AGeV for different values of the in-medium ρ and ω widths. Left panel: $\Gamma_\rho^{\text{tot}}(\rho_0) = 200$ MeV and $\Gamma_\omega^{\text{tot}}(\rho_0) = 60$ MeV. Right panel: $\Gamma_\rho^{\text{tot}}(\rho_0) = 250$ MeV and $\Gamma_\omega^{\text{tot}}(\rho_0) = 125$ MeV.

with respect to the vacuum case, more pronounced in case (b) than (a). However, in both cases, the experimental data are still overestimated around $M \sim 0.7$ GeV, due to the still significant contribution of the $N^*(1535)$. Note that the Dalitz decay of this resonance plays a dominant role in the determination of the dilepton spectrum in the region of and just below the vector meson peak, as separately shown in Fig. 5.5. If on the one side the HADES data seem to favour a less pronounced contribution of the $N^*(1535)$ resonance in this region, on

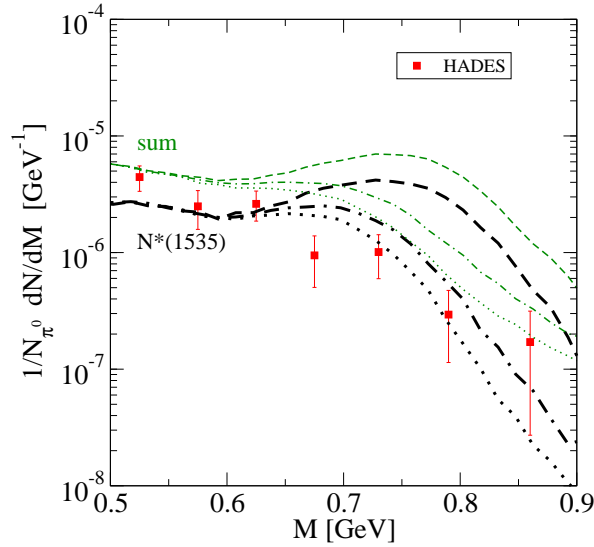


Figure 5.5: The contribution of the $N^*(1535)$ resonance to the dilepton spectrum (thick lines) in comparison to the total spectrum obtained by summing the contribution of all sources considered (thin lines). Dashed lines: vacuum calculation. Dashed-dotted lines: calculation including in-medium ρ and ω widths, with $\Gamma_\rho^{\text{tot}}(\rho_0) = 200$ MeV and $\Gamma_\omega^{\text{tot}}(\rho_0) = 60$ MeV. Dotted lines: calculation including in-medium ρ and ω widths, with $\Gamma_\rho^{\text{tot}}(\rho_0) = 250$ MeV and $\Gamma_\omega^{\text{tot}}(\rho_0) = 125$ MeV. The HADES data [33] are also shown.

the other side dilepton production data in $p+p$ collision have been well described under the same model assumptions for the coupling to the $N^*(1535)$. We see therefore that the contribution of the $N^*(1535)$ Dalitz decay, which is significant in elementary reactions and thus in vacuum, is partially reduced in heavy ion collisions due to in-medium effects.

Energy dependence of the collisional width

Before proceeding, we would like to discuss an approximation which has been made. In the calculations shown in Fig. 5.4 the collisional broadening has been included in first approximation by making no additional assumption what concerns the energy dependence of the in-medium width, i.e. assuming that the collisional width has the same energy dependence as the vacuum width [38, 126]. This approximation is rather crude, but linked to the limits which such a schematic inclusion of in-medium effects carries with it. Obviously a microscopic calculation of the exact energy dependence of the collisional broadening is equivalent to a full model calculation of the in-medium spectral function. The estimated energy dependence would be theoretically consistent but rather model dependent.

To investigate the consequence of this approximation on a schematic level, we extract in the following a possible energy dependence of the collisional broadening on the basis of qualitative considerations and look at the influence that this different choice has on the shape of the dilepton spectrum. For this purpose, we attribute the collisional broadening which a vector meson acquires to an absorption process of the type $V + N \rightarrow R \rightarrow \pi + N$. To simplify, we approximate the corresponding phase space by the phase space for the process $(M + m_N) \rightarrow (m_\pi + m_N)$ and assume that the resonance decay proceeds as a p -wave. This

leads to:

$$\Gamma_V^{\text{coll}}(M, \rho) = \Gamma_V^{\text{coll}}(m_V, \rho) \left(\frac{m_V + m_N}{M + m_N} \right) \left(\frac{p^*(M + m_N, m_N, m_\pi)}{p^*(m_V + m_N, m_N, m_\pi)} \right)^3 \quad (5.52)$$

with p^* defined in Eq. (3.12). As one can see, in this approximation the vector meson threshold is shifted from $2m_\pi$ to m_π for the ρ meson and from $3m_\pi$ to m_π for the ω meson.

The choice affects the shape of the ω width much stronger than the shape of the ρ width. The influence of the choice of the energy dependence of the collisional width is illustrated in Fig. 5.6 for the case $\rho = 2\rho_0$ and for $\Gamma_\rho^{\text{tot}}(\rho_0, m_\rho) = 250$ MeV and $\Gamma_\omega^{\text{tot}}(\rho_0, m_\omega) = 125$ MeV. In particular for the ω meson the shift of the threshold leads to a large enhancement of the ω width at lower invariant masses. However, we have to consider that in our calculations the in-

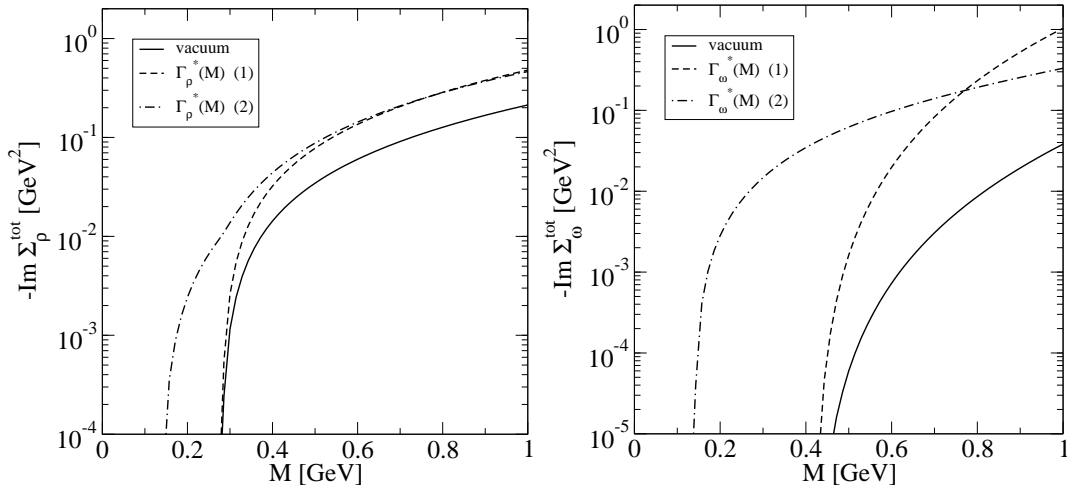


Figure 5.6: Left panel: Imaginary part of ρ meson self energy $-Im\Sigma_\rho^{\text{tot}}(\rho, M) = m_\rho\Gamma_\rho^{\text{tot}}(\rho, M)$ in vacuum (full line) and at $\rho = 2\rho_0$ for $\Gamma_\rho^{\text{tot}}(\rho_0, m_\rho) = 250$ MeV (dashed and dashed-dotted lines). Right panel: Imaginary part of the ω meson self energy $-Im\Sigma_\omega^{\text{tot}}(\rho, M) = m_\omega\Gamma_\omega^{\text{tot}}(\rho, M)$ in vacuum (full line) and at $\rho = 2\rho_0$ for $\Gamma_\omega^{\text{tot}}(\rho_0, m_\omega) = 125$ MeV (dashed and dashed-dotted lines). For both panels the dashed line corresponds to the assumption that the collisional width has the same energy dependence as the vacuum width. The dashed-dotted line corresponds to the assumption that the collisional width has the energy dependence (5.52).

medium vector meson widths enter in the expressions for the ρ and ω meson contributions to the covariant form factors, see Eqs. (5.43), (5.44) and (5.45), whose modulus squared determine the width $\Gamma(R \rightarrow N\gamma^*)$ (3.32). Thus, only in the case that the different choice for the energy dependence of the in-medium vector meson width induces appreciable differences in the corresponding covariant form factors, these differences will be visible in the dilepton spectrum.

Let now $\Gamma_\rho^{*[1]}(M)$ be the ρ meson in-medium width with an energy dependence analogous to the vacuum width and $\Gamma_\rho^{*[2]}(M)$ the ρ meson in-medium width with an energy dependence

according to Eq. (5.52). In correspondence we set

$$F_\rho^{[1]} = \frac{m_\rho^2}{m_\rho^2 - im_\rho \Gamma_\rho^{*[1]}(M) - M^2} \quad (5.53)$$

$$F_\rho^{[2]} = \frac{m_\rho^2}{m_\rho^2 - im_\rho \Gamma_\rho^{*[2]}(M) - M^2}. \quad (5.54)$$

Analogously, for the ω meson we set:

$$F_\omega^{[1]} = \frac{m_\omega^2}{m_\omega^2 - im_\omega \Gamma_\omega^{*[1]}(M) - M^2} \quad (5.55)$$

$$F_\omega^{[2]} = \frac{m_\omega^2}{m_\omega^2 - im_\omega \Gamma_\omega^{*[2]}(M) - M^2}. \quad (5.56)$$

We refer now to the ω meson. The considerations we make are, however, valid also for the ρ meson. Since $(\Gamma_\omega^{*[i]})^2$ appears in the denominator of $|F_\omega^{[i]}|^2$ ($i = 1, 2$), we can in general say that in the region where $\Gamma_\omega^{*[2]} > \Gamma_\omega^{*[1]}$ we have $|F_\omega^{[2]}|^2 \leq |F_\omega^{[1]}|^2$. Consequently, in the region where the strict inequality is valid, the width $\Gamma(R \rightarrow N\gamma^*)$ will decrease. However, we have to notice that the mass region where the strict inequality $|F_\omega^{[2]}|^2 < |F_\omega^{[1]}|^2$ (or $|F_\omega^{[2]}|^2 > |F_\omega^{[1]}|^2$) holds is smaller than the mass region where $\Gamma_\omega^{*[2]} > \Gamma_\omega^{*[1]}$ ($\Gamma_\omega^{*[2]} < \Gamma_\omega^{*[1]}$) since $|F_\omega^{[2]}|^2 \approx |F_\omega^{[1]}|^2 \approx 1$ when $(m_\omega^2 - M^2)^2 \gg (m_\omega \Gamma_\omega^{*[i]})^2$ ($i = 1, 2$). Thus, this region is typically restricted to the region around the vector meson peak. Concerning the ρ meson, $\Gamma_\rho^{*[2]}$ and $\Gamma_\rho^{*[1]}$ are practically identical⁹ in the region of the vector meson peak, as can be seen from Fig. 5.6. Therefore we do not expect differences between $|F_\rho^{[2]}|^2$ and $|F_\rho^{[1]}|^2$. In the case of the ω meson, $\Gamma_\omega^{*[2]}$ and $\Gamma_\omega^{*[1]}$ do slightly differ in the peak region, although the main differences are not in this region but at lower masses, approximately from slightly above m_π up to slightly above $3m_\pi$, due to the different thresholds. As result, we see only small differences, localized around the peak, between $|F_\omega^{[2]}|^2$ and $|F_\omega^{[1]}|^2$. This is illustrated in Fig. 5.7 where the form factors $|F_\rho^{[i]}|^2$ and $|F_\omega^{[i]}|^2$ ($i = 1, 2$) are shown for the case $\rho = 2\rho_0$ and $\Gamma_\rho^{\text{tot}}(\rho_0, m_\rho) = 250$ MeV, $\Gamma_\omega^{\text{tot}}(\rho_0, m_\omega) = 125$ MeV.¹⁰ The dilepton spectrum resulting from the addition of a collisional broadening of the vector meson widths according to (5.52) is shown in Fig 5.8. We observe that the contribution of the Δ resonances, which couple only to the ρ meson, is practically the same in the two cases. Slight differences are visible only in the contribution of the N^* resonances around the vector meson peak. The differences are more evident in the case of larger values of the widths, Fig. 5.8(b). However, even in this case, the total spectra differ at most by a factor 1.3.¹¹

Let us conclude this discussion with a final comment. For a consistent evaluation of the energy dependence resulting from $V + N \rightarrow R \rightarrow \pi + N$ processes, one should indeed sum

⁹Per construction $|F_\rho^{[1]}|^2$ and $|F_\rho^{[2]}|^2$ coincide at the peak. The same consideration holds for the ω meson.

¹⁰In addition one should also consider the interference terms of the kind $F_\rho^{[i]} F_\omega^{[j]}$. These terms can drive either a constructive or destructive interference and therefore it is not possible to comment on their effect in general within a simple scheme as done for the $|F_\omega^{[i]}|^2$ and $|F_\rho^{[i]}|^2$ terms.

¹¹Here we refer to the maximum value of the ratio of the two spectra.

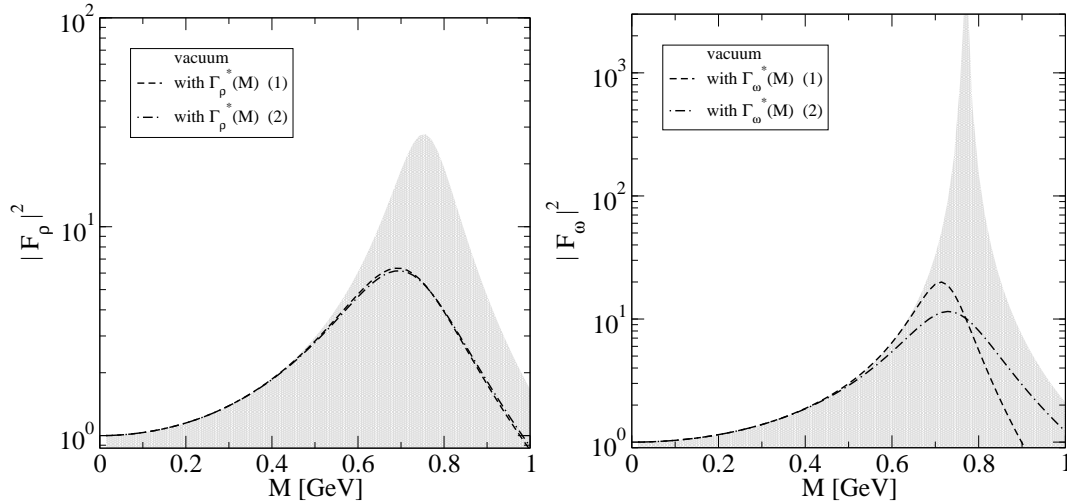


Figure 5.7: Left panel: modulus squared of the ρ meson contribution to the covariant form factor $|F_\rho|^2$ in vacuum (shaded area) and at $\rho = 2\rho_0$ for $\Gamma_\rho^{\text{tot}}(\rho_0, m_\rho) = 250$ MeV (dashed and dashed-dotted lines). Right panel: modulus squared of the ω meson contribution to the covariant form factor, $|F_\omega|^2$, in vacuum (shaded area) and at $\rho = 2\rho_0$ for $\Gamma_\omega^{\text{tot}}(\rho_0, m_\omega) = 125$ MeV (dashed and dashed-dotted lines). For both panels the dashed line corresponds to the assumption that the collisional width has the same energy dependence as the vacuum width. The dashed-dotted line corresponds to the assumption that the collisional width has the energy dependence (5.52).

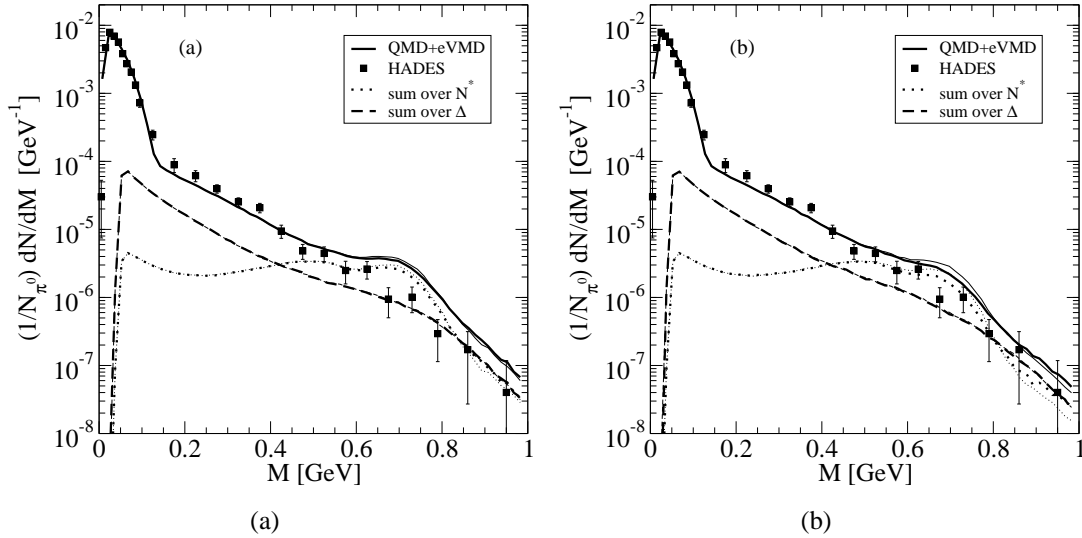


Figure 5.8: Dilepton spectrum in C+C collisions at 2.0 AGeV for different values of the in-medium ρ and ω widths and different choices for the energy dependence of the collisional width. The thick lines refer to an energy dependence estimated from the $V + N \rightarrow R \rightarrow \pi + N$ as discussed in the text. The thin lines correspond to the same calculations shown in Fig. 5.4 and are shown for comparison. Left panel: $\Gamma_\rho^{\text{tot}}(\rho_0) = 200$ MeV and $\Gamma_\omega^{\text{tot}}(\rho_0) = 60$ MeV. Right panel: $\Gamma_\rho^{\text{tot}}(\rho_0) = 250$ MeV and $\Gamma_\omega^{\text{tot}}(\rho_0) = 125$ MeV.

up over all important resonances coupling to the $V + N$ system, each taken with a different weight according to its relative coupling strength, and determine for each mode the corresponding angular momentum dependence of the πN scattering amplitude. Moreover, the

invariant mass squared of the intermediate resonance would be $s = (p_N + p)^2$ which leads to a dependence on the 3-momentum \mathbf{p} of the vector meson. It is then clear that the steps to complete this procedure are analogous to what has already been presented in the previous section where spectral functions for the vector meson have been calculated. In fact, the $V + N \rightarrow R \rightarrow \pi + N$ channel is one of the processes consistently included in our calculation of the spectral functions, since the $N\pi$ channel is one of the channels entering in the expression of the total width of the resonance. Already from this simple argument the importance of using realistic spectral functions can be inferred.

Dropping mass scenario

As the next step we investigated the effect of a dropping mass in-medium scenario à la Brown-Rho. Thus, we performed calculations for an in-medium scenario that differs from the previous one by the additional assumption that the vector meson mass scales with the density according to a $m_V^* = m_V(1 - \alpha\rho_B/\rho_0)$ law, with $\alpha = 0.2$. The results are shown in Fig. 5.9 where Fig. 5.9(a) refers to the choice $\Gamma_\rho^{\text{tot}}(\rho_0) = 200$ MeV, $\Gamma_\omega^{\text{tot}}(\rho_0) = 60$ MeV and Fig. 5.9(b) to the choice $\Gamma_\rho^{\text{tot}}(\rho_0) = 250$ MeV, $\Gamma_\omega^{\text{tot}}(\rho_0) = 125$ MeV. The inclusion of a

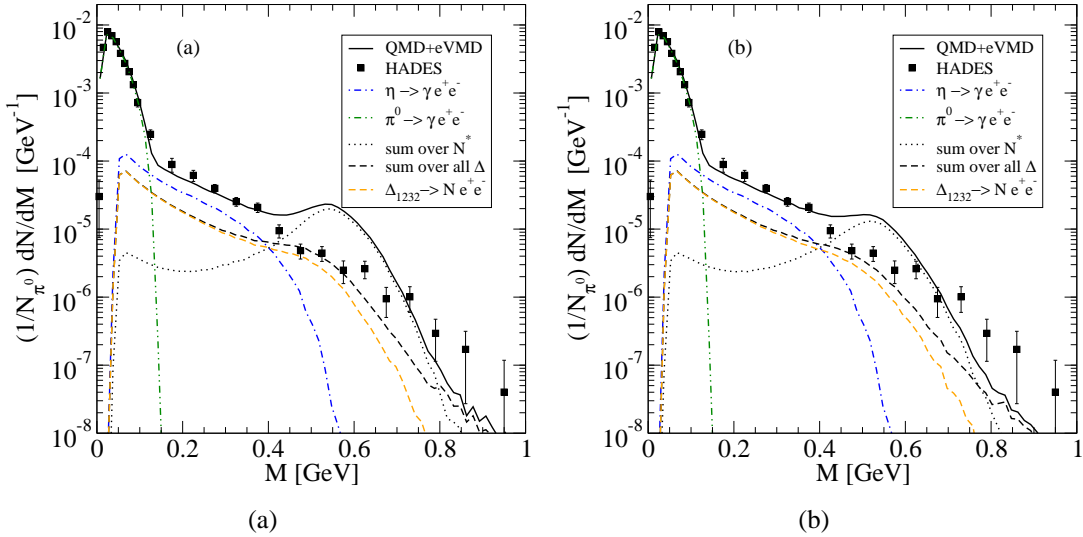


Figure 5.9: Dilepton spectrum in C+C collisions at 2.0 AGeV for different values of the in-medium ρ and ω widths when an in-medium vector meson mass $m_V^* = m_V(1 - \alpha\rho_B/\rho_0)$ is introduced. Left panel: $\Gamma_\rho^{\text{tot}}(\rho_0) = 200$ MeV and $\Gamma_\omega^{\text{tot}}(\rho_0) = 60$ MeV. Right panel: $\Gamma_\rho^{\text{tot}}(\rho_0) = 250$ MeV and $\Gamma_\omega^{\text{tot}}(\rho_0) = 125$ MeV.

dropping in-medium vector meson mass results in a global shift of the vector meson spectral strength to lower masses. Thus, the corresponding theoretical spectrum is enhanced at lower invariant masses with a resulting sizeable overestimation of the experimental data in the $0.4 \leq M \leq 0.7$ GeV region. At the same time, the experimental data are underestimated in the region around and above the vector meson peak. This is due to the lack of spectral strength around the (vacuum) vector meson peak induced by the dropping of the vector meson “pole” mass to lower values. It is interesting to note that, at higher energies, a recent comparison of the dropping mass scenario to new high resolution CERES data has pointed

out a similar underestimation of the vector meson peak [26]. There, however, the analysis focused only on the in-medium ρ meson. Concerning the low mass region, $m_\pi \leq M \leq 0.4$ GeV, the presence of additional strength moves the spectrum closer to the experimental data at $M \sim 0.3 - 0.4$ GeV. However, the region $m_\pi \leq M \leq 0.3$ GeV remains slightly but systematically underestimated. In summary, one can conclude that a naive Brown-Rho scaling is too schematic in order to explain the low mass region. This finding is consistent with previous theoretical analyses of the DLS data at 1 AGeV [29, 30, 31].

In-medium spectral functions

Let us now pass to the introduction of in-medium vector meson properties determined by the in-medium self energies of the vector mesons calculated within NRD+eVMD. First, we present in Fig. 5.10(a) the dilepton spectrum obtained when the ρ and ω mesons are described by the spectral functions determined neglecting in-medium modification of the nucleon resonance widths. These spectral functions can be considered as "first iteration" spectral functions. They induce a depletion of the theoretical spectrum in the mass region $0.45 \leq M \leq 0.75$ GeV not supported by the data. The result can be better understood with the help of Fig. 5.11, where the corresponding in-medium ρ and ω meson contributions to the nucleon resonance covariant form factors are shown at $\rho = \rho_0$ and $\rho = 2\rho_0$ for a vector meson at rest in the nuclear medium (dashed lines). The complex behaviour of the vector meson self energies are reflected in the in-medium form factors which do not present anymore the simple Lorentzian-like shape typical of the vacuum. In particular, we observe a minimum positioned at $0.5 \lesssim M \lesssim 0.6$ GeV between two maxima at $0.4 \lesssim M \lesssim 0.5$ GeV and $M \sim 0.8$ GeV.¹² The particular shape of the in-medium form factor is determined by the behaviour of both the real and imaginary part of the self energy. However, switching off the real part of the self energy, we observed that the depletion present in the form factor between approximately $M \sim 0.5$ GeV and $M \sim 0.7 - 0.8$ GeV is mainly determined by the large value of the imaginary part of the self energy in this region. The latter is shown in Fig. 5.12. The increase is due to the coupling to the important resonances, namely the $N^*(1520)$ for the ρ meson and the $N^*(1535)$ for the ω meson. The corresponding bump structure is a typical feature of this class of models coupling the vector meson to resonance-hole states.

The inclusion of the in-medium properties of the nucleon resonances in the determination of the vector meson spectral functions reduces the value of the imaginary part of the self energy in this region (see Fig. 5.12). In the case of the ω meson, for example, the reduction at $M = 0.57$ GeV is about a factor 2.5. As a consequence, the corresponding form factors, shown in Fig. 5.11, are enhanced. This has an effect on the level of the dilepton spectrum. The dilepton spectrum obtained using self-consistent calculated spectral functions is shown in Fig. 5.10(b). The inclusion of the in-medium properties of the nucleon resonances in the determination of the vector meson spectral functions moves the theoretical spectrum closer to the experimental data in the mass region $0.45 \leq M \leq 0.75$ GeV. This shows the importance of taking into account in-medium modifications of the nucleon resonances to evaluate the vector

¹²The exact positions of the minimum and the maxima, especially of the maximum at lower M , vary with the density. This is the reason why we indicate "regions" for these positions.

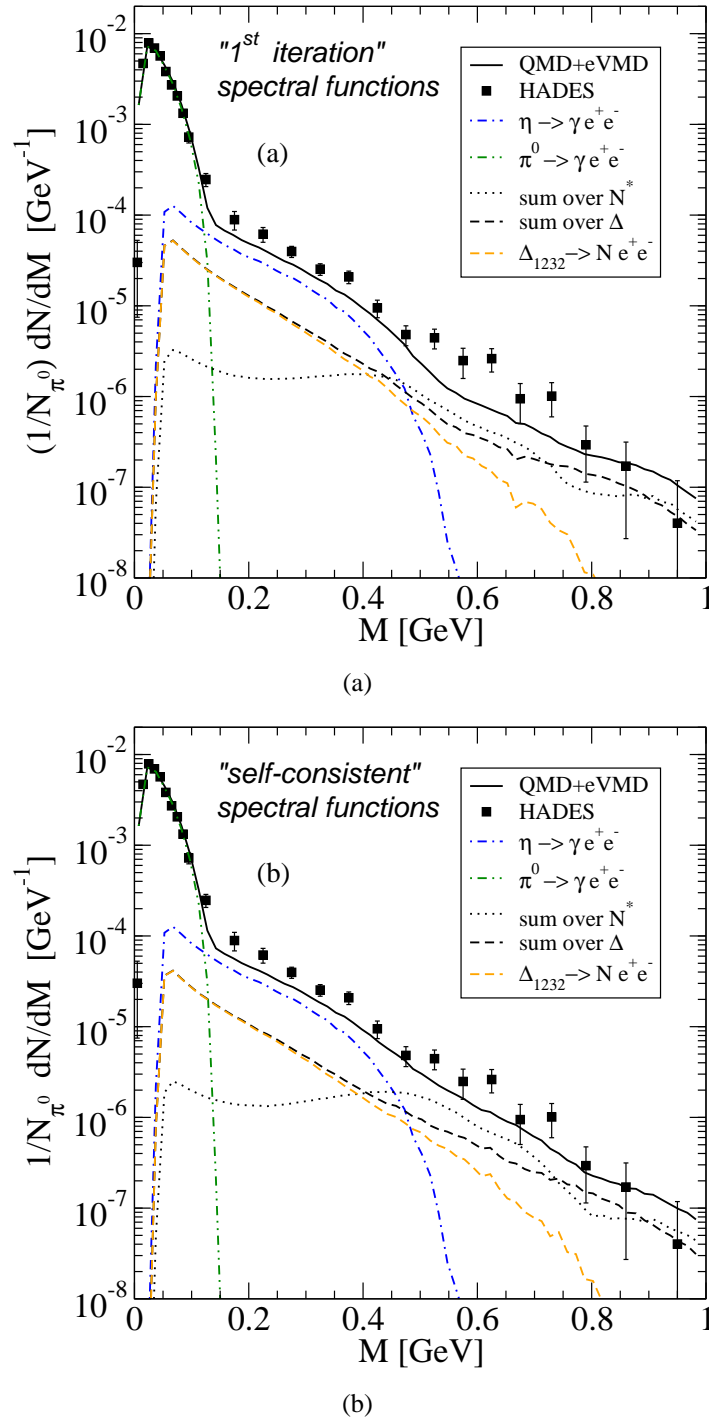


Figure 5.10: Dilepton spectrum in C+C collisions at 2.0 AGeV resulting from the inclusion of ρ - and ω -meson spectral functions calculated within the NRD+eVMD model. The spectral functions affect the branching ratios for the Dalitz decays of the baryon resonances, as explained in the text. The left panel corresponds to the inclusion of vector meson self energies determined from vacuum nucleon resonance properties. The right panel corresponds to the inclusion of vector meson self energies calculated in a self-consistent iteration scheme in which the in-medium modification of the nucleon resonance widths induced by the in-medium spectral functions of the vector mesons is taken into account.

meson in-medium properties resulting from the excitation of nucleon resonance-nucleon hole states. However, some data points remain underestimated. The reduction of the theoretical

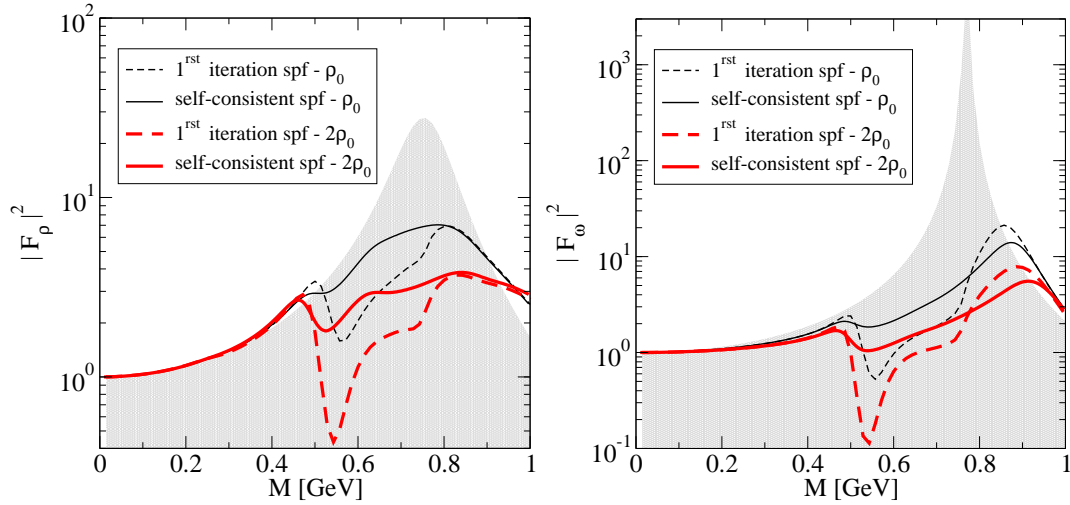


Figure 5.11: Left panel: modulus squared of the ρ meson contribution to the covariant form factor, $|F_\rho|^2$, at $\rho = \rho_0$ (thin lines) and $\rho = 2\rho_0$ (thick lines). The shaded area shows the vacuum value of $|F_\rho|^2$. Right panel: modulus squared of the ω meson contribution to the covariant form factor, $|F_\omega|^2$, at $\rho = \rho_0$ (thin lines) and $\rho = 2\rho_0$ (thick lines). The shaded area shows the vacuum value of $|F_\omega|^2$. For both panels the dashed lines correspond to vector meson self energies calculated from vacuum nucleon resonance properties. The full lines correspond to vector meson self energies calculated in a self-consistent iteration scheme in which the in-medium modifications of the nucleon resonance widths induced by the in-medium spectral functions of the vector mesons are taken into account.

spectrum due to the inclusion of in-medium effects for the vector mesons can intuitively be understood in terms of absorption processes of vector mesons which reduce the number of vector mesons and, consequently, the dilepton yield. In this sense, the underestimation of the experimental data suggests that the NRD+eVMD model predicts a too strong absorption of vector mesons.

Concerning the mass region $M > 0.4$ GeV, although the agreement with the experimental data is not perfect, the level achieved can be considered appreciable if one evaluates the underlying theoretical challenge: the calculation presented here represents a parameter-free determination of the in-medium dilepton spectrum. We operate within an approach which attempts to describe *simultaneously with the same model parameters* dilepton and vector meson production as well as their in-medium modifications. The task is complicated by the current uncertainties especially on the $RN\omega$ couplings due to the lack of experimental data on e.g. $R \rightarrow N\omega$ decay modes. One possible reason for the present underestimation of the experimental data can of course lie in those poorly constrained eVMD model parameters, in particular the $RN\omega$ couplings. The probably most relevant case is the $N^*(1535)$ resonance, with its strong coupling to the ω meson predicted by the eVMD model though a decay of this resonance to $N\omega$ has not been measured yet. Another possible reason can be connected to the fact that in particular the ω meson spectral function does not result to be normalized in the mass region of our interest. The violation of normalization ranges from about 30% at

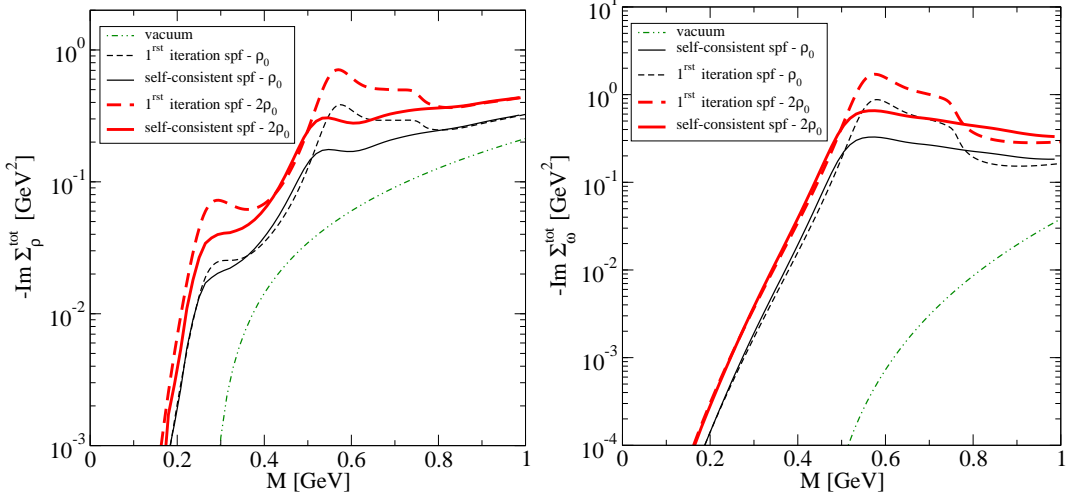


Figure 5.12: Left panel: Imaginary part of the ρ meson self energy in vacuum (dashed-double-dotted line), at $\rho = \rho_0$ (thin lines) and at $\rho = 2\rho_0$ (thick lines). Right panel: Imaginary part of the ω meson self energy in vacuum (dashed-double-dotted line) at $\rho = \rho_0$ (thin lines) and at $\rho = 2\rho_0$ (thick lines). For both panels the dashed lines correspond to vector meson self energies calculated from vacuum nucleon resonance properties. The full lines correspond to vector meson self energies calculated in a self-consistent iteration scheme in which the in-medium modifications of the nucleon resonance widths induced by the in-medium spectral functions of the vector mesons are taken into account.

$\rho = \rho_0$ to about 45% at $\rho = 2\rho_0$.¹³ In principle, this is not an inconsistency, since spectral functions should obey the sum rule in the entire invariant mass range (up to $M = \infty$) and not necessarily already in the finite mass interval in which we work. On the other side, one would expect high invariant mass regions not to influence significantly the results we can extract for lower masses in the framework of phenomenological low energy models.

Regarding the low mass region, $m_\pi \leq M \leq 0.4$ GeV, the introduction of in-medium spectral functions does not provide a solution for the underestimation of the experimental data. On the contrary, due to the finite value of the imaginary part of the self energy at $M \sim 0$ for high vector meson three-momenta \mathbf{p} ($\text{Im}\Sigma_V^{\text{tot}}(M=0) \neq 0$ for $\mathbf{p} \neq 0$), at high momenta we have $|F_V(M=0)|^2 < 1$ with a consequent reduction of strength. We can therefore conclude that to explain the low mass region one has to take into account other effects. It has been shown in Ref. [38] that the account for decoherence effects enhances the theoretical spectrum in the low mass region. The inclusion of such effects are not a matter of this work, therefore we do not discuss them here and refer the reader to Ref. [38] for the description of the decoherence as an in-medium effect. Surely, it will be interesting to take the effect of a partial loss of quantum coherence in medium into account in future investigations. For the sake of completeness, we would like to mention that the particularly significant contribution from pn bremsstrahlung of Ref. [128] has recently been suggested as a possible candidate for the solution of the DLS puzzle [127]. To our present knowledge, the discrepancy between the results of [128] and previous works [125, 130] has not been clarified yet, therefore we do not comment further on this.

¹³Integral evaluated in the mass region up to 1.5 GeV.

Chapter 6

Summary and Conclusions

Combining a nucleon resonance dominance model with an extended vector meson dominance model we have determined the in-medium modifications which the ρ and ω mesons experience in nuclear matter due to a finite baryon density. In addition, non-resonant contributions to the vector meson self energies have been investigated. For both vector mesons we find a substantial broadening of the width and a significant shift of spectral strength down to smaller invariant masses. In particular at small momenta, the coupling of the ρ meson to the $N^*(1520)N^{-1}$ state and of the ω meson to the $N^*(1535)N^{-1}$ state leads to a pronounced double-peak structure in the spectral function. In a first approximation the vector meson spectral functions have been calculated from vacuum nucleon resonance properties. Going beyond this first approximation, we took into account the in-medium modification of the nucleon resonance widths induced by the in-medium modifications of the ρ and ω mesons, which appear among the resonance decay products. This leads to a self-consistent iterative calculation of the vector meson spectral functions. The self-consistent iteration scheme mainly reduces the $N^*(1520)N^{-1}$ and $N^*(1535)N^{-1}$ peaks.

As the next step, we investigated the influence which in-medium modifications of the vector meson properties have on the dilepton production rate in heavy ion collisions. The dilepton spectrum has been calculated exemplary for the reaction C+C at 2.0 AGeV for which experimental data have been recently released by the HADES collaboration. This energy range is complementary to the ultrarelativistic regime since it probes nuclear matter at high net baryon densities and moderate temperatures, while dilepton measurements at the SPS (NA60, CERES) and at RHIC (PHENIX) probe the electromagnetic response at low net baryon densities and high temperatures, most likely even not hadronic but partonic matter. Thus the present investigations are restricted to moderate relativistic energies where the medium is dominated by nucleons and their excitations, i.e. nucleon resonances. We investigated several possible in-medium scenarios. First, we included in-medium effects following standard treatments, namely a schematic collisional broadening of the vector meson width and a dropping of the vector meson mass according to a Brown-Rho scaling law.

Within the schematic collisional broadening scenario we find that the experimental data are still slightly overestimated in the region around the vector meson peak when values of $\Gamma_{\rho}^{\text{tot}}(\rho_0) = 250$ MeV and $\Gamma_{\omega}^{\text{tot}}(\rho_0) = 125$ MeV for the total vector meson width at saturation density are used. Thereby we assumed that the in-medium widths of the vector mesons

increase linearly with density. We discussed the approximation made when assigning an energy dependence to the vector meson width. We, however, did not find too large differences among the various possibilities. Nevertheless, we want to point out the theoretical limitations which such a schematic treatment carries with it.

In the in-medium scenario according to which the vector meson masses decrease linearly with density (Brown-Rho scaling) we find that, even when the collisional broadening of the vector meson widths is additionally taken into account, the corresponding dilepton spectrum overestimates the experimental data at invariant masses below the vector meson peak and underestimates them in the region around and above the vector meson peak. This is a consequence of the global shift of the spectral strength down to lower invariant masses predicted by this scenario, with a consequent lack of spectral strength in the region of the vector meson peak.

In a next step, we went beyond the schematic inclusion of in-medium effects and included the vector meson in-medium properties consistently, i.e. in terms of the in-medium self energies microscopically calculated by combining the nucleon resonance dominance and the extended vector meson dominance models. Doing so, we attempt for the first time to achieve a consistent theoretical description of dilepton spectra based on a unified model for vector meson and dilepton production as well as their in-medium modifications. This surpasses the standard treatments, where the value of the total width at a given density enters as an input parameter and scaling laws for the width are based on assumptions or educated guesses. We find that self energies determined from vacuum nucleon resonance properties give a poor description of the experimental data in the invariant mass region $0.45 \leq M \leq 0.75$ GeV. On the contrary, the self-consistent iteration scheme gives a reasonable description of the data in the same mass region. This demonstrates the importance of including in-medium resonance properties in a consistent way for the determination of the vector meson spectral functions. Taking into account the large uncertainties in the couplings of the nucleon resonances, especially to the ω meson, and the fact that this stands as a parameter-free determination of the in-medium dilepton spectrum, the result can be considered as satisfactory. However, the comparison to data suggests that the in-medium scenario predicted within the present approach is still too strong. For the low mass region of the dilepton spectrum ($m_\pi \leq M \leq 0.4$ GeV) we find that the inclusion of in-medium spectral functions of the ρ and ω mesons do not improve the theoretical result and experimental data remain slightly underestimated.

In summary, we believe that the present investigations provide an essential step towards the understanding of dilepton spectra in heavy ion collisions and vector meson properties in matter. Forthcoming data, in particular for heavy systems, will certainly help to further reduce still existing model uncertainties.

Appendix A

Notation

Units and metric. We use units $\hbar = c = 1$. The metric signature is

$$g_{\mu\nu} = (+, -, -, -) .$$

Indices. Greek indices take values $\mu = 0, \dots, 3$, while spatial indices are denoted by Latin letters, $i, j, \dots = 1, 2, 3$. Repeated upper and lower Lorentz indices are summed over, e.g. $A_\mu B^\mu \equiv \sum_{\mu=0}^3 A_\mu B^\mu$. *Contravariant vectors*, denoted by superscripts, are written as

$$A^\mu = (A^0, \mathbf{A}) = (A^0, A^1, A^2, A^3) ,$$

whereas *covariant vectors*, denoted by subscripts, are defined by

$$A_\mu \equiv g_{\mu\nu} A^\nu = (A^0, -\mathbf{A}) .$$

A scalar product of two four vectors is defined by

$$A \cdot B \equiv A_\mu B^\mu = A^\mu B_\mu = A^0 B^0 - \mathbf{A} \cdot \mathbf{B} .$$

The space-time four-vector is

$$x^\mu = (x^0, \mathbf{x}) = (t, \mathbf{x})$$

and the four-momentum is given by

$$p^\mu = (p^0, \mathbf{p}) = (E, \mathbf{p}) .$$

The components of the contravariant four-gradient are denoted by

$$\partial^\mu \equiv \frac{\partial}{\partial x_\mu} = \left(\frac{\partial}{\partial t}, -\nabla \right) .$$

With our choice of signature the four-momentum operator is represented on functions of the coordinates as $p^\mu = +i\partial^\mu$, so $p^0 = i\partial/\partial x^0 = i\partial/\partial t$ and $p^i = i\partial^i = -i\partial_i = -i\partial/\partial x^i$. Therefore $p^i = -i\nabla^i$ with $\nabla^i = \partial/\partial x^i = \partial_i$ or, in vector notation, $\mathbf{p} = i\nabla$ and $\nabla = \partial/\partial \mathbf{x}$. Finally, we also use the Feynman slash notation: for a four-vector A^μ , we define $\not{A} = a_\mu \gamma^\mu$. In particular, $\not{\partial} = \gamma^\mu \partial_\mu$

Dirac matrices. Dirac γ matrices satisfy

$$\{\gamma^\mu, \gamma^\nu\} \equiv \gamma^\mu \gamma^\nu + \gamma^\nu \gamma^\mu = 2g^{\mu\nu}. \quad (\text{A.1})$$

Therefore $\gamma_0^2 = 1$ and, for each i , $(\gamma^i)^2 = -1$; γ^0 is hermitian while, for each i , γ^i is antihermitian,

$$(\gamma^0)^\dagger = \gamma^0, \quad (\gamma^i)^\dagger = -\gamma^i,$$

or, more compactly, $(\gamma^\mu)^\dagger = \gamma^0 \gamma^\mu \gamma^0$. The matrix γ^5 is defined as

$$\gamma^5 = +i\gamma^0\gamma^1\gamma^2\gamma^3,$$

and satisfies

$$(\gamma^5)^2 = 1, \quad (\gamma^5)^\dagger = \gamma^5, \quad \{\gamma^5, \gamma^\mu\} = 0.$$

We also define

$$\sigma^{\mu\nu} = \frac{i}{2}[\gamma^\mu, \gamma^\nu]. \quad (\text{A.2})$$

A particular usual representation of the γ matrix algebra is the so called *standard representation* in which

$$\gamma^0 = \begin{pmatrix} 1 & 0 \\ 0 & -1 \end{pmatrix}, \quad \gamma^i = \begin{pmatrix} 0 & \sigma^i \\ -\sigma^i & 0 \end{pmatrix}, \quad \gamma^5 = \begin{pmatrix} 0 & 1 \\ 1 & 0 \end{pmatrix}.$$

The Pauli matrices are

$$\sigma^1 = \begin{pmatrix} 0 & 1 \\ 1 & 0 \end{pmatrix}, \quad \sigma^2 = \begin{pmatrix} 0 & -i \\ i & 0 \end{pmatrix}, \quad \sigma^3 = \begin{pmatrix} 1 & 0 \\ 0 & -1 \end{pmatrix}.$$

and satisfy

$$\sigma^i \sigma^j = \delta^{ij} + i\epsilon^{ijk} \sigma^k.$$

In the calculation of cross sections and decay rates we often need to evaluate traces of products of γ matrices. As a consequence of the commutation algebra (A.1) they can be evaluated without ever explicitly calculating a matrix product. Some useful trace identities are:

$$\text{Tr}[1_{4 \times 4}] = 4, \quad (\text{A.3})$$

$$\text{Trace of an odd number of } \gamma_\mu \text{'s vanishes,} \quad (\text{A.4})$$

$$\text{Tr}[\not{a} \not{b}] = 4a \cdot b, \quad (\text{A.5})$$

$$\text{Tr}[\not{a} \not{b} \not{c} \not{d}] = 4[(a \cdot b)(c \cdot d) - (a \cdot c)(b \cdot d) + (a \cdot d)(b \cdot c)], \quad (\text{A.6})$$

$$\text{Tr}[\gamma_5] = 0, \quad (\text{A.7})$$

$$\text{Tr}[\gamma_5 \not{a} \not{b}] = 0, \quad (\text{A.8})$$

$$\text{Tr}[\gamma_5 \not{a} \not{b} \not{c} \not{d}] = 4i\epsilon_{\mu\nu\lambda\sigma} a^\mu b^\nu c^\lambda d^\sigma, \quad (\text{A.9})$$

where $\epsilon_{\mu\nu\lambda\sigma} = +1(-1)$ for $\mu, \nu, \lambda, \sigma$ an even (odd) permutation of 0, 1, 2, 3 and 0 if two indices are the same.

Other useful results for simplifying trace calculations are:

$$\gamma_\mu \gamma^\mu = 4, \quad (\text{A.10})$$

$$\gamma_\mu \not{a} \gamma^\mu = -2 \not{a}, \quad (\text{A.11})$$

$$\gamma_\mu \not{a} \not{b} \gamma^\mu = 4(a \cdot b), \quad (\text{A.12})$$

$$\gamma_\mu \not{a} \not{b} \not{c} \gamma^\mu = -2 \not{c} \not{b} \not{a}. \quad (\text{A.13})$$

Fermions. For fermions, we use the covariant normalization in which we have $2E$ particles/unit volume. Thus, we have the orthogonality relations

$$u^{(r)\dagger} u^{(s)} = 2E \delta_{rs}, \quad v^{(r)\dagger} v^{(s)} = 2E \delta_{rs},$$

with $r, s = 1, 2$. It follows that

$$\bar{u}^{(s)} u^{(s)} = 2m, \quad \bar{v}^{(s)} v^{(s)} = -2m$$

and the completeness relations read

$$\begin{aligned} \sum_{s=1,2} u^{(s)}(p) \bar{u}^{(s)}(p) &= \not{p} + m, \\ \sum_{s=1,2} v^{(s)}(p) \bar{v}^{(s)}(p) &= \not{p} - m. \end{aligned} \tag{A.14}$$

Electromagnetism. The electron charge is denoted by e , and $e < 0$. As is customary in particle physics, we use the Heaviside-Lorentz system of units for electromagnetism. This means that the fine structure constant $\alpha = 1/137$ is related to the electron charge by

$$\alpha = \frac{e^2}{4\pi\hbar c},$$

or simply $\alpha = e^2/(4\pi)$ when we set $\hbar = c = 1$.

Appendix B

The $\gamma^* \rightarrow \ell^+ \ell^-$ decay width

We want to calculate the dilepton decay width of a massive (virtual) photon γ^* . Let be M the photon mass. In the rest frame of the decaying virtual photon, the decay rate $\gamma^* \rightarrow \ell^+ \ell^-$ is given by

$$d\Gamma(\gamma^* \rightarrow \ell^+ \ell^-) = \frac{1}{2M} \sum_f \overline{|\mathcal{A}|^2} \frac{(2\pi)^4}{(2\pi)^6} d\Phi_2 \quad (\text{B.1})$$

where $d\Phi_2$ denotes the differential two-body phase space. The corresponding Feynman diagram is shown in Fig. B.1, where the various factors needed to compute the amplitude \mathcal{A} are shown in detail.

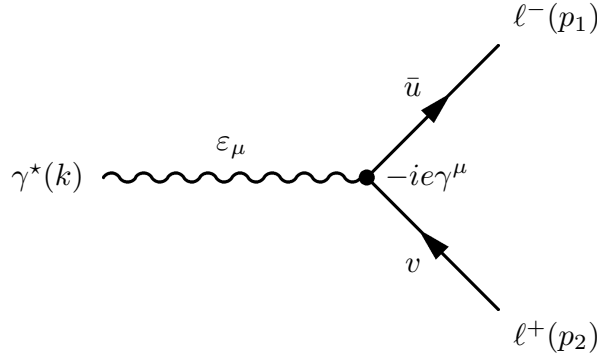


Figure B.1: Feynman diagram for the $\gamma^* \rightarrow \ell^+ \ell^-$ decay.

Applying the Feynman rules, one has:

$$i\mathcal{A} = -ie\epsilon_\mu^\lambda(k)\bar{u}(p_1, s)\gamma^\mu v(p_2, s'). \quad (\text{B.2})$$

To obtain the unpolarized decay width, we must average $|\mathcal{A}|^2$ over the polarization of the initial virtual photon and sum over the spins of the final leptons:

$$\sum_f \overline{|\mathcal{A}|^2} = e^2 \frac{1}{3} \sum_\lambda \epsilon_\mu^\lambda \epsilon_\nu^{*\lambda} \sum_{s, s'} \bar{u}(p_1, s)\gamma^\mu v(p_2, s')\bar{v}(p_2, s')\gamma^\nu u(p_1, s). \quad (\text{B.3})$$

The factor $\frac{1}{3}$ is due to averaging over the initial virtual photon photon polarizations. Using the completeness relation for a massive vector particle

$$\sum_{\lambda} \varepsilon_{\mu}^{\lambda}(k) \varepsilon_{\nu}^{*\lambda}(k) = -g_{\mu\nu} + \frac{k_{\mu} k_{\nu}}{k^2}, \quad (\text{B.4})$$

where the sum is over the three polarization states of the massive vector particle, one obtains

$$\begin{aligned} \sum_f \overline{|\mathcal{A}|^2} &= \frac{4\pi\alpha}{3} \left(-g_{\mu\nu} + \frac{k_{\mu} k_{\nu}}{M^2}\right) \sum_{s,s'} \bar{u}(p_1, s) \gamma^{\mu} v(p_2, s') \bar{v}(p_2, s') \gamma^{\nu} u(p_1, s) \\ &= \frac{4\pi\alpha}{3} \sum_{s,s'} \left\{ -\bar{u}(p_1, s) \gamma^{\mu} v(p_2, s') \bar{v}(p_2, s') \gamma_{\mu} u(p_1, s) \right. \\ &\quad \left. + \frac{1}{k^2} \bar{u}(p_1, s) \not{k} v(p_2, s') \bar{v}(p_2, s') \not{k} u(p_1, s) \right\}. \end{aligned} \quad (\text{B.5})$$

The second term vanishes due to current conservation. The spinor completeness relation, (A.14), allows the sum over $u\bar{u}$ and $v\bar{v}$ states to be performed and one finds

$$\begin{aligned} \sum_f \overline{|\mathcal{A}|^2} &= \frac{4\pi\alpha}{3} \left\{ -\text{Tr}[(\not{p}_1 + m_{\ell}) \gamma^{\mu} (\not{p}_2 - m_{\ell}) \gamma_{\mu}] + 0 \right\} \\ &= \frac{4\pi\alpha}{3} \left\{ -\text{Tr}[\underbrace{\not{p}_1 \gamma^{\mu} \not{p}_2 \gamma_{\mu}}_{-2\not{p}_2} - \underbrace{m_{\ell}^2 \gamma^{\mu} \gamma_{\mu}}_4] \right\} \\ &= \frac{4\pi\alpha}{3} \left\{ 2 \underbrace{\text{Tr}[\not{p}_1 \not{p}_2]}_{4p_1 \cdot p_2} + 4m_{\ell}^2 \underbrace{\text{Tr}[1_{4 \times 4}]}_4 \right\} \\ &= \frac{4\pi\alpha}{3} \left\{ 8(p_1 \cdot p_2) + 16m_{\ell}^2 \right\} \end{aligned} \quad (\text{B.6})$$

where we made use of the trace theorems (A.4), (A.11), (A.10), (A.5) and (A.3). Conservation of 4-momentum at the vertex impose $k = p_1 + p_2$. Therefore one has

$$\begin{aligned} k^2 = M^2 = (p_1 + p_2)^2 &= p_1^2 + p_2^2 + 2p_1 \cdot p_2 = 2m_{\ell}^2 + 2p_1 \cdot p_2 \\ &\Rightarrow p_1 \cdot p_2 = \frac{M^2}{2} - m_{\ell}^2. \end{aligned} \quad (\text{B.7})$$

Introducing (B.7) in (B.6) we finally obtain

$$\sum_f \overline{|\mathcal{A}|^2} = \frac{4\pi\alpha}{3} 8 \left\{ \frac{M^2}{2} - m_{\ell}^2 + 2m_{\ell}^2 \right\} = \frac{16\pi\alpha}{3} \{M^2 + 2m_{\ell}^2\}. \quad (\text{B.8})$$

Substituting in Eq. B.1, one obtains:

$$d\Gamma(\gamma^* \rightarrow \ell^+ \ell^-) = \frac{1}{2M} \frac{4\alpha}{3\pi} (M^2 + 2m_{\ell}^2) d\Phi_2. \quad (\text{B.9})$$

Due to the angle independence of the matrix elements, the angle integration simply leaves us with the integrated two-body phase space, so that

$$\Gamma(\gamma^* \rightarrow \ell^+ \ell^-) = \frac{1}{2M} \frac{4\alpha}{3\pi} (M^2 + 2m_{\ell}^2) \Phi_2. \quad (\text{B.10})$$

The two-body phase space is

$$\Phi_2(M, m_\ell, m_\ell) = \frac{\pi}{2} \sqrt{1 - \frac{4m_\ell^2}{M^2}}. \quad (\text{B.11})$$

Substituting (B.11) in (B.10) one finds

$$\Gamma(\gamma^* \rightarrow \ell^+ \ell^-) = \frac{\alpha}{3M} (M^2 + 2m_\ell^2) \sqrt{1 - \frac{4m_\ell^2}{M^2}} \quad (\text{B.12})$$

or equivalently

$$\boxed{M\Gamma(\gamma^* \rightarrow \ell^+ \ell^-) = \frac{\alpha}{3} (M^2 + 2m_\ell^2) \sqrt{1 - \frac{4m_\ell^2}{M^2}}.} \quad (\text{B.13})$$

Appendix C

Non-resonant contributions to the forward VN scattering

C.1 The Compton-like contribution

We want to evaluate the vector meson-nucleon forward scattering amplitude for the Compton-like scattering process shown in Fig. C.1. The Compton-like scattering corresponds to non-resonant s - and u -channel vector meson-nucleon scattering. To leading order in density, the forward scattering amplitude determines the contribution to the vector meson self energy in nuclear matter due to the excitation of nucleon-nucleon hole states. The corresponding vector meson self energy diagram is depicted in Fig. C.2. Here we restrict ourselves to the calculation of the unpolarized forward scattering amplitude, treating the ρ and ω meson separately.

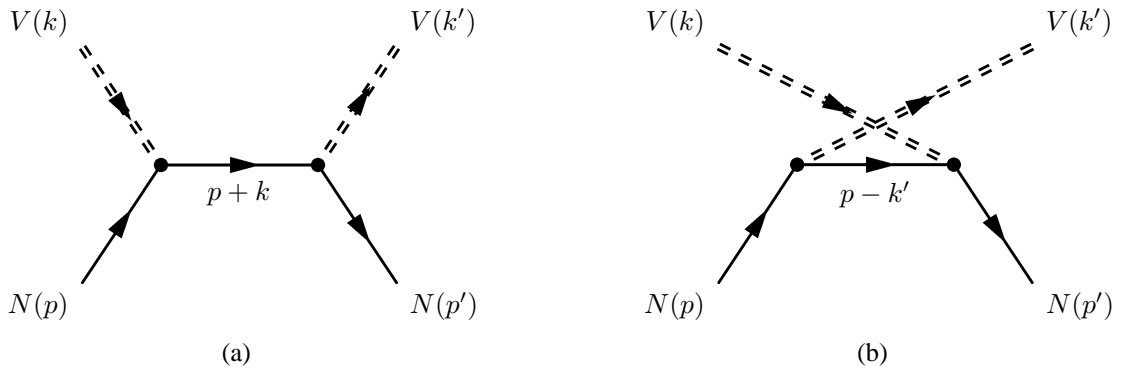


Figure C.1: Feynman diagram for the $NV \rightarrow NV$ Compton-like scattering.

C.1.1 ω meson

We describe the ωNN vertex according to the interaction Lagrangian

$$\delta\mathcal{L}_{\omega NN} = g_{\omega NN} \bar{\psi} \gamma^\mu \psi A_\mu \quad (\text{C.1})$$

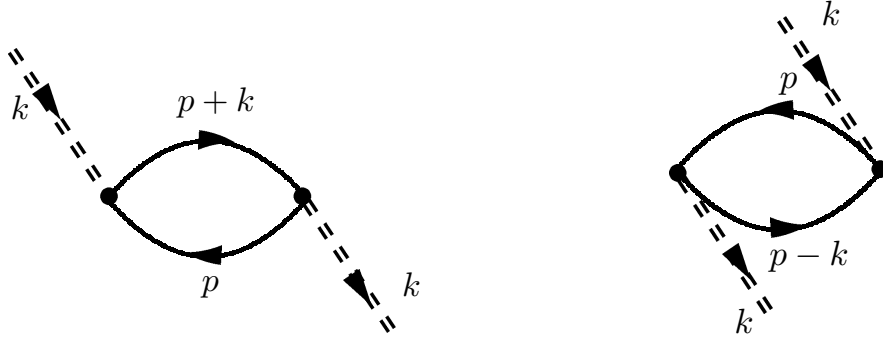


Figure C.2: Vector meson self energy in matter to lowest order in density due to the VN Compton-like scattering.

where A_μ denotes the ω meson field and ψ the nucleon field. The $NN\omega$ vector coupling is taken from the Bonn one-boson-exchange model [84] for nucleon-nucleon scattering ($g_{NN\omega} = 15.9$).

Let \mathcal{M}_1 be the amplitude for the process depicted in Fig. C.1(a) and \mathcal{M}_2 be the amplitude for the process depicted in Fig. C.1(b), which differs from the one of Fig. C.1(a) for the exchange of the initial and final state vector meson. Note that for forward scattering one has $k' = k$ and $p' = p$. The two amplitudes \mathcal{M}_1 and \mathcal{M}_2 are related by crossing symmetry, so that one has $\mathcal{M}_2 = \mathcal{M}_1(k \rightarrow -k)$. Therefore, it is enough to calculate only one of the two amplitudes. We will perform the calculation of \mathcal{M}_1 .

Application of the Feynman rules gives:

$$i\mathcal{M}_1 = \bar{u}^{(s)}(p) (ig_{\omega NN}\gamma^\nu) \frac{i(\not{p} + \not{k} + m_N)}{(p+k)^2 - m_N^2} (ig_{\omega NN}\gamma^\mu) u^{(s)}(p) \varepsilon_\nu^{(\lambda)\star}(k) \varepsilon_\mu^{(\lambda)}(k) \gamma^\nu \quad (\text{C.2})$$

where m_N denotes the nucleon mass and the 4-momentum assignments for the ingoing and outgoing particles are the ones shown in Fig. C.1(a). Performing the average over the nucleon spins and the photon polarizations one has:

$$\begin{aligned} \overline{i\mathcal{M}_1} &= \frac{1}{2} \frac{1}{3} \sum_{\lambda, s} \bar{u}^{(s)}(p) (ig_{\omega NN}\gamma^\nu) \frac{i(\not{p} + \not{k} + m_N)}{(p+k)^2 - m_N^2} (ig_{\omega NN}\gamma^\mu) u^{(s)}(p) \varepsilon_\nu^{(\lambda)\star}(k) \varepsilon_\mu^{(\lambda)}(k) \gamma^\nu \\ &= -ig_{\omega NN}^2 \frac{1}{6} \sum_\lambda \varepsilon_\nu^{(\lambda)\star}(k) \varepsilon_\mu^{(\lambda)}(k) \sum_s \bar{u}^{(s)}(p) \gamma^\nu \frac{\not{p} + \not{k} + m_N}{(p+k)^2 - m_N^2} \gamma^\mu u^{(s)}(p). \end{aligned} \quad (\text{C.3})$$

The sum over the photon polarizations and the nucleon spins can be evaluated with the help of the completeness relation for a massive vector particle (B.4) and of the spinor completeness relation (A.14) respectively. We then arrive at the following expression:

$$\begin{aligned} \overline{i\mathcal{M}_1} &= -ig_{\omega NN}^2 \frac{1}{6} (-g_{\nu\mu} + \frac{k_\nu k_\mu}{k^2}) \frac{1}{(p+k)^2 - m_N^2} \text{Tr}[(\not{p} + m_N)\gamma^\nu (\not{p} + \not{k} + m_N)\gamma^\mu] \\ &= +ig_{\omega NN}^2 \frac{1}{6} \frac{1}{p^2 + k^2 + 2p \cdot k - m^2} \text{Tr}[(\not{p} + m_N) \underbrace{\gamma_\mu (\not{p} + \not{k} + m_N)}_{\gamma^\mu} \gamma^\nu] \\ &\quad - ig_{\omega NN}^2 \frac{1}{6} \frac{1}{k^2} \frac{1}{p^2 + k^2 + 2p \cdot k - m^2} \text{Tr}[(\not{p} + m_N) \not{k} (\not{p} + \not{k} + m_N) \not{k}]. \end{aligned} \quad (\text{C.4})$$

Here we appositely separated the contribution proportional to the $g_{\nu\mu}$ term of the completeness relation (B.4) from the contribution proportional to the $k_\nu k_\mu$ term. We perform this separation in order to show that the latter contribution, although not vanishing for the single amplitudes $\overline{\mathcal{M}}_1$ or $\overline{\mathcal{M}}_2$, it does vanish in the sum of the two amplitudes $\overline{\mathcal{M}}_1 + \overline{\mathcal{M}}_2$. This is a consequence of current conservation. The consideration is completely identical to the one reported in many textbooks when treating the classical Compton scattering (see e.g. [135]).

Let us now evaluate the two traces of Eq. (C.4) with the help of the trace properties (A.3)–(A.6), (A.10) and (A.11):

$$\begin{aligned} \text{Tr}[(\not{p} + m_N) \underbrace{\gamma_\mu (\not{p} + \not{k} + m_N) \gamma^\mu}_{-2(\not{p} + \not{k}) + 4m_N}] &= -2 \text{Tr}[(\not{p} + m_N)(\not{p} + \not{k} - 2m_N)] \\ &= -2 \text{Tr}[\underbrace{\not{p} \not{p}}_{m_N^2} + \not{p} \not{k} - 2m_N^2] \\ &= -2 [4(p \cdot k) - 4m_N^2] \\ &= -8 [(p \cdot k) - m_N^2] \end{aligned} \quad (\text{C.5})$$

$$\begin{aligned} \text{Tr}[(\not{p} + m_N) \not{k} (\not{p} + \not{k} + m_N) \not{k}] &= \text{Tr}[\not{p} \not{k} \not{p} \not{k} + \underbrace{\not{p} \not{k} \not{k} \not{k}}_{k^2} + m_N^2 \underbrace{\not{k} \not{k}}_{k^2}] \\ &= 4[(p \cdot k)^2 - m_N^2 k^2 + (p \cdot k)^2] \\ &\quad + 4k^2(p \cdot k) + 4m_N^2 k^2 \\ &= 4(p \cdot k)[2(p \cdot k) + k^2] \end{aligned} \quad (\text{C.6})$$

where we used $p^2 = m_N^2$ and $\not{k} \not{k} = k^2$. Substituting in (C.4) we obtain:

$$i\overline{\mathcal{M}}_1 = +ig_{\omega NN}^2 \frac{1}{6} \frac{1}{k^2 + 2p \cdot k} \left\{ -8[(p \cdot k) - m_N^2] + 4 \frac{(p \cdot k)}{k^2} [2(p \cdot k) + k^2] \right\}. \quad (\text{C.7})$$

Hence

$$\overline{\mathcal{M}}_1 = \frac{1}{6} g_{\omega NN}^2 \left\{ \frac{-8[(p \cdot k) - m_N^2]}{k^2 + 2p \cdot k} + 4 \frac{(p \cdot k)}{k^2} \right\}. \quad (\text{C.8})$$

Using crossing symmetry we obtain \mathcal{M}_2 :

$$\overline{\mathcal{M}}_2 = \overline{\mathcal{M}}_1(k \rightarrow -k) = \frac{1}{6} g_{\omega NN}^2 \left\{ \frac{8[(p \cdot k) + m_N^2]}{k^2 - 2p \cdot k} - 4 \frac{(p \cdot k)}{k^2} \right\}. \quad (\text{C.9})$$

The sum of the two amplitudes gives the unpolarized forward scattering amplitude for the ω meson Compton-like scattering:

$$\begin{aligned} \overline{\mathcal{M}}_1 + \overline{\mathcal{M}}_2 &= \frac{1}{6} g_{\omega NN}^2 \left\{ \underbrace{\frac{-8[(p \cdot k) - m_N^2]}{k^2 + 2p \cdot k} + \frac{8[(p \cdot k) + m_N^2]}{k^2 - 2p \cdot k}}_{\propto g_{\nu\mu}} + \underbrace{4 \frac{(p \cdot k)}{k^2} - 4 \frac{(p \cdot k)}{k^2}}_{\propto k_\nu k_\mu} \right\} \\ &= \frac{8}{3} g_{\omega NN}^2 \frac{2(p \cdot k)^2 + m_N^2 k^2}{k^4 - 4(p \cdot k)^2}. \end{aligned} \quad (\text{C.10})$$

We had already anticipated that a cancellation between the contributions proportional to the $k_\nu k_\mu$ term of the photon completeness relation would occur in the sum $\overline{\mathcal{M}}_1 + \overline{\mathcal{M}}_2$. The cancellation can be directly read from Eq. (C.10).

C.1.2 ρ meson

We describe the ρNN vertex according to the interaction Lagrangian

$$\delta\mathcal{L}_{\rho NN} = \frac{g_{\rho NN}}{2m_N} \bar{\psi} \sigma^{\mu\nu} \psi F_{\mu\nu} \quad (\text{C.11})$$

where

$$F^{\mu\nu} = \partial^\mu A^\nu - \partial^\nu A^\mu, \quad (\text{C.12})$$

A_μ denotes the rho meson field, ψ denotes the nucleon field, m_N is the nucleon mass and the $NN\rho$ tensor coupling ($g_{NN\rho} = 19.8$) is taken from the Bonn potential [84]. The derivative coupling leads to a momentum dependence of the ρNN vertex. This can be explicitly shown by decomposing the vector meson field in terms of creation and annihilation operators

$$A_\mu(x) = \int \frac{d^3k}{(2\pi)^3 \sqrt{2E_{\mathbf{k}}}} \sum_\lambda [\varepsilon_\mu^{(\lambda)}(\mathbf{k}) a_{(\lambda),\mathbf{k}} e^{-ikx} + \varepsilon_\mu^{(\lambda)*}(\mathbf{k}) a_{(\lambda),\mathbf{k}}^\dagger e^{ikx}] \quad (\text{C.13})$$

and writing down the corresponding expression of $F^{\mu\nu}$:

$$\begin{aligned} F_{\mu\nu} &= \partial_\mu A_\nu - \partial_\nu A_\mu \\ &= \int \frac{d^3k}{(2\pi)^3 \sqrt{2E_{\mathbf{k}}}} \sum_\lambda \{ [\varepsilon_\nu^{(\lambda)}(\mathbf{k}) a_{(\lambda),\mathbf{k}} (-ik_\mu) e^{-ikx} + \varepsilon_\nu^{(\lambda)*}(\mathbf{k}) a_{(\lambda),\mathbf{k}}^\dagger (+ik_\mu) e^{ikx}] \\ &\quad - [\varepsilon_\mu^{(\lambda)}(\mathbf{k}) a_{(\lambda),\mathbf{k}} (-ik_\nu) e^{-ikx} + \varepsilon_\mu^{(\lambda)*}(\mathbf{k}) a_{(\lambda),\mathbf{k}}^\dagger (+ik_\nu) e^{ikx}] \} \\ &= \int \frac{d^3k}{(2\pi)^3 \sqrt{2E_{\mathbf{k}}}} \sum_\lambda \{ -i [k_\mu \varepsilon_\nu^{(\lambda)}(\mathbf{k}) - k_\nu \varepsilon_\mu^{(\lambda)}(\mathbf{k})] a_{(\lambda),\mathbf{k}} e^{-ikx} \\ &\quad + i [k_\mu \varepsilon_\nu^{(\lambda)*}(\mathbf{k}) - k_\nu \varepsilon_\mu^{(\lambda)*}(\mathbf{k})] a_{(\lambda),\mathbf{k}}^\dagger e^{ikx} \}. \end{aligned} \quad (\text{C.14})$$

Thus, $F_{\mu\nu}$ can be written as

$$F_{\mu\nu} = \int \frac{d^3k}{(2\pi)^3 \sqrt{2E_{\mathbf{k}}}} \sum_\lambda [E_{\mu\nu}^{(\lambda)}(\mathbf{k}) a_{(\lambda),\mathbf{k}} e^{-ikx} + E_{\mu\nu}^{(\lambda)*}(\mathbf{k}) a_{(\lambda),\mathbf{k}}^\dagger e^{ikx}] \quad (\text{C.15})$$

when we define

$$\boxed{\begin{aligned} E_{\mu\nu}^{(\lambda)}(\mathbf{k}) &\equiv -i [k_\mu \varepsilon_\nu^{(\lambda)}(\mathbf{k}) - k_\nu \varepsilon_\mu^{(\lambda)}(\mathbf{k})], \\ E_{\mu\nu}^{(\lambda)*}(\mathbf{k}) &\equiv +i [k_\mu \varepsilon_\nu^{(\lambda)*}(\mathbf{k}) - k_\nu \varepsilon_\mu^{(\lambda)*}(\mathbf{k})]. \end{aligned}} \quad (\text{C.16})$$

The expression for the ρ meson Compton-like scattering amplitude can be written down using the standard Feynman rules, provided that one assigns to the external vector meson line the term $E_{\mu\nu}^{(\lambda)}$ in place of the standard polarization vector $\varepsilon_\nu^{(\lambda)}$. For analogy, in the following we will call the tensor $E_{\mu\nu}^{(\lambda)}$ ‘‘polarization tensor’’.

Again, we are interest in the calculations of the forward scattering amplitude. We therefore set $k' = k$, $p' = p$. As for the case of the ω meson, we will calculate the amplitude \mathcal{M}_1 and derive \mathcal{M}_2 from crossing symmetry. We find:

$$i\mathcal{M}_1 = \bar{u}^{(s)}(p) \left(i \frac{g_{\rho NN}}{2m_N} \sigma^{\tau\rho} \right) \frac{i(\not{p} + \not{k} + m_N)}{(p+k)^2 - m_N^2} \left(i \frac{g_{\rho NN}}{2m_N} \sigma^{\mu\nu} \right) u^{(s)}(p) E_{\tau\rho}^{(\lambda)*}(k) E^{\mu\nu(\lambda)}(k) \quad (\text{C.17})$$

and

$$\begin{aligned} \overline{i\mathcal{M}_1} &= -i \frac{g_{\rho NN}^2}{4m_N^2} \frac{1}{3} \sum_{\lambda} E_{\tau\rho}^{(\lambda)*}(k) E_{\mu\nu}^{(\lambda)}(k) \frac{1}{(p+k)^2 - m_N^2} \\ &\quad \times \frac{1}{2} \sum_s \bar{u}^{(s)}(p) \sigma^{\tau\rho} (\not{p} + \not{k} + m_N) \sigma^{\mu\nu} u^{(s)}(p) \\ &= -i \frac{g_{\rho NN}^2}{4m_N^2} \frac{1}{3} \frac{1}{2} \frac{1}{(p+k)^2 - m_N^2} \sum_{\lambda} E_{\tau\rho}^{(\lambda)*}(k) E_{\mu\nu}^{(\lambda)}(k) \\ &\quad \times \frac{i^2}{4} \sum_s \bar{u}^{(s)}(p) (\gamma^{\tau}\gamma^{\rho} - \gamma^{\rho}\gamma^{\tau}) (\not{p} + \not{k} + m_N) (\gamma^{\mu}\gamma^{\nu} - \gamma^{\nu}\gamma^{\mu}) u^{(s)}(p) \\ &= +i \frac{g_{\rho NN}^2}{4m_N^2} \frac{1}{3} \frac{1}{2} \frac{1}{2p \cdot k + k^2} \sum_{\lambda} E_{\tau\rho}^{(\lambda)*}(k) E_{\mu\nu}^{(\lambda)}(k) \\ &\quad \times \text{Tr}[(\not{p} + m_N) (\gamma^{\tau}\gamma^{\rho} - \gamma^{\rho}\gamma^{\tau}) (\not{p} + \not{k} + m_N) (\gamma^{\mu}\gamma^{\nu} - \gamma^{\nu}\gamma^{\mu})] . \end{aligned} \quad (\text{C.18})$$

The second line of (C.18) is obtained from the first line by explicitly substituting the expression (A.2) of the $\sigma^{\tau\rho}$ and $\sigma^{\mu\nu}$ Lorentz tensors. The use of the spinor completeness relation (A.14) leads then to the third line.

Let us now derive the ‘‘completeness relation’’ for the ‘‘polarization tensor’’:

$$\begin{aligned} \sum_{\lambda} E_{\tau\rho}^{(\lambda)*}(k) E_{\mu\nu}^{(\lambda)}(k) &= \sum_{\lambda} \left[k_{\tau} \varepsilon_{\rho}^{(\lambda)*}(k) - k_{\rho} \varepsilon_{\tau}^{(\lambda)*}(k) \right] \left[k_{\mu} \varepsilon_{\nu}^{(\lambda)}(k) - k_{\nu} \varepsilon_{\mu}^{(\lambda)}(k) \right] \\ &= k_{\tau} k_{\mu} \sum_{\lambda} \varepsilon_{\rho}^{(\lambda)*}(k) \varepsilon_{\nu}^{(\lambda)}(k) - k_{\tau} k_{\nu} \sum_{\lambda} \varepsilon_{\rho}^{(\lambda)*}(k) \varepsilon_{\mu}^{(\lambda)}(k) \\ &\quad - k_{\rho} k_{\mu} \sum_{\lambda} \varepsilon_{\tau}^{(\lambda)*}(k) \varepsilon_{\nu}^{(\lambda)}(k) + k_{\rho} k_{\nu} \sum_{\lambda} \varepsilon_{\tau}^{(\lambda)*}(k) \varepsilon_{\mu}^{(\lambda)}(k) . \end{aligned} \quad (\text{C.19})$$

We have now to substitute the completeness relation (B.4) for a massive vector particle. As can be easily seen from (C.19), a mutual cancellation of the expressions obtained by substitution of the term of (B.4) proportional to the vector meson momentum occurs. We find:

$$\begin{aligned} \sum_{\lambda} E_{\tau\rho}^{(\lambda)*}(k) E_{\mu\nu}^{(\lambda)}(k) &= k_{\tau} k_{\mu} (-g_{\rho\nu}) - k_{\tau} k_{\nu} (-g_{\rho\mu}) - k_{\rho} k_{\mu} (-g_{\tau\nu}) + k_{\rho} k_{\nu} (-g_{\tau\mu}) \\ &= - \left[k_{\tau} k_{\mu} g_{\rho\nu} - k_{\tau} k_{\nu} g_{\rho\mu} - k_{\rho} k_{\mu} g_{\tau\nu} + k_{\rho} k_{\nu} g_{\tau\mu} \right] . \end{aligned} \quad (\text{C.20})$$

Thus, in this case, the two amplitudes $\overline{\mathcal{M}_1}$ and $\overline{\mathcal{M}_2}$ are each separately gauge invariant quantities.

Substituting (C.20) in (C.18) we obtain:

$$\begin{aligned}
\overline{i\mathcal{M}_1} &= -\frac{g_{\rho NN}^2}{32m_N^2} \frac{1}{3} \frac{1}{2p \cdot k + k^2} \times \\
&\quad \{ k_\tau k_\mu \text{Tr} [(\not{p} + m_N) (\gamma^\tau \gamma_\nu - \gamma_\nu \gamma^\tau) (\not{p} + \not{k} + m_N) (\gamma^\mu \gamma^\nu - \gamma^\nu \gamma^\mu)] \\
&\quad - k_\tau k_\nu \text{Tr} [(\not{p} + m_N) (\gamma^\tau \gamma_\mu - \gamma_\mu \gamma^\tau) (\not{p} + \not{k} + m_N) (\gamma^\mu \gamma^\nu - \gamma^\nu \gamma^\mu)] \\
&\quad - k_\rho k_\mu \text{Tr} [(\not{p} + m_N) (\gamma_\nu \gamma^\rho - \gamma^\rho \gamma_\nu) (\not{p} + \not{k} + m_N) (\gamma^\mu \gamma^\nu - \gamma^\nu \gamma^\mu)] \\
&\quad + k_\rho k_\nu \text{Tr} [(\not{p} + m_N) (\gamma_\mu \gamma^\rho - \gamma^\rho \gamma_\mu) (\not{p} + \not{k} + m_N) (\gamma^\mu \gamma^\nu - \gamma^\nu \gamma^\mu)] \} \\
&= -\frac{g_{\rho NN}^2}{32m_N^2} \frac{1}{3} \frac{1}{2p \cdot k + k^2} \times \\
&\quad \{ \text{Tr} [(\not{p} + m_N) (\not{k} \gamma_\nu - \gamma_\nu \not{k}) (\not{p} + \not{k} + m_N) (\not{k} \gamma^\nu - \gamma^\nu \not{k})] \\
&\quad + \text{Tr} [(\not{p} + m_N) (-\not{k} \gamma_\mu + \gamma_\mu \not{k}) (\not{p} + \not{k} + m_N) (\gamma^\mu \not{k} - \not{k} \gamma^\mu)] \\
&\quad + \text{Tr} [(\not{p} + m_N) (-\gamma_\nu \not{k} + \not{k} \gamma_\nu) (\not{p} + \not{k} + m_N) (\not{k} \gamma^\nu - \gamma^\nu \not{k})] \\
&\quad + \text{Tr} [(\not{p} + m_N) (\gamma_\mu \not{k} - \not{k} \gamma_\mu) (\not{p} + \not{k} + m_N) (\gamma^\mu \not{k} - \not{k} \gamma^\mu)] \} . \tag{C.21}
\end{aligned}$$

The four traces are identical. Thus:

$$\begin{aligned}
\overline{i\mathcal{M}_1} &= -i \frac{g_{\rho NN}^2}{32m_N^2} \frac{1}{3} \frac{1}{2(p \cdot k) + k^2} \times \\
&\quad 4 \text{Tr} [(\not{p} + m_N) (\not{k} \gamma_\nu - \gamma_\nu \not{k}) (\not{p} + \not{k} + m_N) (\not{k} \gamma^\nu - \gamma^\nu \not{k})] \\
&= -i \frac{g_{\rho NN}^2}{8m_N^2} \frac{1}{3} \frac{1}{2(p \cdot k) + k^2} \times \\
&\quad \text{Tr} [(\not{p} \not{k} \gamma_\nu - \not{p} \gamma_\nu \not{k} + m_N \not{k} \gamma_\nu - m_N \gamma_\nu \not{k}) \times \\
&\quad \quad (\not{p} \not{k} \gamma^\nu - \not{p} \gamma^\nu \not{k} + k^2 \gamma^\nu - \not{k} \gamma^\nu \not{k} + m_N \not{k} \gamma^\nu - m_N \gamma^\nu \not{k})] \\
&= -i \frac{g_{\rho NN}^2}{8m_N^2} \frac{1}{3} \frac{1}{2(p \cdot k) + k^2} \times \\
&\quad \text{Tr} [\not{p} \not{k} \gamma_\nu \not{p} \not{k} \gamma^\nu - \not{p} \not{k} \gamma_\nu \not{p} \gamma^\nu \not{k} + k^2 \not{p} \not{k} \gamma_\nu \gamma^\nu - \not{p} \not{k} \gamma_\nu \not{k} \gamma^\nu \not{k} \\
&\quad \quad - \not{p} \gamma_\nu \not{k} \not{p} \not{k} \gamma^\nu + \not{p} \gamma_\nu \not{k} \not{p} \gamma^\nu \not{k} - k^2 \not{p} \gamma_\nu \not{k} \gamma^\nu + \not{p} \gamma_\nu \not{k} \not{k} \gamma^\nu \not{k} \\
&\quad \quad + m_N^2 \not{k} \gamma_\nu \not{k} \gamma^\nu - m_N^2 \not{k} \gamma_\nu \gamma^\nu \not{k} - m_N^2 \gamma_\nu \not{k} \not{k} \gamma^\nu + m_N^2 \gamma_\nu \not{k} \gamma^\nu \not{k}] . \tag{C.22}
\end{aligned}$$

The expression can be simplified using the properties (A.10)–(A.13) and $\not{k}\not{k} = k^2$. One finds:

$$\begin{aligned}
\not{p} \not{k} \gamma_\nu \not{p} \not{k} \gamma^\nu &= 4(p \cdot k) \not{p} \not{k} , \\
\not{p} \not{k} \gamma_\nu \not{p} \gamma^\nu \not{k} &= -2 \not{p} \not{k} \not{p} \not{k} , \\
k^2 \not{p} \not{k} \gamma_\nu \gamma^\nu &= 4k^2 \not{p} \not{k} , \\
\not{p} \not{k} \gamma_\nu \not{k} \gamma^\nu \not{k} &= -2 \not{p} \not{k} \not{k} \not{k} = -2k^2 \not{p} \not{k} , \\
\not{p} \gamma_\nu \not{k} \not{p} \not{k} \gamma^\nu &= -2 \not{p} \not{k} \not{p} \not{k} , \\
\not{p} \gamma_\nu \not{k} \not{p} \gamma^\nu \not{k} &= 4(p \cdot k) \not{p} \not{k} , \\
k^2 \not{p} \gamma_\nu \not{k} \gamma^\nu &= -2k^2 \not{p} \not{k} , \\
\not{p} \gamma_\nu \not{k} \not{k} \gamma^\nu \not{k} &= k^2 \not{p} \gamma_\nu \gamma^\nu \not{k} = 4k^2 \not{p} \not{k} , \\
m_N^2 \not{k} \gamma_\nu \not{k} \gamma^\nu &= -2m_N^2 \not{k} \not{k} = -2m_N^2 k^2 , \\
m_N^2 \not{k} \gamma_\nu \gamma^\nu \not{k} &= 4m_N^2 \not{k} \not{k} = 4m_N^2 k^2 , \\
m_N^2 \gamma_\nu \not{k} \not{k} \gamma^\nu &= m_N^2 k^2 \gamma_\nu \gamma^\nu = 4m_N^2 k^2 , \\
m_N^2 \gamma_\nu \not{k} \gamma^\nu \not{k} &= -2m_N^2 \not{k} \not{k} = -2m_N^2 k^2 .
\end{aligned} \tag{C.23}$$

Thus:

$$\begin{aligned}
\overline{i\mathcal{M}_1} &= -i \frac{g_{\rho NN}^2}{8m_N^2} \frac{1}{3} \frac{1}{2(p \cdot k) + k^2} \times \\
&\quad \text{Tr} [4(p \cdot k) \not{p} \not{k} + 2 \not{p} \not{k} \not{p} \not{k} + 4k^2 \not{p} \not{k} + 2k^2 \not{p} \not{k} \\
&\quad \quad + 2 \not{p} \not{k} \not{p} \not{k} + 4p \cdot k \not{p} \not{k} + 2k^2 \not{p} \not{k} + 4k^2 \not{p} \not{k} \\
&\quad \quad - 2m_N^2 k^2 - 4m_N^2 k^2 - 4m_N^2 k^2 - 2m_N^2 k^2] \\
&= -i \frac{g_{\rho NN}^2}{8m_N^2} \frac{1}{3} \frac{1}{2(p \cdot k) + k^2} \times \\
&\quad \{ 8(p \cdot k) \text{Tr} [\not{p} \not{k}] + 12k^2 \text{Tr} [\not{p} \not{k}] - 12m_N^2 k^2 \text{Tr} [1_{4 \times 4}] + 4 \text{Tr} [\not{p} \not{k} \not{p} \not{k}] \} .
\end{aligned} \tag{C.24}$$

The traces can be easily calculated using the trace identities (A.3–A.6). We find:

$$\begin{aligned}
\overline{i\mathcal{M}_1} &= -i \frac{g_{\rho NN}^2}{8m_N^2} \frac{1}{3} \frac{1}{2(p \cdot k) + k^2} \times \\
&\quad \{ 32(p \cdot k)^2 + 48k^2(p \cdot k) - 48m_N^2 k^2 + 16 [(p \cdot k)^2 - m_N^2 k^2 + (p \cdot k)^2] \} \\
&= -i \frac{g_{\rho NN}^2}{8m_N^2} \frac{1}{3} \frac{1}{2p \cdot k + k^2} \{ 64(p \cdot k)^2 - 64m_N^2 k^2 + 48k^2(p \cdot k) \} \\
&= -i \frac{g_{\rho NN}^2}{8m_N^2} \frac{1}{3} \frac{1}{2(p \cdot k) + k^2} 16 \{ 4(p \cdot k)^2 - 4m_N^2 k^2 + 3k^2(p \cdot k) \} \\
&= -i \frac{g_{\rho NN}^2}{m_N^2} \frac{2}{3} \frac{1}{2(p \cdot k) + k^2} \{ 4(p \cdot k)^2 - 4m_N^2 k^2 + 3k^2(p \cdot k) \} .
\end{aligned} \tag{C.25}$$

Hence

$$\overline{\mathcal{M}_1} = -\frac{g_{\rho NN}^2}{m_N^2} \frac{2}{3} \frac{1}{2(p \cdot k) + k^2} \{ 4(p \cdot k)^2 - 4m_N^2 k^2 + 3k^2(p \cdot k) \} . \tag{C.26}$$

The expression for \mathcal{M}_2 can be obtained as $\mathcal{M}_2 = \mathcal{M}_1(k \rightarrow -k)$. Thus:

$$\overline{\mathcal{M}_2} = -\frac{g_{\rho NN}^2}{m_N^2} \frac{2}{3} \frac{1}{-2(p \cdot k) + k^2} \{ 4(p \cdot k)^2 - 4m_N^2 k^2 - 3k^2(p \cdot k) \}. \quad (\text{C.27})$$

The unpolarized forward scattering amplitude for the ρ meson Compton-like scattering is then:

$$\overline{\mathcal{M}_1} + \overline{\mathcal{M}_2} = \frac{g_{\rho NN}^2}{m_N^2} \frac{8}{3} k^2 \frac{2m_N^2 k^2 + (p \cdot k)^2}{k^4 - 4(p \cdot k)^2}. \quad (\text{C.28})$$

C.2 The σ -exchange contribution

In this Section we evaluate the vector meson-nucleon forward scattering amplitude for the process involving the exchange of a σ meson shown in Fig. C.3. The process corresponds to non resonant t -channel vector meson-nucleon scattering. To leading order in density, the forward scattering amplitude determines the contribution to the vector meson self energy in nuclear matter. The corresponding vector meson self energy is given by the tadpole diagram shown in Fig. C.4. The diagram describes the excitation of nucleon-nucleon hole states due to the exchange of a σ meson.

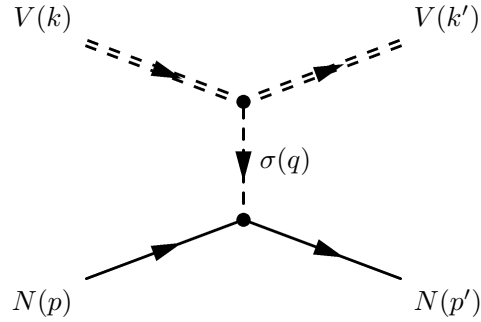


Figure C.3: Feynman diagram for the $NV \rightarrow NV$ scattering proceeding via the exchange of a σ meson.

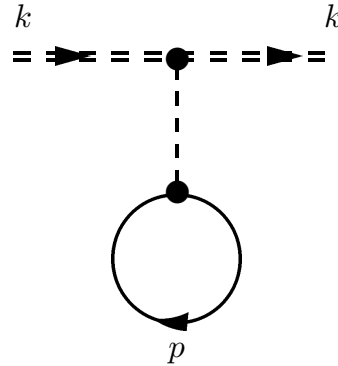


Figure C.4: Vector meson self energy in matter to lowest order in density due to the exchange of a σ meson.

The σNN coupling is described by the interaction Lagrangian

$$\delta\mathcal{L}_{\sigma NN} = g_{\sigma NN} \bar{\psi}\psi\sigma \quad (\text{C.29})$$

where σ and ψ denote the sigma meson and nucleon fields respectively. The coupling $g_{\sigma NN}$ is taken from the Bonn potential [84].

The interaction Lagrangian describing the coupling between the σ meson and the vector meson V ($V=\rho,\omega$) is

$$\delta\mathcal{L}_{\sigma VV} = -\frac{g_{\sigma VV}}{m_{\sigma}} F^{\mu\nu} F^{\mu\nu} \sigma \quad (\text{C.30})$$

where

$$F^{\mu\nu} = \partial^\mu A^\nu - \partial^\nu A^\mu, \quad (\text{C.31})$$

A^μ denotes the vector meson field and m_σ is the σ meson mass used as a scaling mass in the σVV Lagrangian in order to make $g_{\sigma VV}$ dimensionless. The determination of the coupling constant $g_{\sigma VV}$ has been discussed in Section 4.3. The a priori unknown sign of $g_{\sigma VV}$ has been assumed such that the corresponding vector meson self-energy is attractive, in analogy to the attractive part of NN interaction. This follows naturally if one thinks at the σ exchange as an effective 2π exchange process where the intermediate states are dominated by states of energies higher than the vector meson mass. For the ρ meson an example of such a process with an intermediate ω particle-hole state is shown in Fig. C.5(b). On the basis of this argument, the same assumption has been made in Ref. [136].

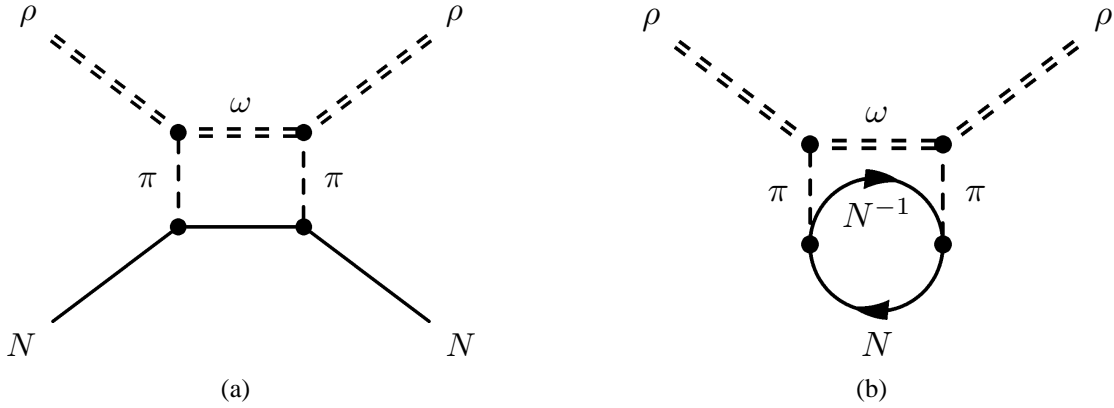


Figure C.5: The 2π -exchange ρN interaction (a) and the corresponding ρ meson self energy in nuclear matter (b).

Application of Feynman rules leads to the following expression for the unpolarized forward scattering amplitude ($k' = k$, $p' = p$):

$$i\bar{\mathcal{A}} = \frac{1}{2} \frac{1}{3} 2 \sum_{s,\lambda} \left(-i \frac{g_{\sigma VV}}{m_\sigma} \right) (i g_{\sigma NN}) \frac{i}{q^2 - m_\sigma^2} \bar{u}^{(s)}(p) u^{(s)}(p) E_{\mu\nu}^{(\lambda)\star}(k) E^{\mu\nu(\lambda)}(k) \quad (\text{C.32})$$

with $E_{\mu\nu}^{(\lambda)\star}(k)$, $E^{\mu\nu(\lambda)}(k)$ defined in (C.16). The factor 2 is due to the symmetry of the diagram of Fig. C.3 under the exchange of the initial and final state vector mesons. Since $p' = p$ we have $q = p' - p = 0$. Thus, performing the sum over the $u\bar{u}$ states with the help of the spinor completeness relation (A.14), we find:

$$\begin{aligned} i\bar{\mathcal{A}} &= i \frac{g_{\sigma VV}}{m_\sigma} g_{\sigma NN} \frac{1}{3} \frac{1}{-m_\sigma^2} \text{Tr}[\not{p} + m_N] \sum_{\lambda} E_{\mu\nu}^{(\lambda)\star}(k) E^{\mu\nu(\lambda)}(k) \\ &= -i \frac{g_{\sigma VV}}{m_\sigma} g_{\sigma NN} \frac{1}{3} \frac{1}{m_\sigma^2} 4m_N \sum_{\lambda} E_{\mu\nu}^{(\lambda)\star}(k) E^{\mu\nu(\lambda)}(k) \end{aligned} \quad (\text{C.33})$$

where we used the trace identities (A.3) and (A.4) to obtain the second line.

Let us now evaluate $\sum_{\lambda} E_{\mu\nu}^{(\lambda)\star}(k) E^{\mu\nu(\lambda)}(k)$ separately:

$$\begin{aligned}
\sum_{\lambda} E_{\mu\nu}^{(\lambda)\star}(k) E^{\mu\nu(\lambda)}(k) &= \sum_{\lambda} (+i) [k_{\mu} \epsilon_{\nu}^{(\lambda)\star}(k) - k_{\nu} \epsilon_{\mu}^{(\lambda)\star}(k)] (-i) [k^{\mu} \epsilon^{\nu(\lambda)\star}(k) - k^{\nu} \epsilon^{\mu(\lambda)}(k)] \\
&= \sum_{\lambda} [k^2 \epsilon_{\nu}^{(\lambda)\star}(k) \epsilon^{\nu(\lambda)}(k) + k^2 \epsilon_{\mu}^{(\lambda)\star}(k) \epsilon^{\mu(\lambda)}(k)] \\
&= 2k^2 \sum_{\lambda} \epsilon_{\nu}^{(\lambda)\star}(k) \epsilon^{\nu(\lambda)}(k) \\
&= 2k^2 \sum_{\lambda} \epsilon_{\nu}^{(\lambda)\star}(k) g^{\nu\sigma} \epsilon_{\sigma}^{(\lambda)}(k) \\
&= 2k^2 g^{\nu\sigma} \sum_{\lambda} \epsilon_{\nu}^{(\lambda)\star}(k) \epsilon_{\sigma}^{(\lambda)}(k) \\
&= 2k^2 g^{\nu\sigma} \left[-g_{\nu\sigma} + \frac{k_{\nu} k_{\sigma}}{k^2} \right] \\
&= 2k^2 \left[-g^{\nu\sigma} g_{\nu\sigma} + \frac{k^2}{k^2} \right] \\
&= 2k^2 [-4 + 1] \\
&= -6k^2.
\end{aligned} \tag{C.34}$$

Substituting (C.34) in (C.33) we obtain:

$$i\bar{\mathcal{A}} = -i \frac{g_{\sigma VV}}{m_{\sigma}} g_{\sigma NN} \frac{1}{3} \frac{1}{m_{\sigma}^2} 4m_N (-6k^2). \tag{C.35}$$

Hence

$$\boxed{\bar{\mathcal{A}} = \frac{g_{\sigma VV}}{m_{\sigma}} g_{\sigma NN} \frac{1}{m_{\sigma}^2} 4m_N 2k^2} \tag{C.36}$$

is the unpolarized forward scattering amplitude.

Bibliography

- [1] P. Gerber and H. Leutwyler,
“Hadrons Below the Chiral Phase Transition,”
Nucl. Phys. B **321** (1989) 387.
- [2] T. D. Cohen, R. J. Furnstahl and D. K. Griegel,
“Quark And Gluon Condensates In Nuclear Matter,”
Phys. Rev. C **45** (1992) 1881.
- [3] M. Lutz, S. Klimt and W. Weise,
“Meson Properties At Finite Temperature And Baryon Density,”
Nucl. Phys. A **542** (1992) 521.
- [4] K. Tsushima, T. Maruyama and A. Faessler,
“Temperature and density dependence of quark dynamical properties: Application of
'thermo field dynamics' to the SU(3) NJL model with instanton effects,”
Nucl. Phys. A **535** (1991) 497;

T. Maruyama, K. Tsushima and A. Faessler,
“Chiral Phase Transition And Dynamical Properties Of Quarks At Finite Temperature
And Density: Application Of The 'Thermo Field Dynamics' To The SU(3) Nambu-
Jona-Lasinio Model With Instanton Effects,”
Nucl. Phys. A **537** (1992) 303.
- [5] G. Q. Li and C. M. Ko,
“Quark condensate in nuclear matter,”
Phys. Lett. B **338** (1994) 118.
- [6] O. Plohl and C. Fuchs,
“Nuclear matter in the chiral limit and the in-medium chiral condensate,”
arXiv:0710.3700 [nucl-th].
- [7] G. E. Brown and M. Rho,
“Scaling effective Lagrangians in a dense medium,”
Phys. Rev. Lett. **66** (1991) 2720.
- [8] B. Friman and H. J. Pirner,
“P-wave polarization of the rho meson and the dilepton spectrum in dense matter,”
Nucl. Phys. A **617** (1997) 496.

- [9] W. Peters, M. Post, H. Lenske, S. Leupold and U. Mosel,
“The spectral function of the rho meson in nuclear matter,”
Nucl. Phys. A **632** (1998) 109.
- [10] M. Post, S. Leupold and U. Mosel,
“The rho spectral function in a relativistic resonance model,”
Nucl. Phys. A **689** (2001) 753.
- [11] M. F. M. Lutz, G. Wolf and B. Friman,
“Scattering of vector mesons off nucleons,”
Nucl. Phys. A **706**, 431 (2002) [Erratum-ibid. A **765**, 431 (2006)].
- [12] B. Friman, M. Lutz and G. Wolf,
“From meson nucleon scattering to vector mesons in nuclear matter,”
arXiv:nucl-th/0003012.
- [13] M. Herrmann, B. L. Friman and W. Norenberg,
“Properties Of Rho Mesons In Nuclear Matter,”
Nucl. Phys. A **560** (1993) 411.
- [14] R. Rapp, G. Chanfray and J. Wambach,
“Rho meson propagation and dilepton enhancement in hot hadronic matter,”
Nucl. Phys. A **617** (1997) 472.
- [15] M. Urban, M. Buballa, R. Rapp and J. Wambach,
“Momentum dependence of the pion cloud for rho mesons in nuclear matter,”
Nucl. Phys. A **641** (1998) 433.
- [16] F. Klingl, N. Kaiser and W. Weise,
“Current correlation functions, QCD sum rules and vector mesons in baryonic matter,”
Nucl. Phys. A **624** (1997) 527.
- [17] D. Cabrera, E. Oset and M. J. Vicente Vacas,
“Chiral approach to the rho meson in nuclear matter,”
Nucl. Phys. A **705** (2002) 90.
- [18] M. Post, S. Leupold and U. Mosel,
“Hadronic spectral functions in nuclear matter,”
Nucl. Phys. A **741** (2004) 81.
- [19] P. Muehlich, V. Shklyar, S. Leupold, U. Mosel and M. Post,
“The spectral function of the omega meson in nuclear matter from a coupled-channel
resonance model,”
Nucl. Phys. A **780** (2006) 187.
- [20] T. Hatsuda and S. H. Lee,
“QCD sum rules for vector mesons in nuclear medium,”
Phys. Rev. C **46** (1992) 34.

- [21] S. Leupold, W. Peters and U. Mosel,
“What QCD sum rules tell about the rho meson,”
Nucl. Phys. A **628** (1998) 311.
- [22] G. Agakishiev *et al.* [CERES Collaboration],
“Enhanced production of low mass electron pairs in 200-GeV/u S-Au collisions at the CERN SPS,”
Phys. Rev. Lett. **75** (1995) 1272 .
- [23] M. Masera [HELIOS Collaboration],
“Dimuon production below mass 3.1 GeV/c² in p-W and S-W interactions at 200 GeV/c/A,”
Nucl. Phys. A **590** (1995) 93C.
- [24] R. Rapp and J. Wambach,
“Low mass dileptons at the CERN-SPS: Evidence for chiral restoration?,”
Eur. Phys. J. A **6** (1999) 415.
- [25] R. Arnaldi *et al.* [NA60 Collaboration],
“First measurement of the rho spectral function in high-energy nuclear collisions,”
Phys. Rev. Lett. **96** (2006) 162302.
- [26] D. Adamova *et al.*,
“Modification of the rho-meson detected by low-mass electron positron pairs in central Pb-Au collisions at 158-A-GeV/c,”
arXiv:nucl-ex/0611022.
- [27] R. J. Porter *et al.* [DLS Collaboration],
“Dielectron cross section measurements in nucleus nucleus reactions at 1.0-A-GeV,”
Phys. Rev. Lett. **79** (1997) 1229.
- [28] W. K. Wilson *et al.* [DLS Collaboration],
“Inclusive dielectron cross sections in p + p and p + d interactions at beam energies from 1.04-GeV to 4.88-GeV,”
Phys. Rev. C **57** (1998) 1865.
- [29] E. L. Bratkovskaya, W. Cassing, R. Rapp and J. Wambach,
“Dilepton production and m(T)-scaling at BEVALAC/SIS energies,”
Nucl. Phys. A **634** (1998) 168.
- [30] C. Ernst, S. A. Bass, M. Belkacem, H. Stoecker and W. Greiner,
“Intermediate mass excess of dilepton production in heavy ion collisions at BEVALAC energies,”
Phys. Rev. C **58** (1998) 447.
- [31] E. L. Bratkovskaya and C. M. Ko,
“Low-mass dileptons and dropping rho meson mass,”
Phys. Lett. B **445** (1999) 265.

- [32] T. Eberl *et al.*,
“Di-electron measurements in C + C reactions at 2-GeV-A with HADES,”
Nucl. Phys. A **752** (2005) 433.
- [33] G. Agakichiev *et al.* [HADES Collaboration],
“Dielectron production in C-12 + C-12 collisions at 2-AGeV with HADES,”
Phys. Rev. Lett. **98** (2007) 052302.
- [34] M. I. Krivoruchenko, B. V. Martemyanov, A. Faessler and C. Fuchs,
“Electromagnetic transition form factors and dilepton decay rates of nucleon resonances,”
Annals Phys. **296** (2002) 299.
- [35] R. Rapp and J. Wambach,
“Chiral symmetry restoration and dileptons in relativistic heavy-ion collisions,”
Adv. Nucl. Phys. **25** (2000) 1.
- [36] H. van Hees and R. Rapp,
“Comprehensive interpretation of thermal dileptons at the SPS,”
Phys. Rev. Lett. **97** (2006) 102301.
- [37] G. Agakishiev *et al.* [CERES/NA45 Collaboration],
“Low-mass $e^+ e^-$ pair production in 158-A-GeV Pb Au collisions at the CERN SPS, its dependence on multiplicity and transverse momentum,”
Phys. Lett. B **422** (1998) 405.
- [38] K. Shekhter, C. Fuchs, A. Faessler, M. Krivoruchenko and B. Martemyanov,
“Dilepton production in heavy ion collisions at intermediate energies,”
Phys. Rev. C **68** (2003) 014904.
- [39] D. Trnka *et al.* [CBELSA/TAPS Collaboration],
“First observation of in-medium modifications of the omega meson,”
Phys. Rev. Lett. **94** (2005) 192303.
- [40] K. Ozawa *et al.* [E325 Collaboration],
“Observation of rho / omega meson modification in nuclear matter,”
Phys. Rev. Lett. **86** (2001) 5019.
- [41] M. Naruki *et al.*,
“Experimental signature of the medium modification for rho and omega mesons in 12-GeV p + A reactions,”
Phys. Rev. Lett. **96** (2006) 092301.
- [42] M. Djalali Chaden,
Quark Matter 2006.

- [43] A. Faessler, C. Fuchs and M. I. Krivoruchenko,
“Dilepton spectra from decays of light unflavored mesons,”
Phys. Rev. C **61** (2000) 035206.
- [44] L. G. Landsberg,
“Electromagnetic Decays Of Light Mesons,”
Phys. Rept. **128** (1985) 301.
- [45] V. A. Matveev, R. M. Muradian and A. N. Tavkhelidze,
“Automodellism in the large - angle elastic scattering and structure of hadrons,”
Lett. Nuovo Cim. **7** (1973) 719;
- S. J. Brodsky and G. R. Farrar,
“Scaling Laws At Large Transverse Momentum,”
Phys. Rev. Lett. **31** (1973) 1153;
- S. J. Brodsky and G. R. Farrar,
“Scaling Laws For Large Momentum Transfer Processes,”
Phys. Rev. D **11** (1975) 1309.
- [46] H. J. Behrend *et al.* [CELLO Collaboration],
“A Measurement of the π^0 , η and η' electromagnetic form-factors,”
Z. Phys. C **49** (1991) 401.
- [47] J.J. Sakurai,
“Currents and Mesons,”
University of Chicago Press, Chicago (1969).
- [48] M. E. Peskin and D. V. Schroeder,
“An Introduction To Quantum Field Theory,”
Reading, USA: Addison-Wesley (1995).
- [49] H. F. Jones and M. D. Scadron,
“Multipole gamma N Delta form-factors and resonant photoproduction and electroproduction,”
Annals Phys. **81** (1973) 1.
- [50] R. C. E. Devenish, T. S. Eisenschitz and J. G. Korner,
“Electromagnetic $N N^*$ Transition Form-Factors,”
Phys. Rev. D **14** (1976) 3063.
- [51] T. L. Trueman,
“Kinematic structure of vertex functions,”
Phys. Rev. **182** (1969) 1469;
- W. R. Theis and P. H. Hertel,

- “Electromagnetic-transition form factors free of kinematic singularities,” *Nuovo Cim. A* **66** (1970) 152;
- F. E. Close and W. N. Cottingham,
“The Kinematic And Symmetry Structure Of $E^+ E^- \rightarrow$ Hadron Pairs,”
Nucl. Phys. B **99** (1975) 61;
- W. A. Bardeen and W. K. Tung,
“Invariant amplitudes for photon processes,”
Phys. Rev. **173** (1968) 1423 [Erratum-ibid. *D* **4** (1971) 3229];
- R. Tarrach,
“Invariant Amplitudes For Virtual Compton Scattering Off Polarized Nucleons Free From Kinematical Singularities, Zeros And Constraints,”
Nuovo Cim. A **28** (1975) 409.
- [52] V. A. Matveev, R. M. Muradian and A. N. Tavkhelidze,
“Automodellism in the large - angle elastic scattering and structure of hadrons,”
Lett. Nuovo Cim. **7** (1973) 719;
- S. J. Brodsky and G. R. Farrar,
“Scaling Laws At Large Transverse Momentum,”
Phys. Rev. Lett. **31** (1973) 1153;
- S. J. Brodsky and G. R. Farrar,
“Scaling Laws For Large Momentum Transfer Processes,”
Phys. Rev. D **11** (1975) 1309;
- A. I. Vainshtein and V. I. Zakharov,
“Remarks On Electromagnetic Form-Factors Of Hadrons In The Quark Model,”
Phys. Lett. B **72** (1978) 368.
- [53] A. Faessler, C. Fuchs, M. I. Krivoruchenko and B. V. Martemyanov,
“Dilepton production in proton proton collisions at BEVALAC energies,”
J. Phys. G **29** (2003) 603.
- [54] M. I. Krivoruchenko,
“Electromagnetic nucleon form-factors,”
Talk given at International Conference on Mesons and Nuclei at Intermediate Energies, Dubna, Russia, 3-8 May 1994.
- [55] P. Mergell, U. G. Meissner and D. Drechsel,
“Dispersion theoretical analysis of the nucleon electromagnetic form-factors,”
Nucl. Phys. A **596** (1996) 367.

- [56] S. Dubnicka,
“Present status of theoretical predictions of electromagnetic form-factor behaviours,”
Acta Phys. Polon. B **27** (1996) 2525.
- [57] B. V. Geshkenbein and M. V. Terentev,
“The Phenomenological Formula For The Pion Electromagnetic Form-Factor,”
Sov. J. Nucl. Phys. **40** (1984) 487.
- [58] E. L. Bratkovskaya, W. Cassing and U. Mosel,
“Perspectives of e^+e^- production in $p p$, $p d$ and $p Be$ reactions at SIS energies,”
Nucl. Phys. A **686** (2001) 568.
- [59] D. E. Groom *et al.* [Particle Data Group Collaboration],
“Review of particle physics,”
Eur. Phys. J. C **15** (2000) 1.
- [60] S. Stein *et al.*,
“Electron Scattering At 4-Degrees With Energies Of 4.5-Gev - 20-Gev,”
Phys. Rev. D **12** (1975) 1884.
- [61] W. Bartel *et al.*,
“Electroproduction of pions near the Delta(1236) isobar and the form-factor of $G^*(M)(q^{*2})$ of the $(\gamma N \Delta)$ vertex,”
Phys. Lett. B **28** (1968) 148.
- [62] K. Baetzner *et al.*,
“Separation of $\sigma(s)$ and $\sigma(t)$ in the region of the delta(1236) resonance and determination of the magnetic dipole transition form-factor,”
Phys. Lett. B **39** (1972) 575.
- [63] V. V. Frolov *et al.*,
“Electroproduction of the Delta(1232) resonance at high momentum transfer,”
Phys. Rev. Lett. **82** (1999) 45.
- [64] D. M. Manley and E. M. Saleski,
“Multichannel Resonance Parametrization Of πN Scattering Amplitudes,”
Phys. Rev. D **45** (1992) 4002.
- [65] R. S. Longacre and J. Dolbeau,
“K-matrix fits to $N\pi \rightarrow N\pi$ and $N\pi\pi$ in the resonance region $\sqrt{s} = 1380$ to 1740 MeV,”
Nucl. Phys. B **122** (1977) 493;
- R. Longacre, A. H. Rosenfeld, T. A. Lasinski, G. Smadja, R. J. Cashmore and D. W. G. Leith,
“ N^* resonance parameters and K-matrix fits to the reactions $\pi N \rightarrow \Delta\pi + \rho N + \epsilon N$,”
Phys. Lett. B **55** (1975) 415.

- [66] R. Koniuk,
 “Baryon - Vector Meson Couplings In A Quark Model With Chromodynamics,”
 Nucl. Phys. B **195** (1982) 452.
- [67] S. Capstick and W. Roberts,
 “Quasi two-body decays of nonstrange baryons,”
 Phys. Rev. D **49** (1994) 4570.
- [68] V. Burkert,
 “Electroproduction Of Baryon Resonances Above The Delta (1232),”
 Proc. of the Topical Workshop on "Excited Baryons 1988", Troy, New York (1988),
 eds. G. Adams, N. Mukhopadhyay and P. Stoler, World Scientific, Singapore (1989),
 p. 122.
- [69] V. D. Burkert,
 “ E_{1+}/M_{1+} and S_{1+}/M_{1+} from and analysis of $p(e, e'p)\pi^0$ in the region of the $\Delta(1232)$
 resonance at $Q^2 = 3.2$ (GeV/c)²,”
 Phys. Rev. Lett. **75** (1995) 3614.
- [70] R. Siddle *et al.*,
 “Coincidence π^0 electroproduction experiments in the first resonance region at momen-
 tum transfers of 0.3, 0.45, 0.60, 0.76 GeV/c²,”
 Nucl. Phys. B **35** (1971) 93.
- [71] R. Beck *et al.*,
 “Measurement of the $E2/M1$ Ratio in the $N \rightarrow \Delta$ Transition using the reaction $p(\gamma \rightarrow$
 $, p)\pi^0$,”
 Phys. Rev. Lett. **78** (1997) 606.
- [72] I. G. Aznaurian and S. G. Stepanian,
 “The $P_{33}(1232)$ resonance contribution into the amplitudes $M_{1+}^{3/2}$, $E_{1+}^{3/2}$, $S_{1+}^{3/2}$ from an
 analysis of the $p(e, e'p)\pi^0$ data at $Q^2 = 2.8, 3.2$ and 4 (GeV/c)² within dispersion rela-
 tion approach”
 Phys. Rev. D **59** (1999) 054009.
- [73] J. C. Alder *et al.*,
 “Pi0 electroproduction at the first resonance at momentum transfers q-squared=0.6, 1.0
 and 1.56 gev-squared,”
 Nucl. Phys. B **46** (1972) 573.
- [74] M. Post and U. Mosel,
 “Coupling of baryon resonances to the N omega channel,”
 Nucl. Phys. A **688** (2001) 808.
- [75] V. L. Eletsky, M. Belkacem, P. J. Ellis and J. I. Kapusta,
 “Properties of rho and omega mesons at finite temperature and density as inferred from

- experiment,”
Phys. Rev. C **64** (2001) 035202.
- [76] G. Penner and U. Mosel,
“ $\pi N \rightarrow \omega N$ in a coupled-channel approach,”
Phys. Rev. C **65** (2002) 055202 [Erratum-ibid. C **65** (2002) 059901].
- [77] M. Gell-Mann, D. Sharp and W. G. Wagner,
“Decay rates of neutral mesons,”
Phys. Rev. Lett. **8** (1962) 261.
- [78] C. Fuchs, M. I. Krivoruchenko, H. L. Yadav, A. Faessler, B. V. Martemyanov and K. Shekhter,
“Off-shell omega production in proton proton collisions near threshold,”
Phys. Rev. C **67** (2003) 025202.
- [79] A. Faessler, C. Fuchs, M. I. Krivoruchenko and B. V. Martemyanov,
“Exclusive Phi production in proton proton collisions in the resonance model,”
Phys. Rev. C **68** (2003) 068201.
- [80] R. M. Barnett *et al.* [Particle Data Group],
“Review of particle physics. Particle Data Group,”
Phys. Rev. D **54** (1996) 1.
- [81] F. Hibou *et al.*,
“Near-threshold production of ω mesons in the $pp \rightarrow pp\omega$ reaction,”
Phys. Rev. Lett. **83** (1999) 492.
- [82] S. Abd El-Samad *et al.* [COSY-TOF Collaboration],
“Production of omega mesons in proton proton collisions,”
Phys. Lett. B **522** (2001) 16.
- [83] S. Barsov *et al.*,
“Study of omega-meson production in p p collisions at ANKE,”
Eur. Phys. J. A **31** (2007) 95.
- [84] R. Machleidt,
“The high-precision, charge-dependent Bonn nucleon-nucleon potential (CD-Bonn),”
Phys. Rev. C **63** (2001) 024001.
- [85] S. Zschocke, O. P. Pavlenko and B. Kampfer,
“In-medium spectral change of omega mesons as a probe of QCD four-quark condensate,”
Phys. Lett. B **562** (2003) 57.
- [86] R. Thomas, S. Zschocke and B. Kampfer,
“Evidence for in-medium changes of four-quark condensates,”
Phys. Rev. Lett. **95** (2005) 232301.

- [87] J. Aichelin,
“‘Quantum’ molecular dynamics: A Dynamical microscopic n body approach to investigate fragment formation and the nuclear equation of state in heavy ion collisions,”
Phys. Rept. **202** (1991) 233.
- [88] H. Sorge, H. Stoecker and W. Greiner,
“Poincare Invariant Hamiltonian Dynamics: Modeling Multi-Hadronic Interactions In A Phase Space Approach,”
Annals Phys. **192** (1989) 266.
- [89] E. Lehmann, R. K. Puri, A. Faessler, G. Batko and S. W. Huang,
“Consequences of a covariant description of heavy ion reactions at intermediate-energies,”
Phys. Rev. C **51** (1995) 2113.
- [90] S. A. Bass *et al.*,
“Microscopic models for ultrarelativistic heavy ion collisions,”
Prog. Part. Nucl. Phys. **41** (1998) 255.
- [91] M. Bleicher *et al.*,
“Relativistic hadron hadron collisions in the ultra-relativistic quantum molecular dynamics model,”
J. Phys. G **25** (1999) 1859.
- [92] V. S. Uma Maheswari, C. Fuchs, A. Faessler, L. Sehn, D. S. Kosov and Z. Wang,
“In-medium dependence and Coulomb effects of the pion production in heavy ion collisions,”
Nucl. Phys. A **628** (1998) 669.
- [93] P. A. M. Dirac,
“Forms Of Relativistic Dynamics,”
Rev. Mod. Phys. **21** (1949) 392;
- J. Samuel,
“Constraints In Relativistic Hamiltonian Mechanics,”
Phys. Rev. D **26** (1982) 3475.
- [94] C. Fuchs, E. Lehmann, L. Sehn, F. Scholz, T. Kubo, J. Zipprich and A. Faessler,
“Heavy ion collisions and the density dependence of the local mean field,”
Nucl. Phys. A **603** (1996) 471.
- [95] C. Fuchs, A. Faessler, E. Zabrodin and Y. M. Zheng,
“Probing the nuclear equation of state by K⁺ production in heavy ion collisions,”
Phys. Rev. Lett. **86** (2001) 1974.

- [96] C. Fuchs,
“Kaon production in heavy ion reactions at intermediate energies,”
Prog. Part. Nucl. Phys. **56** (2006) 1.
- [97] H. Feldmeier,
“Fermionic molecular dynamics,”
Nucl. Phys. A **515** (1990) 147.
- [98] H. Feldmeier and J. Schnack,
“Fermionic molecular dynamics: Ensembles and fluctuations therein,”
Nucl. Phys. A **583** (1995) 347.
- [99] H. Feldmeier, K. Bieler and J. Schnack,
“Fermionic molecular dynamics for ground states and collisions of nuclei,”
Nucl. Phys. A **586** (1995) 493.
- [100] H. Feldmeier and J. Schnack,
“Fermionic Molecular Dynamics,”
Prog. Part. Nucl. Phys. **39** (1997) 393.
- [101] H. Feldmeier and J. Schnack,
“Molecular Dynamics for Fermions,”
Rev. Mod. Phys. **72** (2000) 655.
- [102] A. Ono, H. Horiuchi, T. Maruyama and A. Ohnishi,
“Fragment Formation Studied With Antisymmetrized Version Of Molecular Dynamics
With Two Nucleon Collisions,”
Phys. Rev. Lett. **68** (1992) 2898.
- [103] A. Ono, H. Horiuchi, T. Maruyama and A. Ohnishi,
“Antisymmetrized Version Of Molecular Dynamics With Two Nucleon Collisions And
Its Application To Heavy Ion Reactions,”
Prog. Theor. Phys. **87** (1992) 1185.
- [104] A. Ono, H. Horiuchi,
“Antisymmetrized molecular dynamics for heavy ion collisions,”
Prog. Part. Nucl. Phys. **53** (2004) 501.
- [105] H. Feldmeier, T. Neff, R. Roth and J. Schnack,
“A unitary correlation operator method,”
Nucl. Phys. A **632** (1998) 61.
- [106] T. Neff and H. Feldmeier,
“Tensor correlations in the Unitary Correlation Operator Method,”
Nucl. Phys. A **713** (2003) 311.

- [107] A. Ono and H. Horiuchi,
“Antisymmetrized molecular dynamics of wave packets with stochastic incorporation of Vlasov equation,”
Phys. Rev. C **53** (1996) 2958.
- [108] R. Wada *et al.*,
“Reaction mechanisms and multifragmentation processes in Zn-64 + Ni-58 at 35A-MeV to 79A-MeV,”
Phys. Rev. C **62** (2000) 034601.
- [109] C. Hartnack, R. K. Puri, J. Aichelin, J. Konopka, S. A. Bass, H. Stoecker and W. Greiner,
“Modelling the many-body dynamics of heavy ion collisions: Present status and future perspective”
Eur. Phys. J. A **1** (1998) 151.
- [110] D.T. Khoa, N. Ohtsuka, M.A. Matin, A. Faessler, S.W. Huang, E. Lehmann and R.K. Puri,
“In-medium effects in the description of heavy-ion collisions with realistic NN interactions,”
Nucl. Phys. A **548** (1992) 102.
- [111] J. Aichelin and H. Stoecker,
“Quantum molecular dynamics. A Novel approach to N body correlations in heavy ion collisions,”
Phys. Lett. B **176** (1986) 14.
- [112] H. Kruse, B. V. Jacak and H. Stoecker,
“Microscopic theory of pion production and sideways flow in heavy ion collisions,”
Phys. Rev. Lett. **54** (1985) 289.
- [113] J. J. Molitoris and H. Stoecker,
“Further Evidence For A Stiff Nuclear Equation Of State From A Transverse Momentum Analysis Of Ar (1800-Mev/Nucleon) + Kcl,”
Phys. Rev. C **32** (1985) 346.
- [114] S. Huber and J. Aichelin,
“Production of Delta and N* resonances in the one boson exchange model,”
Nucl. Phys. A **573** (1994) 587.
- [115] S. Teis, W. Cassing, M. Effenberger, A. Hombach, U. Mosel and G. Wolf,
“Pion-production in heavy-ion collisions at SIS energies,”
Z. Phys. A **356** (1997) 421.
- [116] A. I. Baz, Ya. B. Zeldovich, A. M. Perelomov,
“Scattering Reactions and Decay in Non-Relativistic Quantum Mechanics,”
Nauka, Moscow (1971).

- [117] P. Danielewicz and S. Pratt,
“Delays Associated With Elementary Processes In Nuclear Reaction Simulations,”
Phys. Rev. C **53** (1996) 249.
- [118] J. Aichelin and C. Hartnack,
“On the influence of resonance lifetimes on observables in heavy ion collisions,”
proceedings to the XXV Int. Workshop on Gross Properties of Nuclei and Nuclear
Excitations, Hirschegg 1997, ed. by H. Feldmeier et al., Hirschegg, Austria, 1997.
- [119] A. B. Larionov, M. Effenberger, S. Leupold and U. Mosel,
“Resonance life time in BUU: Observable consequences,”
Phys. Rev. C **66** (2002) 054604.
- [120] C. Sturm *et al.* [KAOS Collaboration],
“Evidence for a soft nuclear equation of state from kaon production in heavy ion collisions,”
Phys. Rev. Lett. **86** (2001) 39.
- [121] A. Sibirtsev, W. Cassing and U. Mosel,
“Heavy meson production in proton nucleus reactions with empirical spectral functions,”
Z. Phys. A **358** (1997) 357.
- [122] J. Smyrski *et al.*,
“Near-threshold eta meson production in proton proton collisions,”
Phys. Lett. B **474** (2000) 182.
- [123] G. Faeldt and C. Wilkin,
“The Reaction $p d \rightarrow \text{He-3 } \eta$ near threshold,”
Nucl. Phys. A **587** (1995) 769.
- [124] R. Averbeck, R. Holzmann, V. Metag and R. S. Simon,
“Neutral pions and eta mesons as probes of the hadronic fireball in nucleus nucleus collisions around 1-A-GeV,”
Phys. Rev. C **67** (2003) 024903.
- [125] R. Shyam and U. Mosel,
“Role of baryonic resonances in the dilepton emission in nucleon nucleon collisions,”
Phys. Rev. C **67** (2003) 065202.
- [126] M. D. Cozma, C. Fuchs, E. Santini and A. Fassler,
“Dilepton production at HADES: Theoretical predictions,”
Phys. Lett. B **640** (2006) 170.
- [127] E.L. Bratkovskaya,
“Dileptons from heavy-ion collisions: from SIS to FAIR and off-shell transport”

Talk given at the International Workshop on Electromagnetic Probes of Strongly Interacting Matter: The Quest for Medium Modifications of Hadrons, ECT Trento, Italy, 18-22 June 2007.*

- [128] L. P. Kaptari and B. Kampfer,
“Di-electron bremsstrahlung in intermediate-energy p n and D p collisions,”
Nucl. Phys. A **764** (2006) 338.
- [129] T. Inoue and E. Oset,
“eta in the nuclear medium within a chiral unitary approach,”
Nucl. Phys. A **710** (2002) 354.
- [130] M. Schafer, H. C. Donges, A. Engel and U. Mosel,
“Dilepton production in nucleon-nucleon interactions,”
Nucl. Phys. A **575** (1994) 429.
- [131] C. Gale and J. I. Kapusta,
“Dilepton Radiation From High Temperature Nuclear Matter,”
Phys. Rev. C **35** (1987) 2107;
- C. Gale and J. I. Kapusta,
“Dilepton Radiation From Nucleon-Nucleon Collisions,”
Phys. Rev. C **40** (1989) 2397.
- [132] G. Q. Li, C. M. Ko, G. E. Brown and H. Sorge,
“Dilepton production in proton nucleus and nucleus nucleus collisions at SPS energies,”
Nucl. Phys. A **611** (1996) 539.
- [133] S. Leupold,
“Life time of resonances in transport simulations,”
Nucl. Phys. A **695** (2001) 377.
- [134] H. W. Barz, B. Kampfer, G. Wolf and M. Zetenyi,
“Propagation of broad meson resonances in a BUU type transport model: Application to di-electron production,”
arXiv:nucl-th/0605036.
- [135] F. Halzen and A. D. Martin,
“Quarks And Leptons: An Introductory Course In Modern Particle Physics,”
New York, Usa: Wiley (1984).
- [136] B. Friman and M. Soyeur,
“Photoproduction of vector mesons off nucleons near threshold,”
Nucl. Phys. A **600** (1996) 477.

Zusammenfassung

Motiviert durch die Erwartung, dass eine Signatur für die Wiederherstellung der spontanen Symmetriebrechung im chiralen Sektor in geeigneten Experimenten gefunden werden könnte, wurde in den letzten beiden Jahrzehnten sowohl theoretisch als auch experimentell an den Eigenschaften von Hadronen in heißer und dichter Materie geforscht. Man erwartet, daß sich durch den chiralen Phasenübergang die Hadroneneigenschaften ändern würden, insbesondere wird die Beziehung zwischen Mediummodifikationen der Hadronenmassen und der Restauration der chiralen Symmetrie in Materie endlicher Dichte und hoher Temperatur seit langem diskutiert. Nach den Vorhersagen wird das skalare Kondensat, das durch die spontane chirale Symmetriebrechung einen Vakuumerwartungswert erhält, mit zunehmender Dichte und Temperatur abnehmen [1, 2, 3, 4, 5, 6]. Bringt man die Mediummodifikationen der Hadronenmassen direkt mit der Änderung des skalaren Kondensates in Verbindung, wäre eine ähnliche Abnahme der Hadronenmassen mit zunehmender Dichte und Temperatur zu erwarten, wie von Brown und Rho vorgeschlagen [7]. Diese Idee regte die Suche nach Signaturen in verschiedenen Kernreaktionen an. Experimente mit Schwerionenstößen bieten die Möglichkeit, Hadroneneigenschaften bei hohen Temperaturen und Dichten weit oberhalb der normalen Dichte zu untersuchen. Außerdem werden dazu auch Experimente, in denen elementare Hadronen mit Kernen zur Kollision gebracht werden, eingesetzt. Die Anstrengungen im Bereich der Hadronen wurden hauptsächlich auf die leichten Vektormesonen konzentriert, da deren direkter Zerfall zu Dileptonenpaaren die Möglichkeit bietet, die Mediummodifikationen von Hadronen in einem fast ungestörten Reaktionskanal zu untersuchen.

Nachdem die Suche nach Mediummodifikationen von Vektormesonen ihren historischen Ursprung in der Verbindung von Absenkung der Vektormesonennasse mit der Skalierung des chiralen Kondensates hatte, wurden auch Modifikationen der spektralen Eigenschaften der Vektormesonen im Kontext von Hadronenmodellen umfassend untersucht. Durch Vielkörperkorrelationen (dressing) wird oft eine signifikante Reduzierung der Teilchenlebensdauern bewirkt, was in einem "Schmelzen" der Mesonen in Kernen resultiert.

Die Verbindung zwischen Hadroneneigenschaften und ihren Mediummodifikationen einerseits und den Änderungen des nichtperturbativen Quark- und Gluonkondensates durch ein Medium andererseits ist nichttrivial. Einen Ansatz dafür bilden Analysen basierend auf QCD-Summenregeln [20], die die Vermutung der Absenkung der Vektormesonennassen bei endlicher Dichte (Brown and Rho [7]) unterstützen, jedoch noch mit relativ hohen Unsicherheiten verbunden sind.

In [21] wurde gezeigt, dass die Summenregeln nur begrenzte Möglichkeiten für Vorhersagen in Bezug auf die spezifischen Eigenschaften wie die Masse oder die Breite der Hadro-

nen haben, da Integrale über die spektrale Verteilung des Hadrons laufen. Damit kann man Masse-Breite-Korrelationen eingrenzen, d.h. Regionen in einer fiktiven Masse-Breite-Ebene. Im Fall des ρ Mesons beispielsweise sagt die Analyse nach den Summenregeln voraus, dass die spektrale Stärke der Mesonen in Kernmaterie zu kleineren invarianten Massen verschoben wird. Es ist jedoch allein anhand der Summenregelanalysen nicht möglich zu bestimmen, ob diese zusätzliche Stärke durch Absenkung der Masse oder Stoßverbreiterung entsteht.

Die erste experimentelle Beobachtung der Modifikation spektraler Eigenschaften des ρ Mesons in heißer und dichter Materie geht zurück auf das Jahr 1990, als Dileptonenspektren in ultrarelativistischen Schwerionenstößen von den CERES [22] und HELIOS [23] Kollaborationen am CERN gemessen wurden. Die gemessenen Dileptonenspektren zeigten eine deutliche Erhöhung relativ zu Standardquellen (hadronic cocktail) in der Region unterhalb des Vektormesonpeaks, was eine generelle Verschiebung der spektralen Stärke zu kleineren invarianten Massen nahelegte. Es konnte jedoch durch den Vergleich von theoretischen Berechnungen und experimentellen Daten nicht geklärt werden, ob die spektrale Stärke bei kleineren Massen mit einer Absenkung der Massen, wie in [7, 20] vorausgesagt, oder einer Ausdehnung der Spektralfunktion durch Stoßverbreiterung, wie in Rechnungen hadronischer Modelle erwartet [24], verbunden ist, was hauptsächlich durch die Auflösung bei kleinen Massen in der Region um den Vektormesonpeak bedingt war. Neuere Messungen der Dileptonenspektren in Schwerionenstößen mit höherer Auflösung, die von der NA60 [25] und der CERES [26] Kollaboration gemacht wurden, unterstützen das Szenario einer Mediumverbreiterung des ρ Mesons anstelle einer Massenverschiebung.

Eine zweite Reihe von Schwerionenexperimenten wurde bei niedrigeren Energien von 1.0 AGeV im Laborsystem von der DLS Kollaboration am BEVALAC [27, 28] durchgeführt. Auch in diesem Fall wurden die Dileptonenspektren in der Region kleiner Massen von den Transportrechnungen unterschätzt, im Gegensatz zu ähnlichen Messungen an den elementaren $p + p$ und $p + d$ Systemen. Diese Situation verbessert sich nicht wie im ultrarelativistischen Fall, wenn man Mediumspektralfunktionen oder ein Szenario der Massenabsenkung berücksichtigt [29, 30]. In diesem Energiebereich, der die Phase hoher Dichte und niedriger Temperatur untersucht, wird die experimentelle Lage jedoch mit den schon existierenden Daten und den zukünftigen Messungen der HADES Kollaboration an der GSI [32, 33] signifikant verbessert werden.

In dieser Arbeit wurde eine systematische Untersuchung der von Vektormesonen im Medium erhaltenen Eigenschaften und ihres Einflusses auf das Dileptonenspektrum in Schwerionenstößen durchgeführt. Die zeitliche Dynamik der Schwerionenreaktionen wurde mithilfe des Relativistischen Quanten-Molekular-Dynamik-Transportmodells (RQMD) beschrieben.

Die Mediemeigenschaften der ρ und ω Mesonen in Kernmaterie wurden durch ein Nukleonresonanzmodell kombiniert mit einem Vektormesondominanz-Modell (VMD) bestimmt. Man geht dabei von der Annahme aus, dass die dominanten Vielteilcheneffekte durch die Ankopplung der Vektormesonen an Nukleonloch-Resonanz-Anregungen (RN^{-1}) beschrieben werden können. Die Ankopplung elektromagnetischer Ströme an Hadronen erfolgt im Rahmen des etablierten VMD-Modells über intermediäre Vektormesonen. In dieser Arbeit wurde

das in Tübingen erweiterte VMD-Modell benutzt. Zusätzlich werden nicht-resonante Beiträge zur Selbstenergie der Vektormesonen berücksichtigt. Für beide Vektormesonen wurde eine Verbreiterung und eine signifikante Verschiebung der Spektralstärke zu kleinen invarianten Massen gefunden. Die Kopplung des ρ Mesons an den $N^*(1520)N^{-1}$ Zustand und des ω Mesons an den $N^*(1535)N^{-1}$ Zustand führt insbesondere bei kleinen Impulsen zu einem ausgeprägten Doppelpack in der Spektralfunktion. Zuerst wurden die Spektralfunktionen der Vektormesonen aus Vakuumeigenschaften der Nukleonresonanzen berechnet. Als nächstes wurden Mediummodifikationen der Nukleonresonanzbreiten, die durch Mediummodifikationen der ρ und ω Mesonen induziert werden, berücksichtigt. Dies führt zu einer selbstkonsistenten Berechnung der Spektralfunktionen der Vektormesonen, da nun die Selbstenergie der Mesonen von der Mediumbreite der Nukleonresonanzen abhängt, die wiederum durch die mesonische Selbstenergie bestimmt wird. Diese selbstkonsistente Berechnung wird iterativ geführt. Das iterative Schema beeinflusst hauptsächlich die Ergebnisse bei kleinen Massen und reduziert die Höhen der $N^*(1520)N^{-1}$ und $N^*(1535)N^{-1}$ Peaks.

Im folgenden Schritt wurde der Einfluss von Mediummodifikationen der Vektormesoneigenschaften auf die Dileptonenproduktion untersucht. Das Dileptonenspektrum wurde exemplarisch für die Reaktion C+C bei 2.0 AGeV berechnet, für die vor kurzem experimentelle Daten von der HADES Kollaboration veröffentlicht wurden. Zuerst wurden Mediumeffekte in einem Standardverfahren behandelt, wobei eine schematische Stoßverbreiterung der Vektormesonbreite und eine Absenkung der Vektormesonmasse entsprechend des Brown-Rho Skalengesetzes eingeschlossen wurden.

Das schematische Szenario der Stoßverbreiterung ergab, dass die Experimentaldaten in der Masseregion der Vektormesonpeaks leicht überschätzt werden, wenn man dichteabhängige Mediumbreiten der Vektormesonen (mit $\Gamma_{\rho}^{\text{tot}}(\rho_0) = 250$ MeV und $\Gamma_{\omega}^{\text{tot}}(\rho_0) = 125$ MeV bei Nuklearer Sättigungsdichte ρ_0) annimmt. Wir diskutieren desweiteren Näherungen, die durch die Energieabhängigkeit der Vektormesonbreite nötig sind. Besonderer Wert wurde dabei darauf gelegt, die theoretischen Beschränkungen aufzuzeigen, die eine derartige schematische Herangehensweise mit sich bringt.

In dem – relativ naiven – Mediumszenario, worin die Vektormesonmassen linear mit der anwachsenden Dichte absinken (Brown-Rho scaling), wird gefunden, dass das experimentelle Dileptonenspektrum bei invarianten Massen unterhalb des Vektormesonpeaks überschätzt und in der Region des und überhalb des Vektormesonpeaks unterschätzt wird, auch wenn zusätzlich eine Stoßverbreiterung berücksichtigt wird. Dieses Verhalten ist eine Konsequenz der von diesem Szenario vorhergesagten Verschiebung der Spektralstärke zu kleineren invarianten Massen mit dem daraus folgenden Mangel an Spektralstärke in der Region des Vektormesonpeaks.

Als letzten Schritt gehen wir über die schematische Behandlung von Mediumeffekten hinaus und berücksichtigen die Mediumeigenschaften von Vektormesonen in einer konsistenten Weise durch die mikroskopische Berechnung der Selbstenergie im Medium im Rahmen des Nukleonresonanzmodells kombiniert mit Vektormesondominanz. Zum ersten Mal wird hier versucht, eine konsistente theoretische Beschreibung des Dileptonenspektrums basierend auf einem einheitlichen Modell für Vektormesonen- und Dileptonen-Produktion sowie ihrer Mediummodifikationen durchzuführen. Das übertrifft die Standardverfahren, in

denen die totale Breite bei gegebener Dichte als Parameter eingesetzt wird und die Skalierung der Breite in Abhängigkeit der Dichte nur als Annahme eingeht.

Wir erhalten als Ergebnis, dass die Selbstenergie, die aus den Vakuumeigenschaften der Nukleonresonanzen bestimmt wird, eine unzureichende Beschreibung der Experimentaldaten im Bereich der invarianten Massen von $0.45 \leq M \leq 0.75$ GeV liefert. Das selbstkonsistente Schema kann jedoch die Daten in derselben Masseregion angemessen beschreiben. Dies zeigt, dass die Berücksichtigung der Mediumeigenschaften der Nukleonresonanzen bei der Bestimmung der Spektralfunktionen der Vektormesonen große Bedeutung hat. In Anbetracht der großen Unsicherheiten in den Kopplungen der Nukleonresonanzen insbesondere an das ω Meson und der Tatsache, dass diese Berechnung eine *parameterfreie* Bestimmung des Dileptonenspektrum im Medium darstellt, kann das Ergebnis als zufriedenstellend angesehen werden. Dennoch lässt der Vergleich mit den experimentellen Daten darauf schließen, dass die Mediummodifikationen, die in dem verwendeten Ansatz vorhergesagt werden, eventuell zu stark sind. Im Bereich kleiner Massen ($m_\pi \leq M \leq 0.4$ GeV) finden wir, dass die Einbeziehung der Mediumspektralfunktionen der ρ und ω Mesonen das theoretische Ergebnis nicht verbessern und die Experimentaldaten noch leicht unterschätzt werden.

Abschließend kann man feststellen, dass eine konsistente mikroskopische Beschreibung der Vektormesoneigenschaften im nuklearen Medium im Rahmen von Transportrechnungen einen wesentlichen Schritt zu einem besseren Verständnis der Dileptonenspektren liefert. Zukünftige experimentelle Daten, vor allem für Reaktionen schwerer Kerne, werden sicherlich dazu beitragen, noch bestehende Modellunsicherheiten weiter einzuschränken.

Acknowledgments

I would like to thank here all the people who, directly or indirectly, supported me during my PhD.

Going back with my thoughts to the summer 2004, I cannot help but remembering that day, 23 July 2004, when my Diploma supervisor Prof. Massimo Di Toro announced me that he had been asked by Prof. Amand Fäßler for suited candidates for a PhD position at the Institute for Theoretical Physics of the Tübingen University and he wanted to suggest my name. I accepted almost immediately. At that time I was sure I wanted to start a PhD after my Diploma, though my imagination did not go beyond the idea of starting it in Catania, where I studied. This is more or less how everything started. It is therefore imperative for me to thank Prof. M. Di Toro for having suggested my name, Prof. Amand Fäßler for accepting me in his group as well as the DFG for the economical support through the grant GRK683.

Vorrei ringraziare anche i miei genitori. E' stato doloroso per loro lasciarmi andare via, ma mi hanno lasciato fare, senza impormi senza di colpa. L'hanno fatto per il mio bene, immagino, per non contrastare la mia volonta' di intraprendere la strada della ricerca "in ambito internazionale". E cosi', per darmi la possibilita' di sentirmi realizzata, hanno in silenzio sopportato il dolore causato dal mio allontanamento.

A particular thank you goes to Prof. Christian Fuchs. He accepted me in his team and inserted me in the challenging project which constitutes now the content of this thesis. He has been always open to comments and discussions and helped me in various technical and conceptual problems connected with my work.

I would like to thank our collaborators, Dr. B. Martemyanov and Dr. M.I. Krivoruchenko. I appreciated a lot many interesting discussions with them. They helped me during my work too, and often "had" to answer to questions which were coming into my mind. Dr. B. Martemyanov, in particular, taught me how to calculate self energies. It was really exciting to learn something new...thanks for that!

I would like to thank all the people of the institute I went to the mensa and I used to drink coffee with: Ludwig, Diana, Oli, Edward, Vadim, Mohamed, Viktor, Dan, Marcel, Vito, Alan. They often had to listen to my "stories" and to stand my moods.

A particular thank you goes to my ex-college and friend Diana, who is now working at the University of Graz. She was already in Tübingen when I arrived and then left in July 2007. I miss her a lot. We had so many discussions! About physics, our daily work, our hopes and expectations... how sad, silent and boring would have been these years without you!

From the deep of my heart I would like to thank you, Klemens. Though our relationship

has been full of ups and downs in the past, in the last year you have been near me and have filled my days with your love.

Finally, I would like to thank Prof. Christian Fuchs, Dr. B. Martemyanov, Dr. M.I. Krivoruchenko and Klemens for the careful reading of this manuscript, The HADES collaboration for providing the filter function and the experimental data and in particular Dr. Christian Sturm for the explanations given concerning the use of the HADES filter.